NAVAL POSTGRADUATE SCHOOL
Monterey, California

DTIC
S ELECTE D
B
MAR 0 4 1991

THESIS

AN ENGINEERING STUDY OF ALTITUDE
DETERMINATION DEFICIENCIES OF THE SERVICE
AIRCRAFT INSTRUMENTATION PACKAGE (SAIP)

by

Steven R. Eastburg

December, 1991

Thesis Advisor:	O. Biblarz
Second Reader:	E. L. Pagenkopf

Approved for public release; distribution is unlimited.

91 2 21 041

REPORT DOCUMENTATION PAGE

Form Approved
OMB No. 0704-0188

1a REPORT SECURITY CLASSIFICATION UNCLASSIFIED	1b RESTRICTIVE MARKINGS

2a SECURITY CLASSIFICATION AUTHORITY	3. DISTRIBUTION/AVAILABILITY OF REPORT
2b DECLASSIFICATION/DOWNGRADING SCHEDULE	Approved for public release; distribution is unlimited.

4. PERFORMING ORGANIZATION REPORT NUMBER(S)	5. MONITORING ORGANIZATION REPORT NUMBER(S)

6a. NAME OF PERFORMING ORGANIZATION Naval Postgraduate School	6b. OFFICE SYMBOL (If applicable) AA	7a. NAME OF MONITORING ORGANIZATION Naval Postgraduate School

6c. ADDRESS (City, State, and ZIP Code) Monterey, CA 93943-5000	7b. ADDRESS (City, State, and ZIP Code) Monterey, CA 93943-5000

8a. NAME OF FUNDING/SPONSORING ORGANIZATION Pacific Missile Test Center	8b. OFFICE SYMBOL (If applicable) 3333	9. PROCUREMENT INSTRUMENT IDENTIFICATION NUMBER

8c. ADDRESS (City, State, and ZIP Code) Pt. Mugu, CA 93042-5000	10 SOURCE OF FUNDING NUMBERS

PROGRAM ELEMENT NO	PROJECT NO.	TASK NO	WORK UNIT ACCESSION NO

11. TITLE (Include Security Classification)
AN ENGINEERING STUDY OF ALTITUDE DETERMINATION DEFICIENCIES OF THE SERVICE AIRCRAFT INSTRUMENTATION PACKAGE (SAIP)

12. PERSONAL AUTHOR(S)
Steven R. Eastburg

13a. TYPE OF REPORT AeE Degree Thesis	13b TIME COVERED FROM _____ TO _____	14. DATE OF REPORT (Year, Month, Day) 1991 December	15 PAGE COUNT 125

16 SUPPLEMENTARY NOTATION
The views expressed in this thesis are those of the author and do not reflect the official policy of the Department of Defense or U.S. Government

17 COSATI CODES			18. SUBJECT TERMS (Continue on reverse if necessary and identify by block number)
FIELD	GROUP	SUB-GROUP	Pitot-static, Static Pressure Measurement, Service Aircraft Instrumentation Package

19 ABSTRACT (Continue on reverse if necessary and identify by block number)

Altitude determination errors of the U.S. Navy's Service Aircraft Instrumentation Package (SAIP), an airborne positioning pod, were examined in a multifaceted study involving in-flight evaluations, wind tunnel testing and pressure sensitivity experiments. The original objectives of the research related to identifying aerodynamic sources of pod static pressure inaccuracies and recommending specific remedies to alleviate these errors. After an extensive evaluation, results revealed that the problem exists not in the aerodynamic measurement performance of the probe, but in the electronic circuitry residing within the Air Data Unit (ADU). The ADU houses multiple pressure transducers, each associated with different static and dynamic pressure ports, in a single module. This circuit configuration leads to electrical interference and an attendant degradation of the static pressure output voltage. Accurate static pressure voltages, which can be subsequently converted into appropriate SAIP barometric altitudes, are obtained by electrically isolating the three ADU dynamic pressure transducers from the single operative static pressure transducer and remaining ADU circuitry.

20 DISTRIBUTION/AVAILABILITY OF ABSTRACT ☒ UNCLASSIFIED/UNLIMITED ☐ SAME AS RPT ☐ DTIC USERS	21 ABSTRACT SECURITY CLASSIFICATION UNCLASSIFIED
22a. NAME OF RESPONSIBLE INDIVIDUAL Dr. O. Biblarz	22b TELEPHONE (Include Area Code) 408-646-3096	22c OFFICE SYMBOL AA/Bi

DD Form 1473, JUN 86   *Previous editions are obsolete.*   SECURITY CLASSIFICATION OF THIS PAGE

S/N 0102-LF-014-6603

AN ENGINEERING STUDY OF ALTITUDE
DETERMINATION DEFICIENCIES OF THE SERVICE
AIRCRAFT INSTRUMENTATION PACKAGE (SAIP)

by

Steven R. Eastburg
Lieutenant, United States Navy
B.S., United States Naval Academy, 1981
M.S., University of Southern California, 1988
M.S., Naval Postgraduate School, 1990

Submitted in December 1990 in partial fulfillment
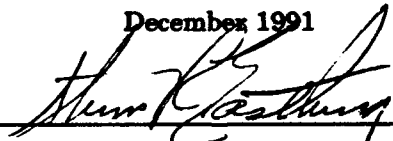of the requirements for the degree of
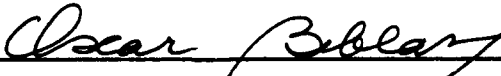
AERONAUTICAL ENGINEER

from the
NAVAL POSTGRADUATE SCHOOL
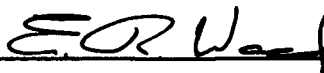December 1991

Author: _____
Steven R. Eastburg

Approved by: _____
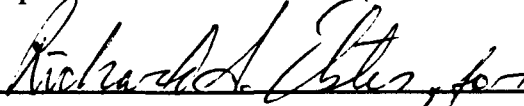O. Biblarz, Thesis Advisor

_____
Eric L. Pagenkopf, Second Reader

_____
E. R. Wood, Chairman,
Department of Aeronautics and Astronautics

_____
Dean of Faculty and Graduate Studies

ii

ABSTRACT

Altitude determination errors of the U.S. Navy's Service Aircraft Instrumentation Package (SAIP), an airborne positioning pod, were examined in a multifaceted study involving in-flight evaluations, wind tunnel testing and pressure sensitivity experiments. The original objectives of the research related to identifying aerodynamic sources of pod static pressure inaccuracies and recommending specific remedies to alleviate these errors.

After an extensive evaluation, results revealed that the problem exists not in the aerodynamic measurement performance of the probe, but in the electronic circuitry residing within the Air Data Unit (ADU). The ADU houses multiple pressure transducers, each associated with different static and dynamic pressure ports, in a single module. This circuit configuration leads to electrical interference and an attendant degradation of the static pressure output voltage. Accurate static pressure voltages, which can be subsequently converted into appropriate SAIP barometric altitudes, are obtained by electrically isolating the three ADU dynamic pressure transducers from the single operative static pressure transducer and remaining ADU circuitry.

iii

Accession For		
NTIS GRA&I	☑	
DTIC TAB	☐	
Unannounced	☐	
Justification		
By		
Distribution/		
Availability Codes		
Dist	Avail and/or Special	
A-1		

QUALITY INSPECTED 3

TABLE OF CONTENTS

LIST OF TABLES

LIST OF FIGURES

LIST OF SYMBOLS

a	Local speed of sound
α	Angle-of-attack
ADU	Air Data Unit
ASA	Airflow Sensor Assembly
β	Angle-of-sideslip
C_p	Coefficient of pressure
γ	Specific heat ratio of gas
DPU/DIU	Data Processing Unit/Data Interface Unit
DVM	Digital voltmeter
EATS	Extended Area Tracking System
g	Gravitational constant
θ	Angle of rotation about SAIP longitudinal axis
IRIG	Inter-range Instrumentation Group
KIAS	Knots indicated air speed
M	Local Mach number
M_∞	Free-stream Mach number
NCA	Nose Cone Assembly
NPS	Naval Postgraduate School
P	Local pressure

P_∞	Free-stream pressure
P3	Total pressure
P(A1), P(A2)	Differential angle-of-attack pressures
P(B1), P(B2)	Differential angle-of-sideslip pressures
P_s	Static pressure
PMTC	Pacific Missile Test Center
ρ	Gas density
R	Gas constant
SAIP	Service Aircraft Instrumentation Package
T	Local temperature
T_∞	Free-stream temperature
U_m	Measured wind tunnel velocity
V	Local velocity
V_∞	Free-stream velocity
ϕ	Angle of rotation about SAIP vertical axis
Z	Altitude

ACKNOWLEDGEMENTS

I. INTRODUCTION

A. BACKGROUND

1. System Description

The U.S. Navy's Service Aircraft Instrumentation Package (SAIP) is an airborne positioning pod designed to be carried aboard aircraft being tracked within the Extended Area Test System (EATS), a tracking system used by the Pacific Missile Test Center (PMTC), Point Mugu, California. EATS is intended to be a multilateration system which is capable of providing continuous three-dimensional tracking of participating aircraft operating within the PMTC test range.

The SAIP is designed to mount on aircraft equipped with the LAU-7/A (series) launcher or equivalent, and can be attached to aircraft at various locations on the fuselage and wings. The pod consists of a five-inch diameter stainless steel tube which contains various electronic subassemblies, and a fiberglass nose cone which houses the unit's air-data and antenna subsystems (Figure 1). The SAIP is a self-contained subsystem and functions independently of indigenous systems aboard the carrier aircraft with the exception of the vehicle's electrical system, which provides 115 VAC and 28 VDC power to the pod. The pod's only source of communication with the EATS

1
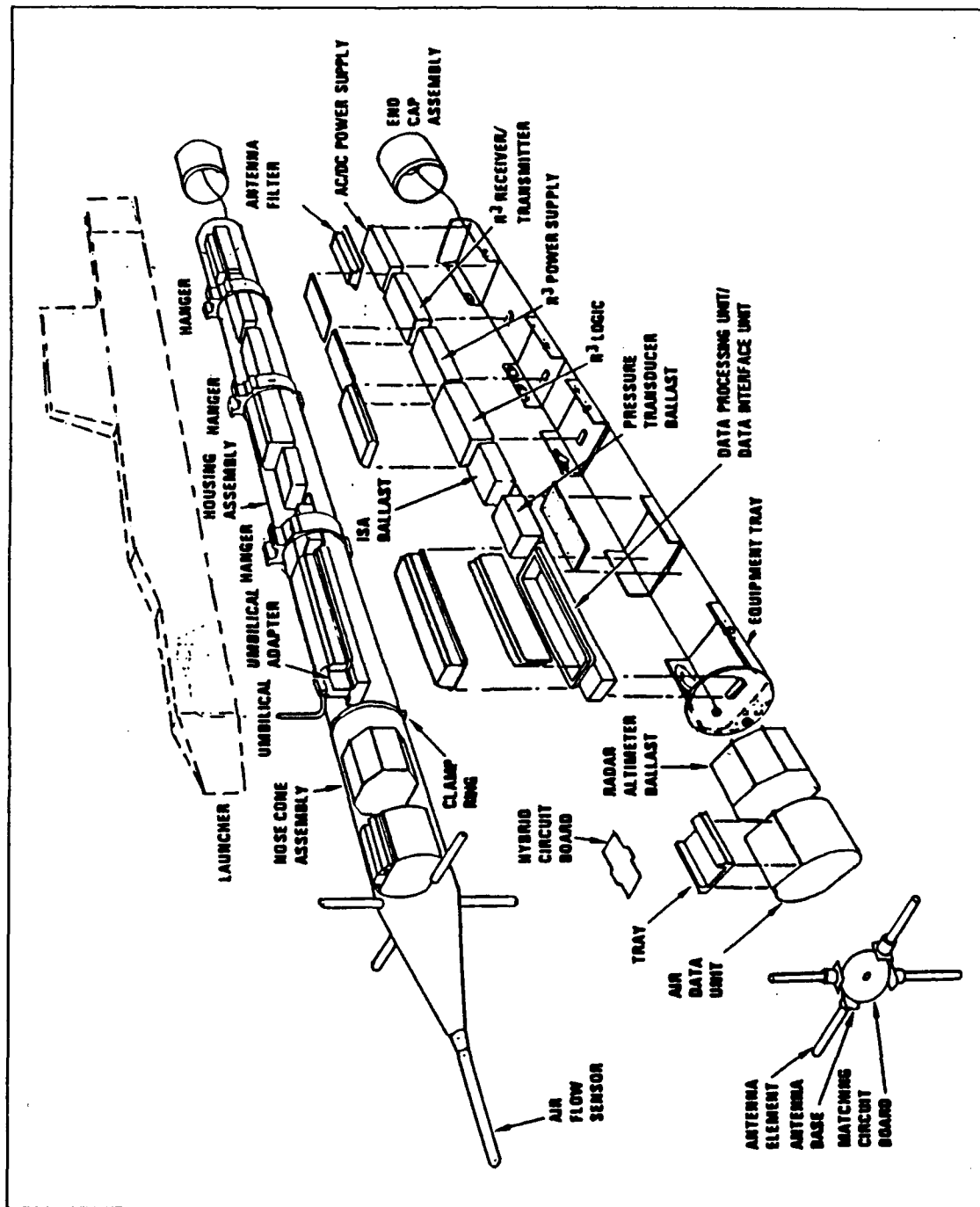
Figure 1. Service Aircraft Instrumentation Package (SAIP); Configuration -003 [Ref. 1]

2

in which it is employed is through its antenna system which receives and transmits RF signals at 141 MHz.[Ref. 1]

Among the electronics which are contained within the SAIP pod are an airflow sensor assembly which is exposed to the oncoming air flow, an air-data unit consisting of various pressure transducers, a component for digitizing and formatting of data for downlink communication, and an AC/DC power supply. Collectively, these electronics enable the tracking system master station to obtain range from the SAIP, and static pressure (altitude), air speed, attitude and weapons system data from the aircraft. The SAIP is required to operate throughout the entire flight envelope of the aircraft, including at both subsonic and supersonic airspeeds, in all attitude regimes, and with lift devices and landing gear both deployed and retracted.

2. System Performance

Altitude data obtained from flight tests of SAIPs have revealed that significant deviations from specified altitude accuracies are routinely experienced in operating the units. In addressing performance criteria for static pressure of the SAIP, the system's functional specification indicates that "the altitude error in 50 percent of the track updates shall be less than the larger of 100 feet or three percent of the participant altitude" [Ref. 1]. In comparison, standard military aircraft barometric altimeters typically maintain sea-level accuracies on the order of 75 feet [Ref. 2].

3

A number of tests of SAIP units have been conducted specifically to evaluate the pods' altitude accuracy in a dynamic flight environment. One of these in-flight evaluations was done at PMTC in May 1989, in which several SAIPs attached to A-6E and A-7E aircraft revealed that the barometric pressure measuring equipment aboard the units was providing altitude data which were grossly in error. In these tests, three aircraft carrying four SAIPs evaluated the pods' altitude accuracy in both low and high speed flight regimes. While SAIP altitudes corresponded well with true altitudes while the aircraft were stationary, at ground speeds of 150 knots on the takeoff roll, the pods reported altitude errors of approximately 146 feet, which is 146% of the total EATS altitude error budget. Measurements obtained at an altitude of 4,000 feet and at flight speeds ranging from 375 to 500 knots resulted in at least one SAIP reporting an altitude 420 feet below the known altitude, constituting 280% of the EATS altitude budget.[Ref. 3]

A subsequent flight test to evaluate SAIP altitude accuracy was performed at PMTC on 7 September 1989. In these tests, four well-calibrated SAIPs carried aboard an A-6E aircraft were used to evaluate SAIP accuracy at altitudes of 4,000 and 10,000 feet. During these trials, the aircraft commenced its data runs at 250 knots, accelerated to 500 knots, and then decelerated to 250 knots. While significant deviations from actual altitudes were obtained from the SAIPs at both altitudes and at all airspeeds, it was discovered that higher aircraft speeds and elevations substantially aggravated

4

errors in the reported SAIP altitudes. Specifically, errors on the order of 500-600 feet were experienced at an altitude of 4,000 feet, and errors ranging from 900-1,000 feet were observed at an aircraft altitude of 10,000 feet.[Ref. 4]

B. THESIS PURPOSE

A three-fold purpose of this thesis was envisioned:

1) To evaluate flight test data of the single static port-type (first-generation) SAIP and multiple static port-type (second-generation) SAIP, both of which are currently in use, in order to determine the adequacy of these designs to meet existing specifications;

2) To perform tests of the multiple static port-type SAIP at the Naval Postgraduate School's low speed wind tunnel, and to provide an evaluation of the potential of this second-generation system to meet specifications based on wind tunnel test results; and

3) To recommend design improvements to the second-generation SAIP hardware in an effort to enhance the system's altitude measurement accuracy.

II. THEORY

A. AERODYNAMIC SOURCES OF ERROR

The degree of accuracy which can be obtained in the measurement of static pressure using pressure ports in aerodynamic bodies depends upon a number of factors, such as the location of the ports on the body, the dimensions of the holes and the direction and variation in the flow direction. Measurement accuracy can potentially be degraded when the static pressure taps are not positioned a distance sufficiently aft of the base of the probe's nose. An accelerating flow in the vicinity of a probe's nose has the effect of reducing the static pressure at a tap in the region, while in areas of the body where the flow is stagnating, an increase in static pressure will normally occur [Ref. 5]. Aerodynamic flow instabilities, including rotational flow, and effects such as compressibility and boundary layer separation can also have a deleterious effect upon static pressure measurement accuracy.

B. INCOMPRESSIBLE FLOW AROUND A CIRCULAR CYLINDER

The dynamics of air flow impingement upon a circular cylinder has been treated extensively in the literature. The flow around such an object serves as a basis for the principle of the fixed yaw-probe. This flow situation is shown

6

in Figure 2, where the cylinder illustrated is exposed to a uniform flow. In the case of inviscid, irrotational and incompressible flow over such a cylinder of
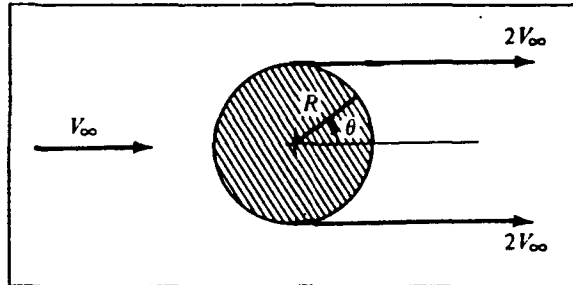
Figure 2.   Uniform Flow Over a
Circular Cylinder [Ref. 6]

radius R, it can be routinely shown that the coefficient of pressure at the surface of the cylinder, C_p, is given by

$$C_p = 1 - 4\sin^2\theta \tag{1}$$

This ideal pressure distribution can be plotted as shown in Figure 3. The curve illustrates that C_p varies from a value of 1.0 at the stagnation points at the leading and trailing edges of the cylinder, to -3.0 at the top and bottom points on the cylinder's surface, where the flow reaches a maximum velocity.

C.   REAL FLOW AROUND A CIRCULAR CYLINDER

The pressure distribution described by Equation (1) can also be presented as a function of θ for various values of Reynolds number, as illustrated in
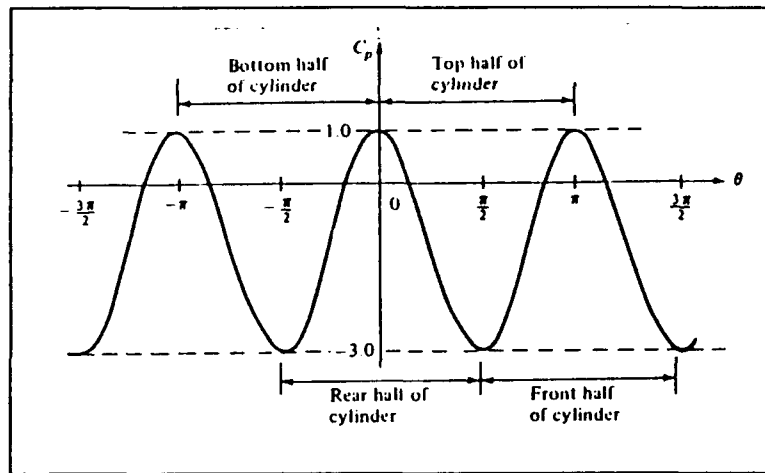
Figure 3. C_p Distribution at Circular Cylinder Surface (inviscid, incompressible flow) [Ref. 4]

Figure 4. It can be seen from the figure that the actual pressure distribution in certain regions is significantly different from the results obtained for inviscid flow. The subcritical Reynolds number case represents a flow situation
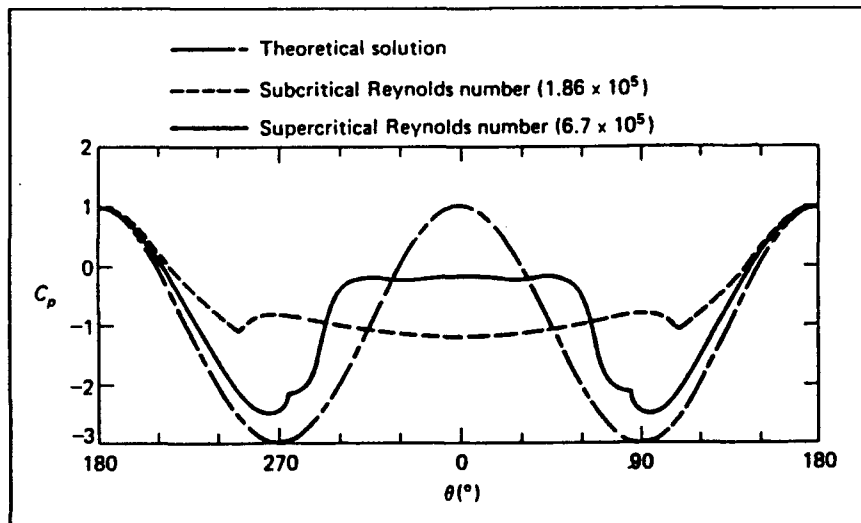
Figure 4. Pressure Distribution Over a Circular Cylinder as a Function of Reynolds Number [Ref. 7]

8

about a cylinder where the forebody boundary layer is laminar, while in the supercritical Reynolds number flow, the boundary layer in the cylinder transitions to turbulent flow [Ref. 7].

D.   COMPRESSIBLE FLOW AROUND A CIRCULAR CYLINDER

A more complete analysis can also be presented for steady, irrotational and compressible flow around a circular cylinder. The flow direction in this problem, as illustrated in Figure 5, is oriented at an angle θ on the cylinder surface and an angle ϕ with respect to the cylinder axis. For the compressible
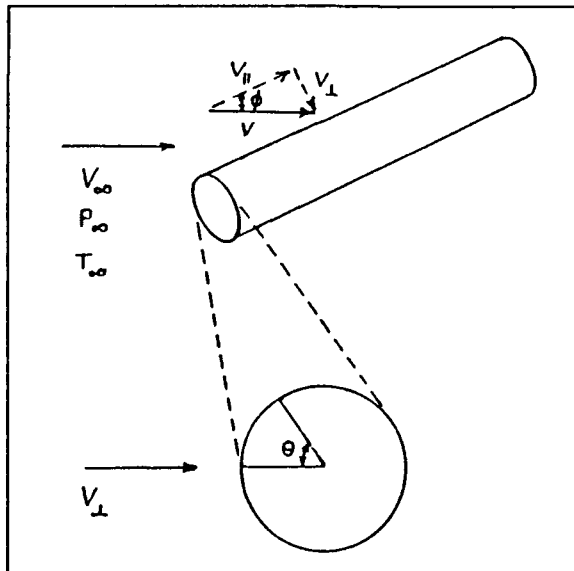
Figure 5. Configuration For Compressible Flow Around a Circular Cylinder

flow situation, it can be shown that the local velocity, V, at the cylinder surface is expressed as

$$V^2 = V_\infty^2 (4\sin^2\phi\sin^2\theta + \cos^2\phi) \qquad (2)$$

From the definition of Mach number, $M = V/a$, where a is defined as the local speed of sound, and from isentropic relations, it is possible to find an expression for the local Mach number, M, at the surface of the cylinder:

$$M^2 = \frac{M_\infty^2\, f(\phi,\theta)}{\left[1 + \frac{\gamma-1}{2}M_\infty^2\right] - \left[\frac{\gamma-1}{2}M_\infty^2\, f(\phi,\theta)\right]} \qquad (3)$$

where $f(\phi,\theta)$ is defined as

$$f(\phi,\theta) = 4\sin^2\phi\sin^2\theta + \cos^2\phi \qquad (4)$$

The ratio between the local pressure at the cylinder surface and the free-stream pressure is

$$\frac{P}{p_\infty} = \left[\frac{1 + \frac{\gamma-1}{2} M_\infty^2}{1 + \frac{\gamma-1}{2} M^2} \right]^{\frac{\gamma}{\gamma-1}} \qquad (5)$$

where $\gamma = 1.4$ for air [Ref. 8]. The relationships between the pressures in this flow condition may also be described in terms of the coefficient of pressure, given by

$$C_p = \left[\frac{p}{p_\infty} - 1 \right] \frac{2}{\gamma M_\infty^2} \qquad (6)$$

Equations (2), (3), (5) and (6) represent the relations which describe the idealized flow of a perfect gas over a circular cylinder, and serve as a fundamental basis for the principle of the fixed yaw-probe design. These equations, which are valid for both compressible and incompressible flow, fully describe the mechanics of a flow field approaching such a probe from any direction, as would be expected in the flow about a SAIP pod configured for use aboard an aircraft. While the relations also accommodate deviations from the true cylindrical geometry which are caused by flow field impingement upon the cylinder from varying directions, they only partially represent flow with the boundary layer separated.

11

E. IDEALIZED PRESSURE DISTRIBUTION

A BASIC language computer program written to evaluate Equations (2) through (6) for various values of free stream Mach number and different impingement angles appears in Appendix A. Plots of the program's output for $M_\infty=.20$ appear in Figures 6 and 7 and output for $M_\infty=.80$ is plotted in Figures 8 and 9. Figures 6 and 8, distributions of p/p_∞ versus impingement angle θ, illustrate the sinusoidal nature of the pressure ratio, and reveal that very little actual variation in the ratio occurs as the freestream direction changes. Enhanced resolution of the variation of pressure is seen in Figures 7 and 9, where the pressure coefficient has been plotted as a function of the impingement direction θ. It can be seen from the latter two figures that the variation of C_p is sinusoidal in nature, similar to the results depicted in Figure 3.

Important differences exist between the incompressible and compressible flow pressure coefficient variations. While the relative phases of the resultant sinusoids in Figures 7 and 9 are identical, the amplitude of the incompressible flow pressure coefficient varies from approximately -3.0 to 1.0, while the amplitude of the coefficient under conditions of compressible flow takes on values ranging from approximately -1.9 to 1.2. The resultant effect of compressibility, as depicted in the foregoing figures, is to narrow the magnitude of these amplitude differences.

12
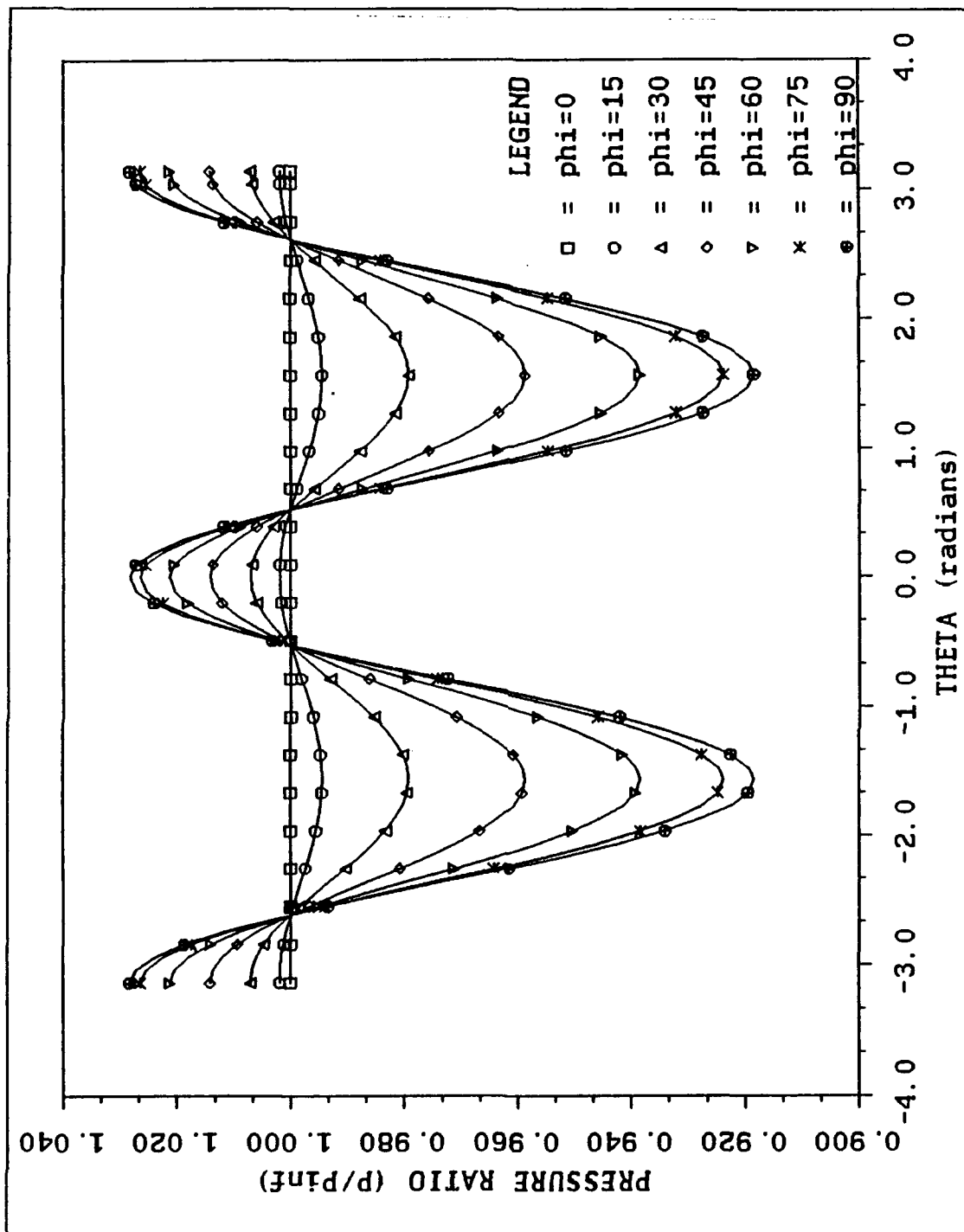
Figure 6. P/P∞ Distribution at Circular Cylinder Surface; M∞=.20 (inviscid, incompressible flow)
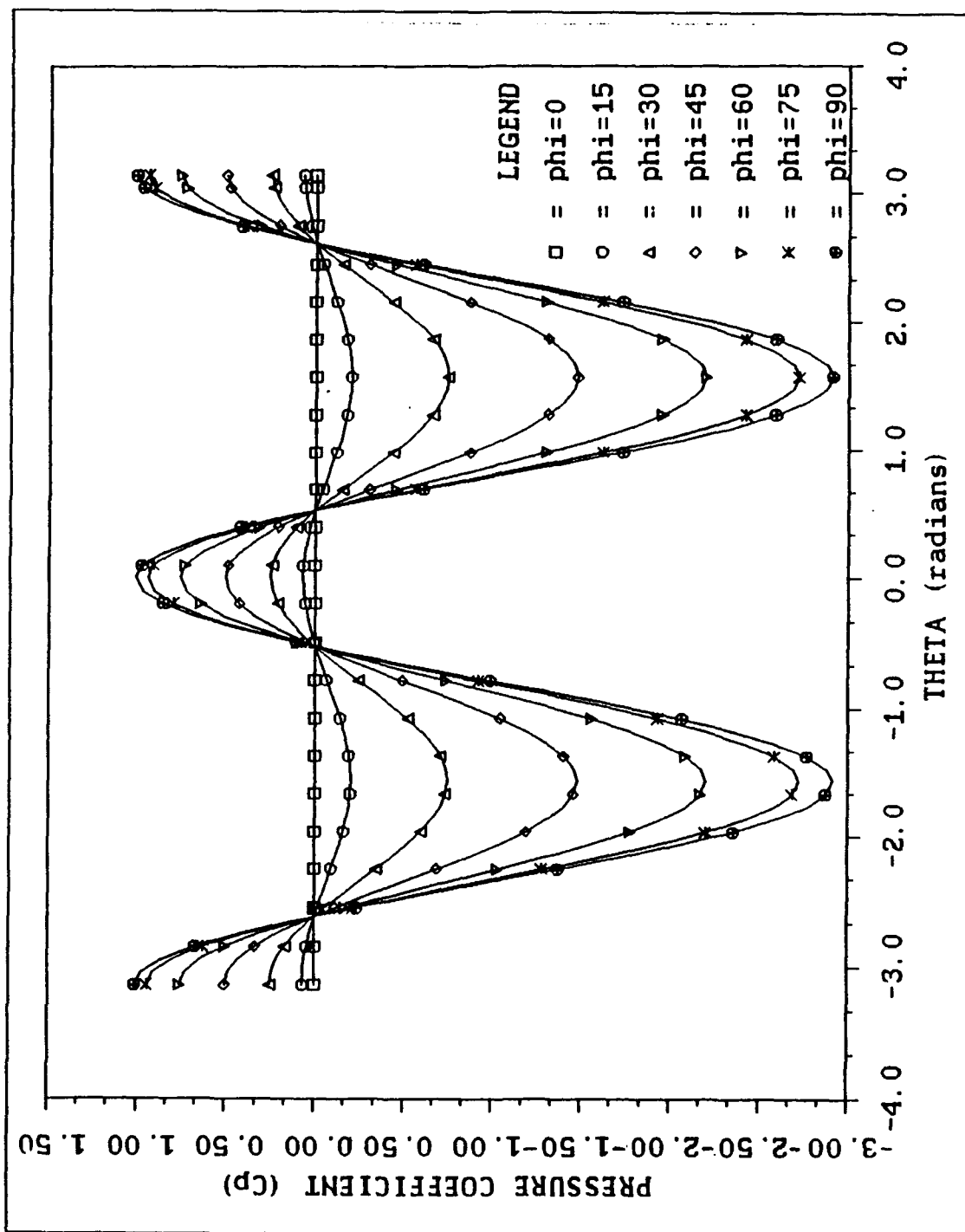
Figure 7. C_p Distribution at Circular Cylinder Surface; $M\infty$=.20 (inviscid, incompressible flow)

14
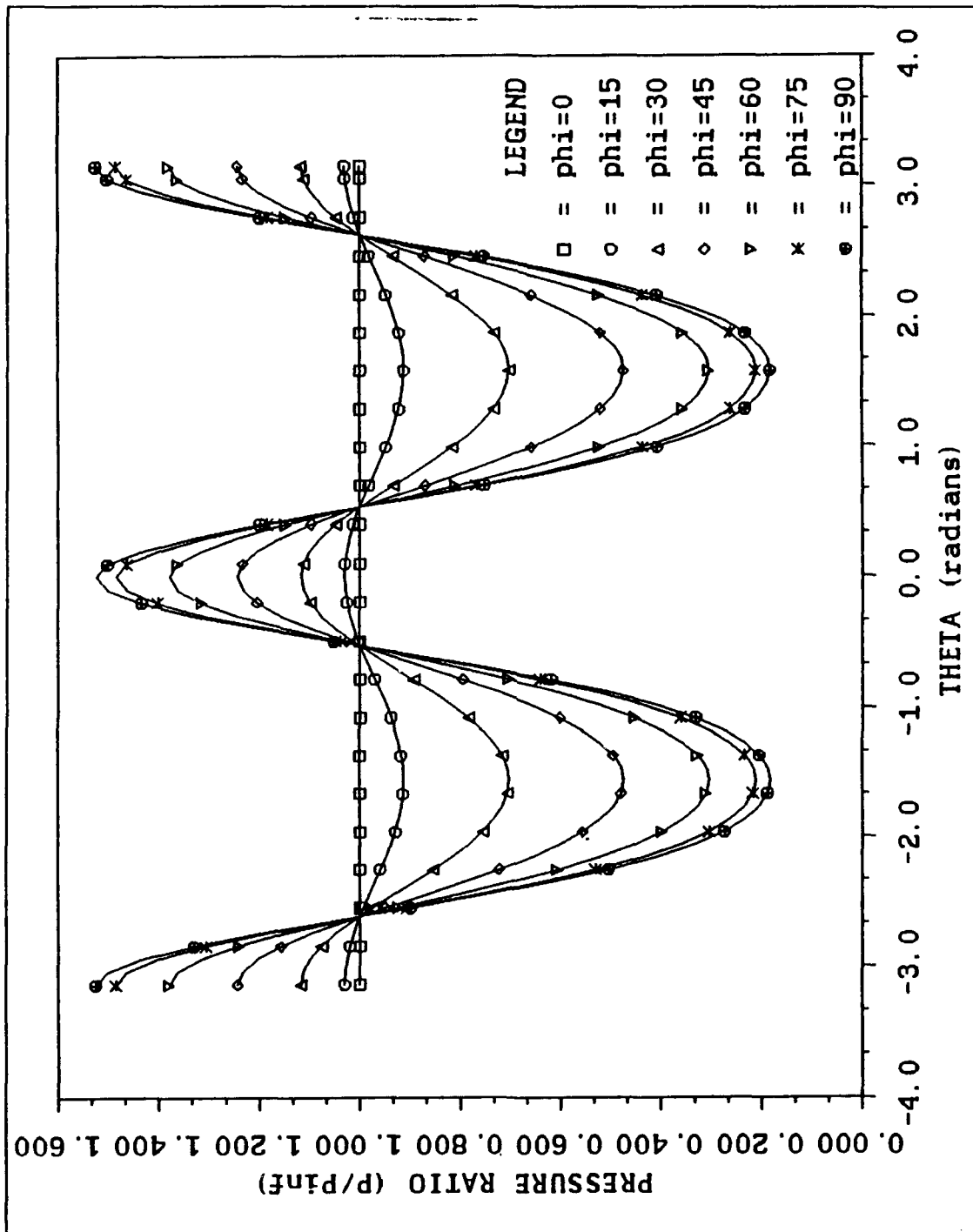
Figure 8. P/P_∞ Distribution at Circular Cylinder Surface; $M_\infty = .80$ (inviscid, compressible flow)

15
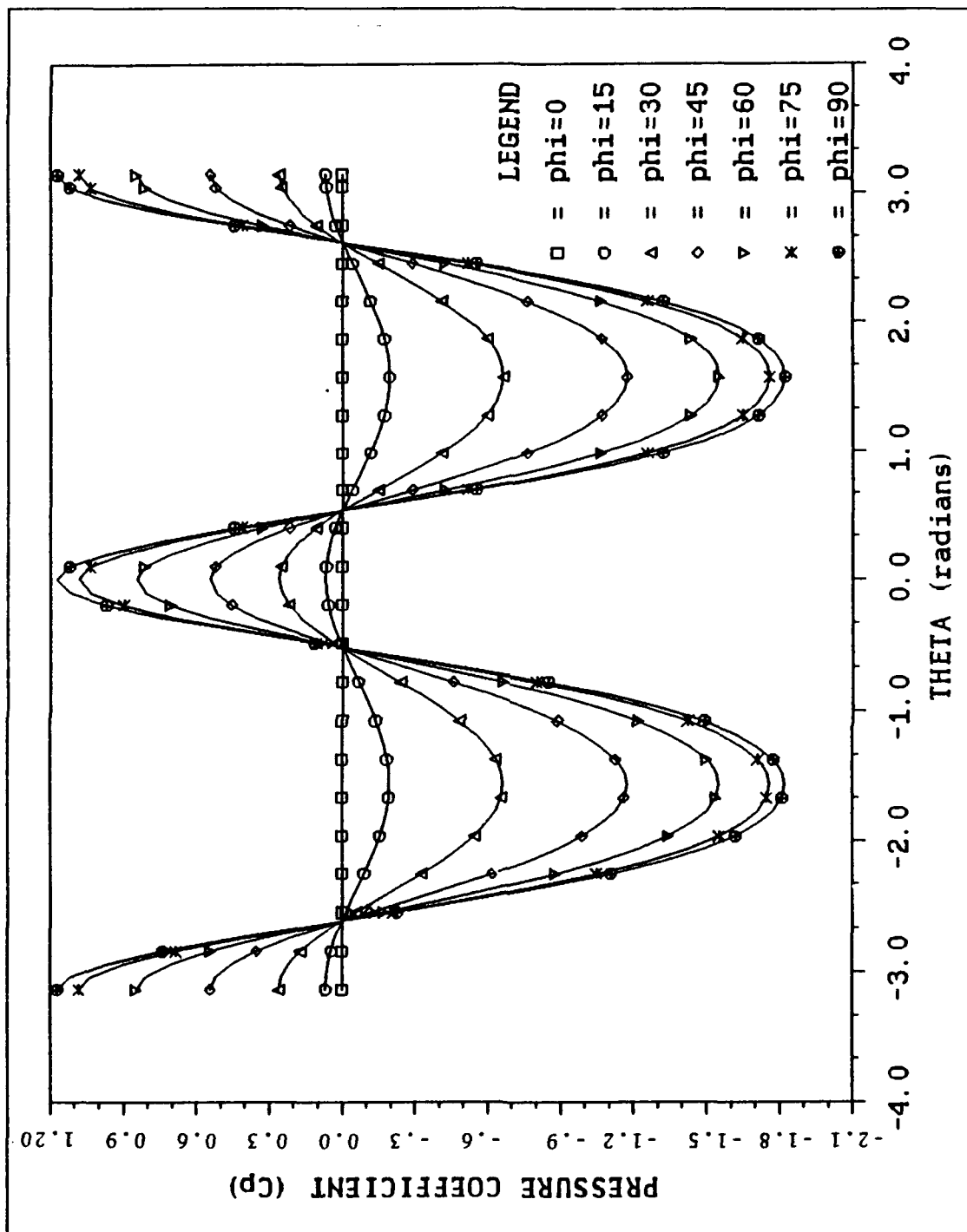
Figure 9. C_p Distribution at Circular Cylinder Surface; M∞=.80 (inviscid, compressible flow)

16

III. FLIGHT TEST ANALYSIS

A. FLIGHT TEST OBJECTIVES AND PROCEDURE

1. Objectives

The primary flight test to evaluate SAIP airborne altitude measurement accuracy was initiated by PMTC personnel and conducted on 7 September 1989 aboard an A-6E configured to carry four SAIP units. Among the objectives of the tests, as promulgated in the published test plan, were the following:

1. To evaluate raw, processed and filtered state output data from SAIP units;

2. To determine altitude errors associated with different wing stations on the A-6E aircraft; and

3. To determine errors in pressure measurements associated with the different static port configurations existent in the first- and second-generation SAIP pods.[Ref. 9, enclosure (1)]

2. Procedure

A total of ten runs of approximately four to five minutes duration each were performed during the series of three test flights. Runs were performed at 4,000 feet and at 10,000 feet (as determined by the aircraft barometric altimeter) in order to obtain data on the influence of altitude upon

17

SAIP accuracy. In order to acquire data on the impact which the presence of a centerline fuel tank would have upon SAIP altitude accuracy, the tank was removed from the aircraft following the first flight. Two first-generation and two second-generation SAIP units were carried on each of the test flights. The only difference in the two designs was that the first-generation SAIP incorporated a single static pressure port while the second-generation unit was equipped with 12 static ports located around the probe's circumference and manifolded into a single static pressure line. A more extensive discussion of SAIP design is contained in Section IV.A.2.

Test runs were initiated in straight and level flight at the assigned altitude and at a nominal aircraft speed of 250 knots indicated air speed (KIAS) (416.67 ft/sec). During the runs, airspeed was increased to 500 KIAS (833.33 ft/sec) and subsequently decreased to 250 KIAS while maintaining a constant altitude. Start and stop times of each run were recorded, as were the times at which both acceleration and deceleration were commenced and terminated. These procedures were followed during each of the runs at the two different altitudes. By executing constant altitude runs with varying aircraft speed and by also establishing data points were the aircraft was at constant velocity at varying altitudes, a possible SAIP altitude error dependence upon both velocity and ambient air density could be investigated.

During each of the maneuvers, SAIP altitude information was relayed from the pods' antenna subsystem to the various ground stations for post-

18

mission evaluation. The EATS' System Evaluator General Data Tape was used
to continuously record the test aircraft's altitude, heading, airspeed and the
Inter-range Instrumentation Group (IRIG) time. The aircraft instrumentation
tape recorder (pilot-activated MARS-1414) was used to catalog aircraft
heading, ground speed (knots), true air speed (knots, Mach number), altitude
(radar, barometric and "true") and time.

While a total of ten data gathering runs were conducted during the
series of three flights, data from only four of the runs were either available or
were of utility in analyzing SAIP altitude accuracy. The runs which resulted
in useful data included a test at 4,000 feet and one at 10,000 feet, both with
a centerline fuel tank installed, and two similar trials at the same altitudes
with the centerline tank removed. In the runs which were analyzed, the first-
generation pods were attached to wing stations one and four and the second-
generation SAIPs were placed on stations two and five. The wing stations and
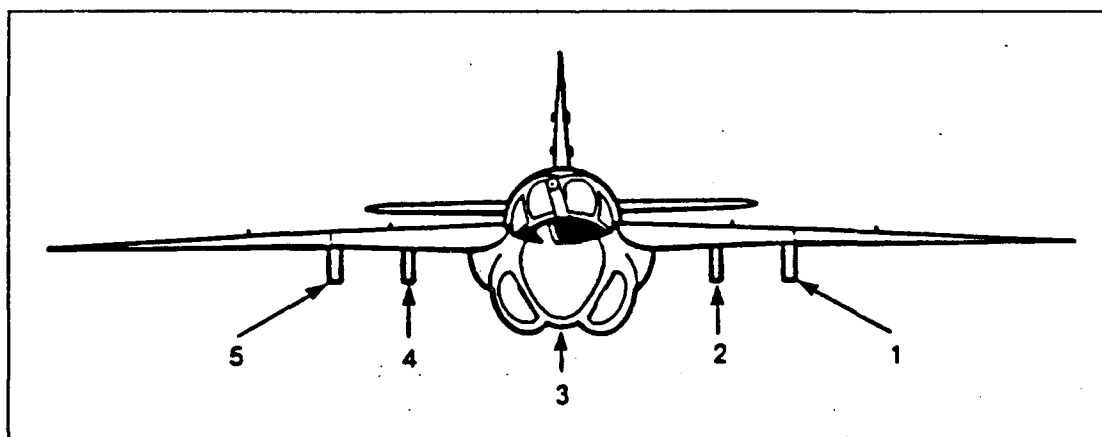
Figure 10. A-6E Wing Station Configuration

19

their respective identifications are illustrated in Figure 10. The SAIP pods which were used in the tests were configured on the individual wing stations as follows:

- Station 1: SAIP B (first-generation)

- Station 2: SAIP A (second-generation)

- Station 3: Fuel Tank

- Station 4: SAIP D (first-generation)

- Station 5: SAIP C (second-generation)

B.   DATA ANALYSIS PROCEDURE

1.   Data Correlation

Data obtained during the flight tests by the EATS ground stations, which recorded SAIP-telemetered altitude information, and by the aircraft, which recorded the actual barometric altitude against which SAIP measurement accuracy was compared, were correlated for purposes of analysis by the common IRIG time. Data points corresponding to these respective altitudes were selected at ten-second intervals for subsequent comparison and statistical analysis.

2. DATASTAT Program

To analyze the results of the flight tests, the altitudes reported by the aircraft and by each of the four SAIPs at each ten-second interval were input to the FORTRAN program DATASTAT (Appendix B), which was written to calculate the differences in altitude reported by the aircraft and each individual SAIP, and to subsequently determine the mean values and standard deviations of these differences. These altitude differences were plotted against the relative run time to illustrate the variation in time of the reported position differences. The differences were also plotted verses aircraft speed in order to establish the variation of SAIP altitude accuracy with velocity.

3. Altitude Error Velocity Dependence

a. Analysis

In the analysis of SAIP altitude error, the parameter of primary importance in judging SAIP performance is the "altitude deficit", ΔZ, which can be expressed as the difference in aircraft-reported altitude and SAIP-reported altitude

$$\Delta Z = Z_{aircraft} - Z_{SAIP} \qquad (7)$$

Since this altitude deficit originates as a pressure deficit, the difference in reported altitudes may be described by the hydrostatic equation

$$\frac{dP}{P} = -g\frac{dz}{RT} \tag{8}$$

where P = pressure

   g = gravitational constant

   R = gas constant

   T = temperature

For small changes in pressure, this may be written as

$$\frac{\Delta P}{P} \approx -g\frac{\Delta Z}{RT} \tag{9}$$

Equation (8) yields the following integral,

$$P = P_o\left[1-\frac{\beta Z}{T_o}\right]^{\frac{g}{R\beta}} \tag{10}$$

where, for the atmosphere, $T = T_o - \beta Z$

$$\beta = 6.5 \ ^\circ K/km$$

$$= .0019817 \ ^\circ K/ft$$

$$g/R\beta \approx 5.26$$

Substituting (10) into (9), we get

$$\Delta P = -\frac{g}{RT_o} \frac{P_o \left[1 - \frac{\beta Z}{T_o}\right]^{\frac{g}{R\beta}}}{\left[1 - \frac{\beta Z}{T_o}\right]} \Delta Z \qquad (11)$$

$$= -\frac{gP_o}{RT_o} \left[1 - \frac{\beta Z}{T_o}\right]^{4.26} \Delta Z \qquad (12)$$

Since $\beta Z/T_o < 1$, the binomial approximation

$$\left[1 - \frac{\beta Z}{T_o}\right]^{4.26} \approx 1 - 4.26 \frac{\beta Z}{T_o} \qquad (13)$$

may be applied to Equation (12), yielding,

$$\Delta P \approx \left[\frac{gP_o}{RT_o}\right] \left[1 - 4.26 \frac{\beta Z}{T_o}\right] \Delta Z \qquad (14)$$

Because gP_o/RT_o is a constant, Equation (14) may also be written as a proportionality

$$\Delta P \propto \left[1 - 4.26 \frac{\beta Z}{T_o}\right] \Delta Z \qquad (15)$$

For operations under standard conditions, T_o may be taken as 288°K.

Now, since $\Delta P \approx q = .5\rho V^2$, then by plotting

$$\log \left[\left(1 - \frac{4.26\beta Z}{T_o}\right)\Delta Z\right] \qquad (16)$$

versus $\log(V)$, a slope of the resulting curve of two would reveal the existence of a velocity-squared influence on pressure. Accordingly, it would then be possible to conclude with a high degree of confidence that dynamic pressure impingement on the SAIP pods' pressure ports is giving rise to erroneous altitude determinations.

b. DATAFIT Program

The FORTRAN program DATAFIT (Appendix C) was written to calculate the above parameters based on input aircraft velocities and differences in altitude between the carrier aircraft and the individual SAIP units. By subsequently plotting DATAFIT output and lines of constant slope

24

two for each of the four runs, the velocity-squared dependence may be investigated.

C. DATA ANALYSIS RESULTS

1. Statistical Analysis

The aircraft- and SAIP-reported altitudes which were input to the programs DATASTAT and DATAFIT for runs two through five appear in Appendix D. The output of DATASTAT appears in Tables 1 through 4. SAIPs A-D were mounted as discussed in Section III.A.2 and as depicted in Figure 10.

TABLE 1. STATISTICAL MEASURES OF SAIP PERFORMANCE;
RUN #2, 4,000 FEET, CENTERLINE FUEL TANK
INSTALLED

Alt_{AC} - Alt_{SAIP}	SAIP A	SAIP B	SAIP C	SAIP D
Mean Value (feet)	623.46	586.79	549.82	536.07
Standard Deviation (feet)	230.05	254.29	230.80	213.12

TABLE 2. STATISTICAL MEASURES OF SAIP PERFORMANCE;
RUN #3, 10,000 FEET, CENTERLINE FUEL TANK
INSTALLED

Alt_{AC} - Alt_{SAIP}	SAIP A	SAIP B	SAIP C	SAIP D
Mean Value (feet)	974.91	980.06	870.52	963.15
Standard Deviation (feet)	206.89	251.81	222.67	198.58

TABLE 3. STATISTICAL MEASURES OF SAIP PERFORMANCE;
RUN #4, 4,000 FEET, CENTERLINE FUEL TANK
REMOVED

Alt_{AC} - Alt_{SAIP}	SAIP A	SAIP B	SAIP C	SAIP D
Mean Value (feet)	626.94	592.00	604.22	526.56
Standard Deviation (feet)	226.31	289.61	256.35	228.68

TABLE 4. STATISTICAL MEASURES OF SAIP PERFORMANCE;
RUN #5, 10,000 FEET, CENTERLINE FUEL TANK
REMOVED

Alt$_{AC}$ - Alt$_{SAIP}$	SAIP A	SAIP B	SAIP C	SAIP D
Mean Value (feet)	980.05	1006.82	963.77	463.55
Standard Deviation (feet)	169.70	210.69	197.28	166.85

The above tabulated results reveal no distinct correlation between either relative SAIP position on the aircraft, pod design (first- or second-generation) or the existence of a centerline fuel tank upon SAIP altitude accuracy. A number of observations can be made, however, based on the tabulated results. On the average, SAIP altitude error at 4,000 feet was 14.35% of the assigned altitude with the fuel tank installed and 14.69% of the altitude with the tank removed. At 10,000 feet, SAIP error was 9.47% of the assigned altitude with a centerline tank attached and 8.54% with it removed. The system's required altitude accuracy at 4,000 and 10,000 feet, as stipulated by the functional specification, is 120 and 300 feet, respectively [Ref. 1]. The only significant (and inexplicable) anomaly resulting from the statistical analysis was associated with SAIP D (first-generation) performance; during

run five, this particular pod reported altitudes which, on the average, had errors of approximately one-half of those of pods A-C.

2. Graphical Analysis

The results of the flight tests which were performed by maintaining constant altitude, and hence keeping ambient air density constant, and varying the aircraft speed appear in Figures 11 through 14. These plots of aircraft-reported and SAIP-reported positions versus relative run time can be scrutinized to determined if SAIP altitude accuracy depends upon aircraft velocity. Specifically, the data reveal that the greatest SAIP altitude errors occurred in the range of highest aircraft velocity (in the middle of each run). Figures 15 through 22, plots of the variations of the reported altitudes with aircraft speed, clearly illustrate the possible dependence of SAIP altitude error upon aircraft velocity.

3. Altitude Error Velocity Dependence

Plots of the output of the program DATAFIT appear in Figures 23 through 26, corresponding to the four runs in which valid data were collected. Also depicted in the figures are lines with a constant slope of two. From the figures it can be seen that data from two of the four runs (runs #2 and #4) manifest a velocity-squared relationship. While not all of the data points are corroborative, the figures reveal very significantly that it is highly possible that that SAIP altitude error exhibits a velocity-squared dependence.

28
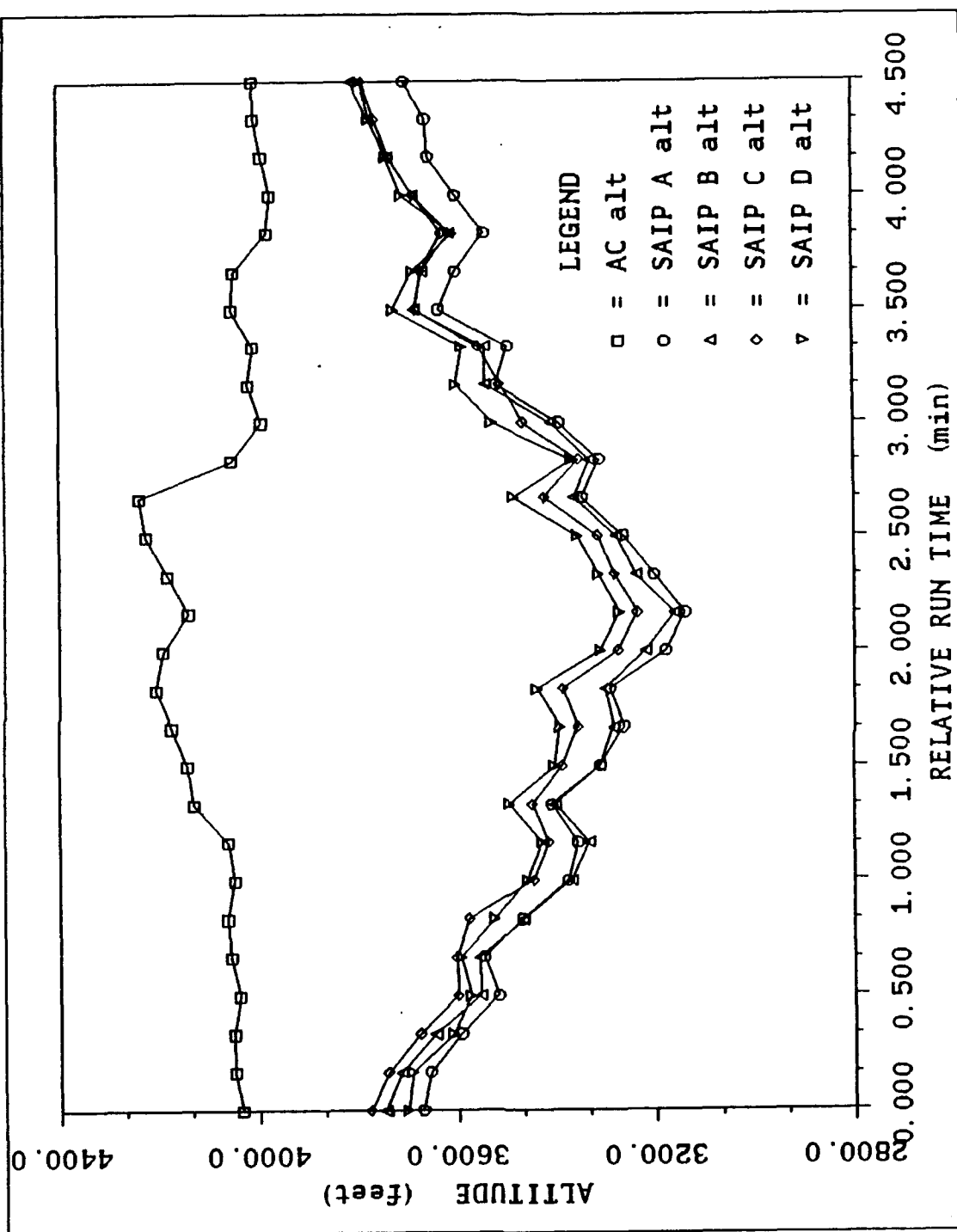
Figure 11. Reported Altitude vs. Run Time (Run #2: 4,000 feet, centerline tank installed)

29
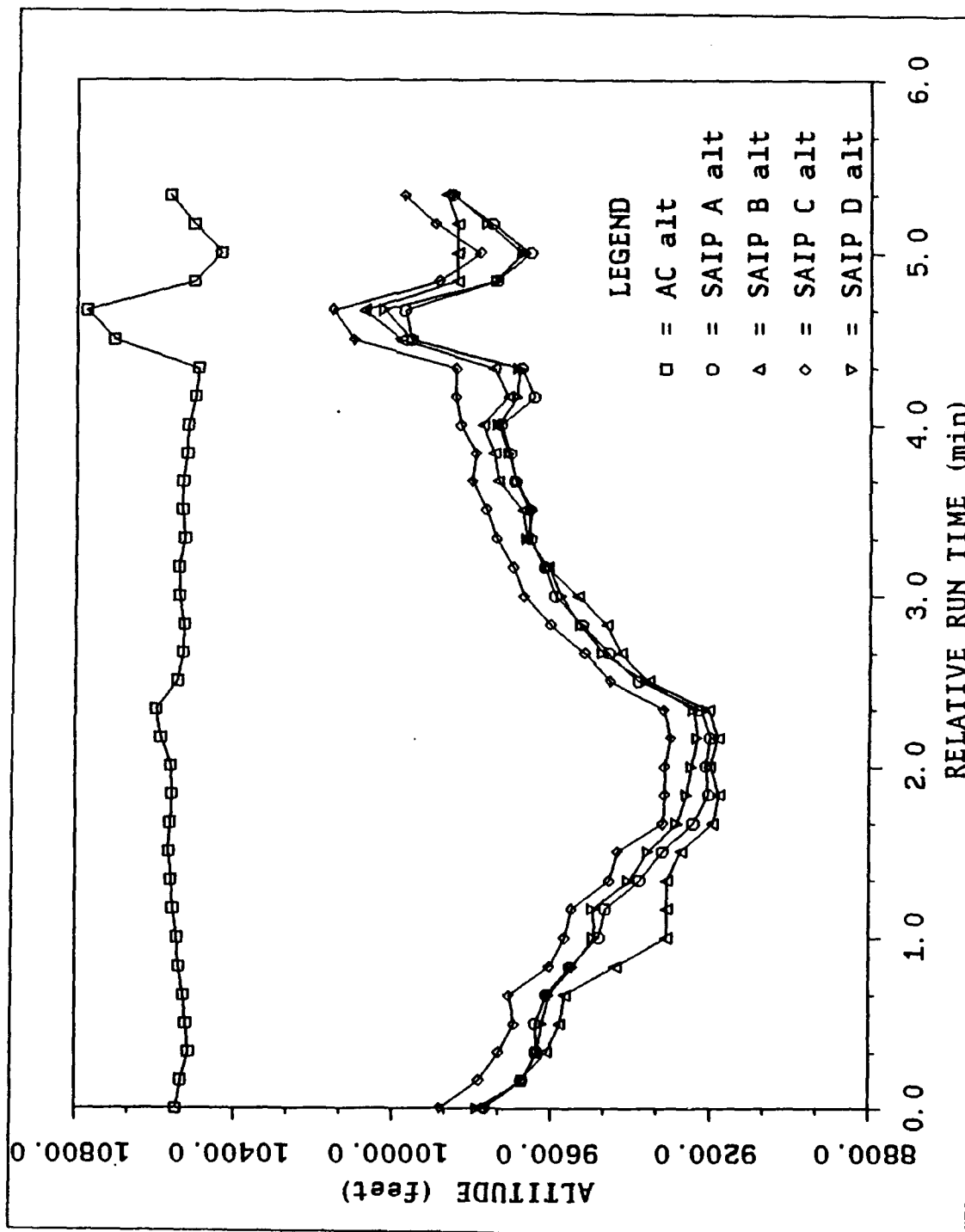
Figure 12. Reported Altitude vs. Run Time (Run #3: 10,000 feet, centerline tank installed)
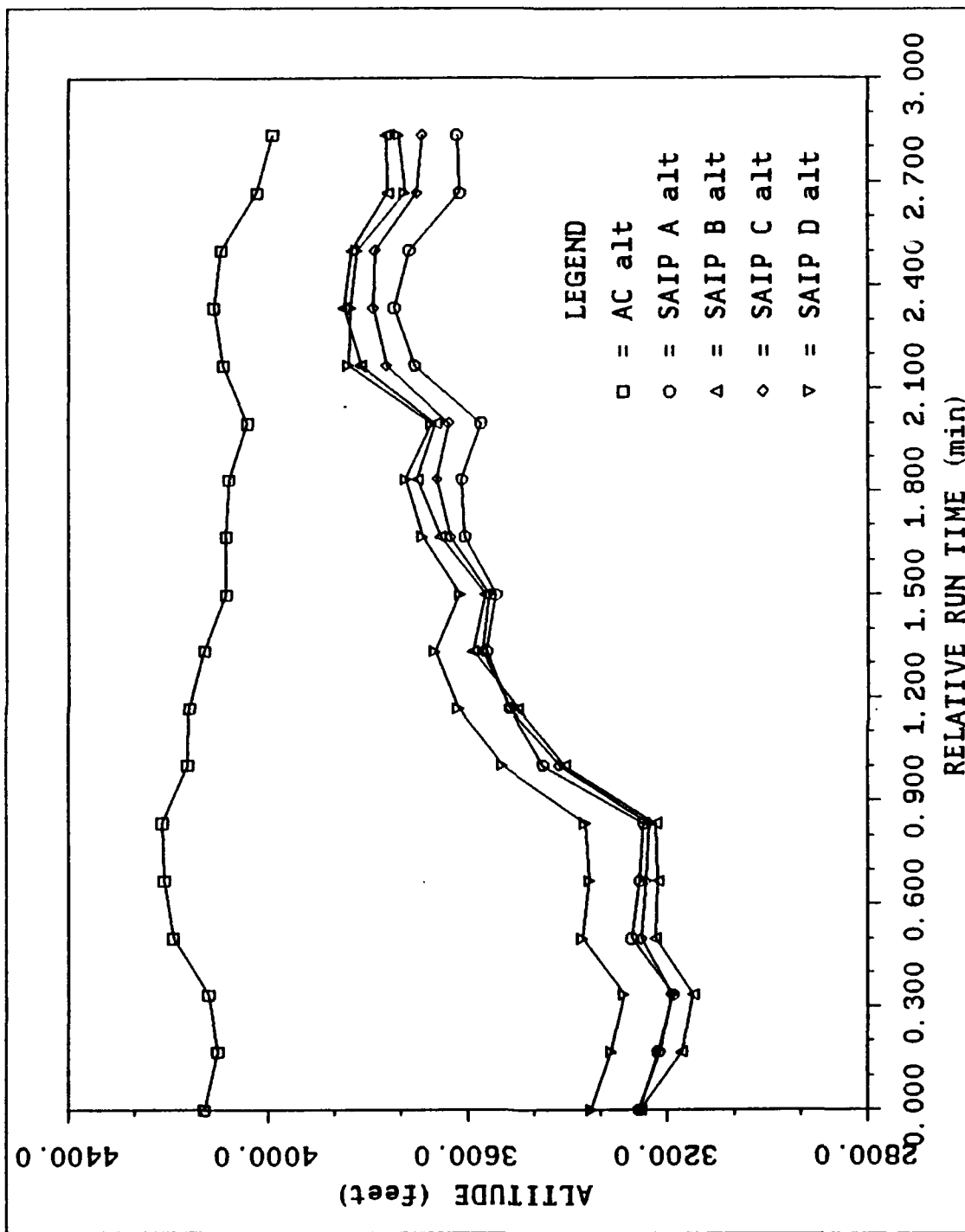
Figure 13. Reported Altitude vs. Run Time (Run #4: 4,000 feet, centerline tank removed)
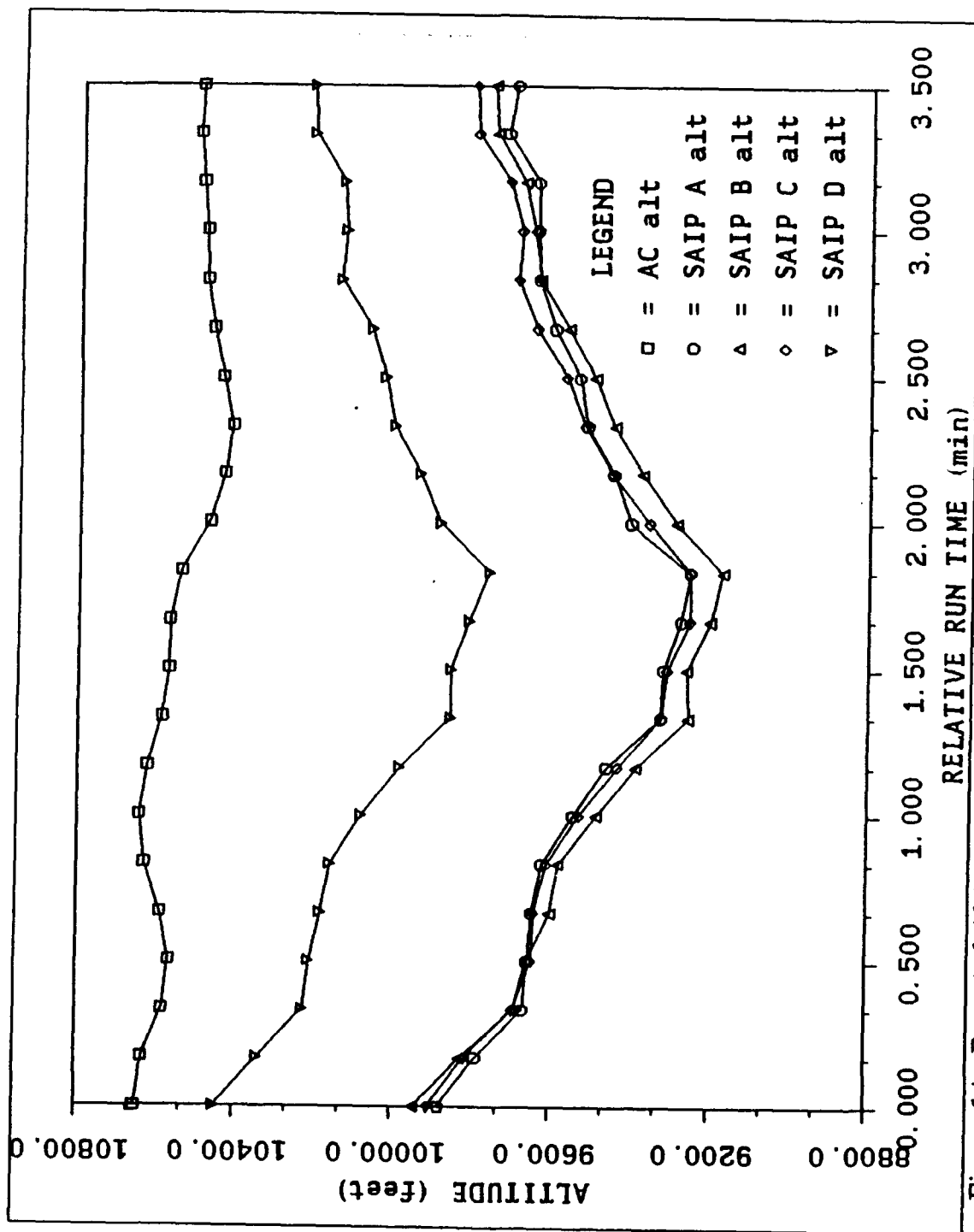
Figure 14. Reported Altitude vs. Run Time (Run #5: 10,000 feet, centerline tank removed)

32
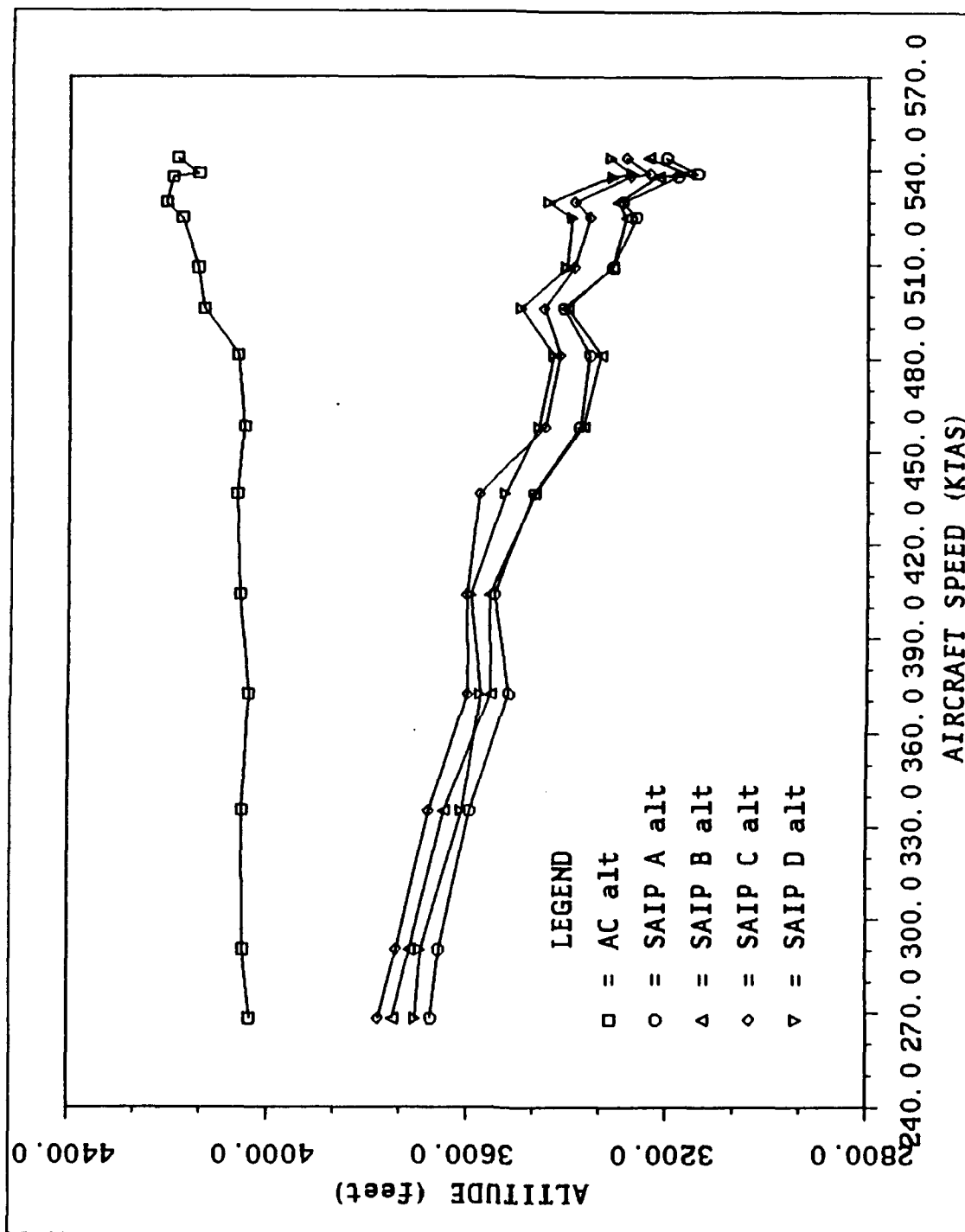
Figure 15. Reported Altitude vs. Aircraft Speed (Run #2: Acceleration)

33
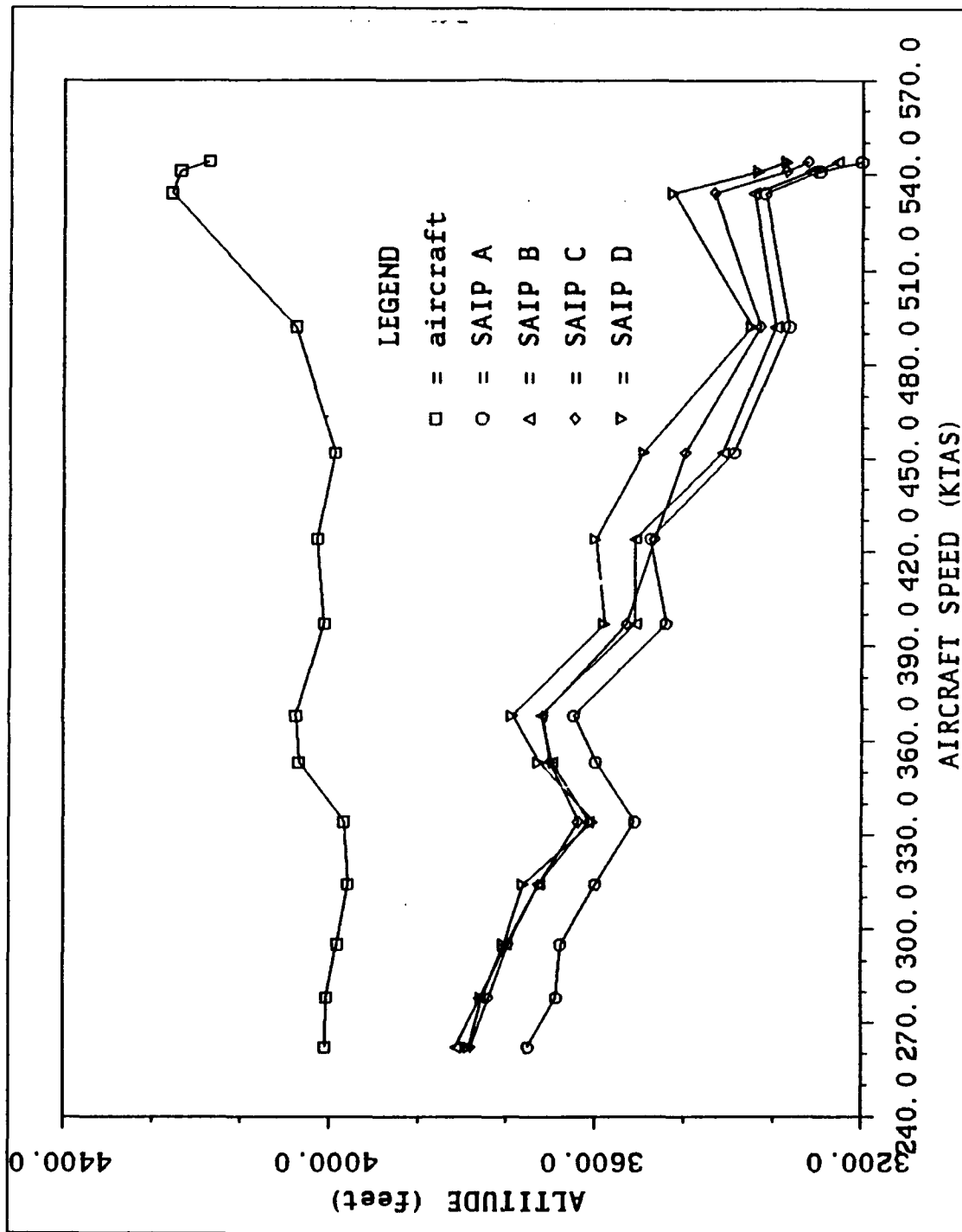
Figure 16. Reported Altitude vs. Aircraft Speed (Run #2: Deceleration)

34
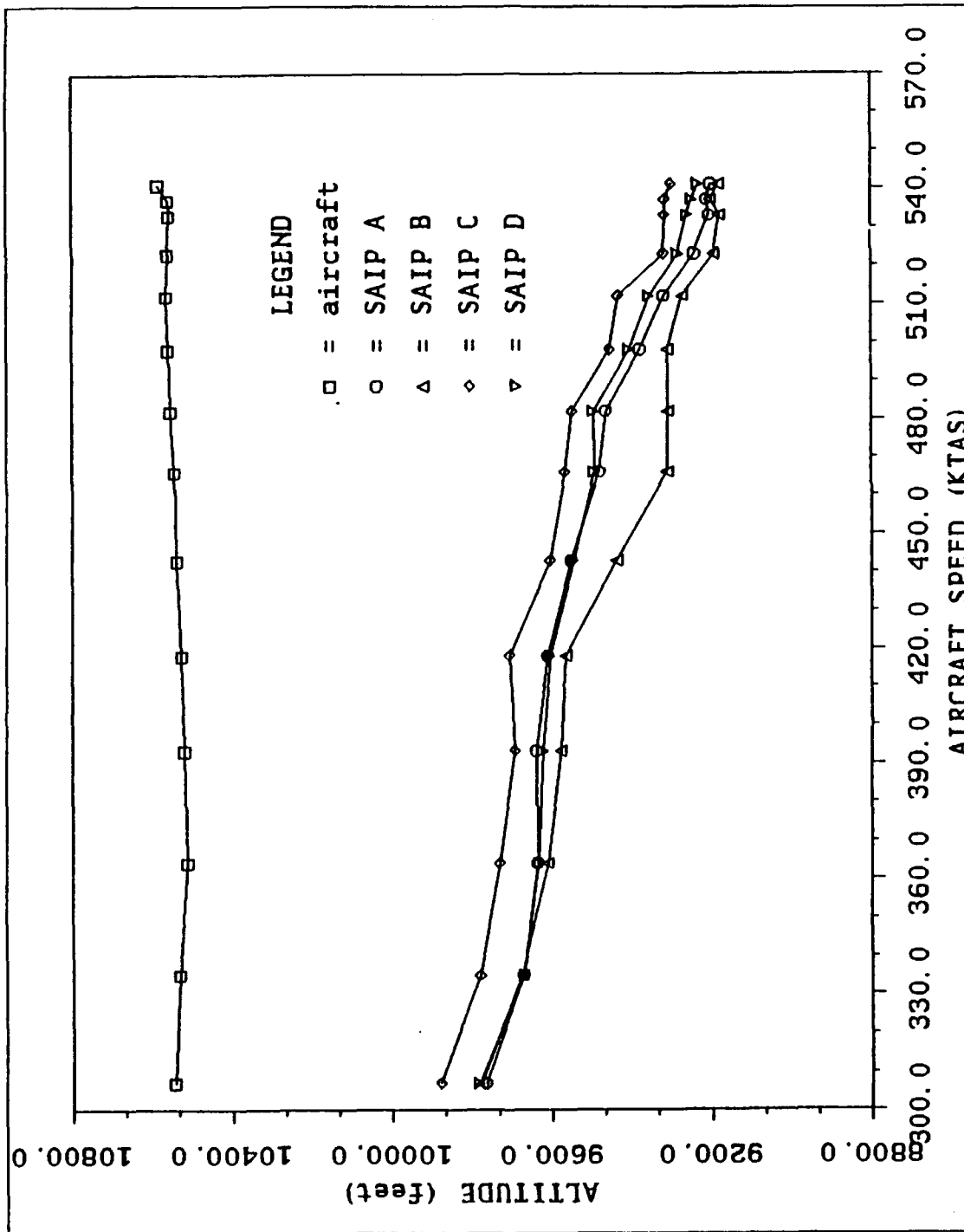
Figure 17. Reported Altitude vs. Aircraft Speed (Run #3: Acceleration)
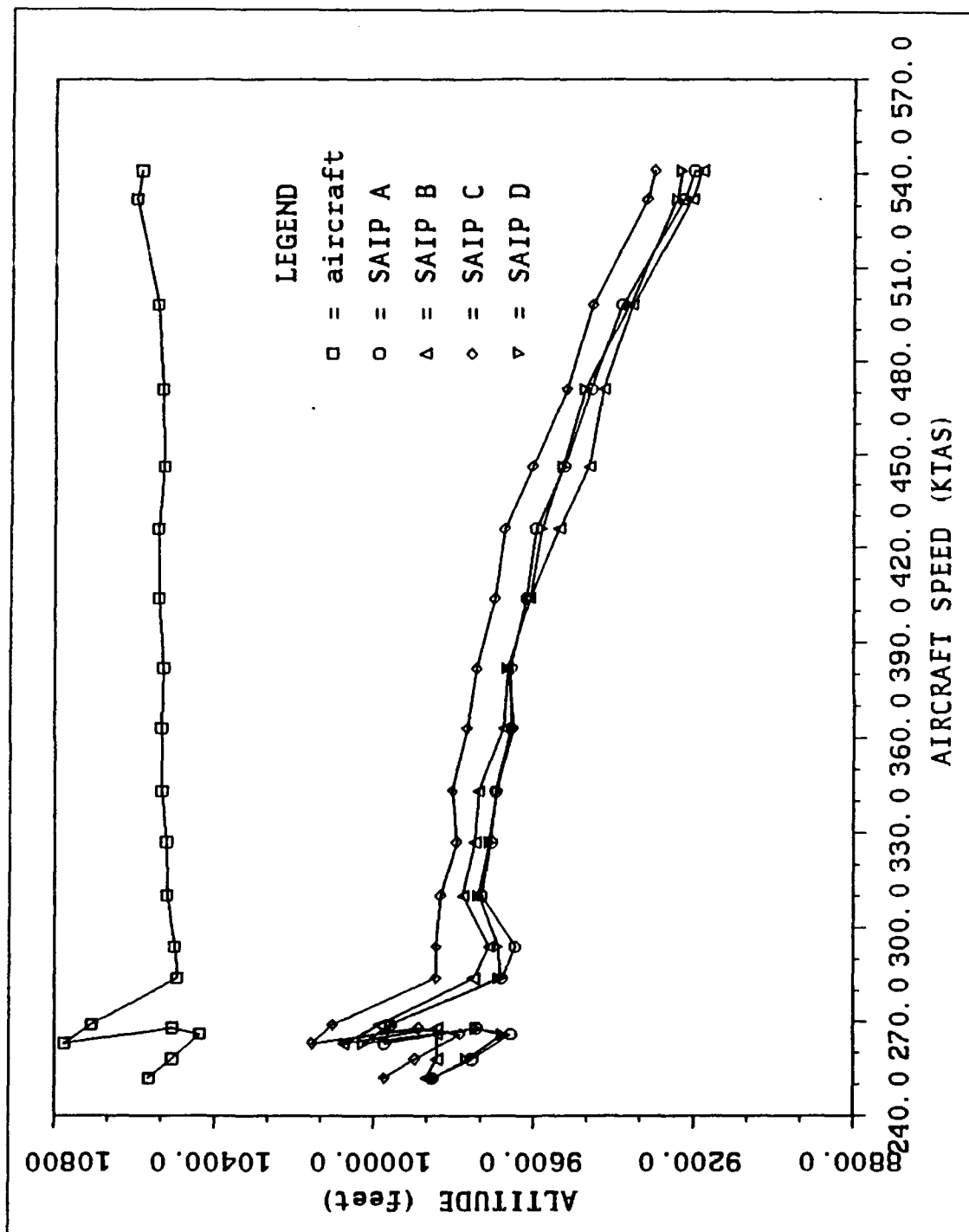
Figure 18. Reported Altitude vs. Aircraft Speed (Run #3: Deceleration)
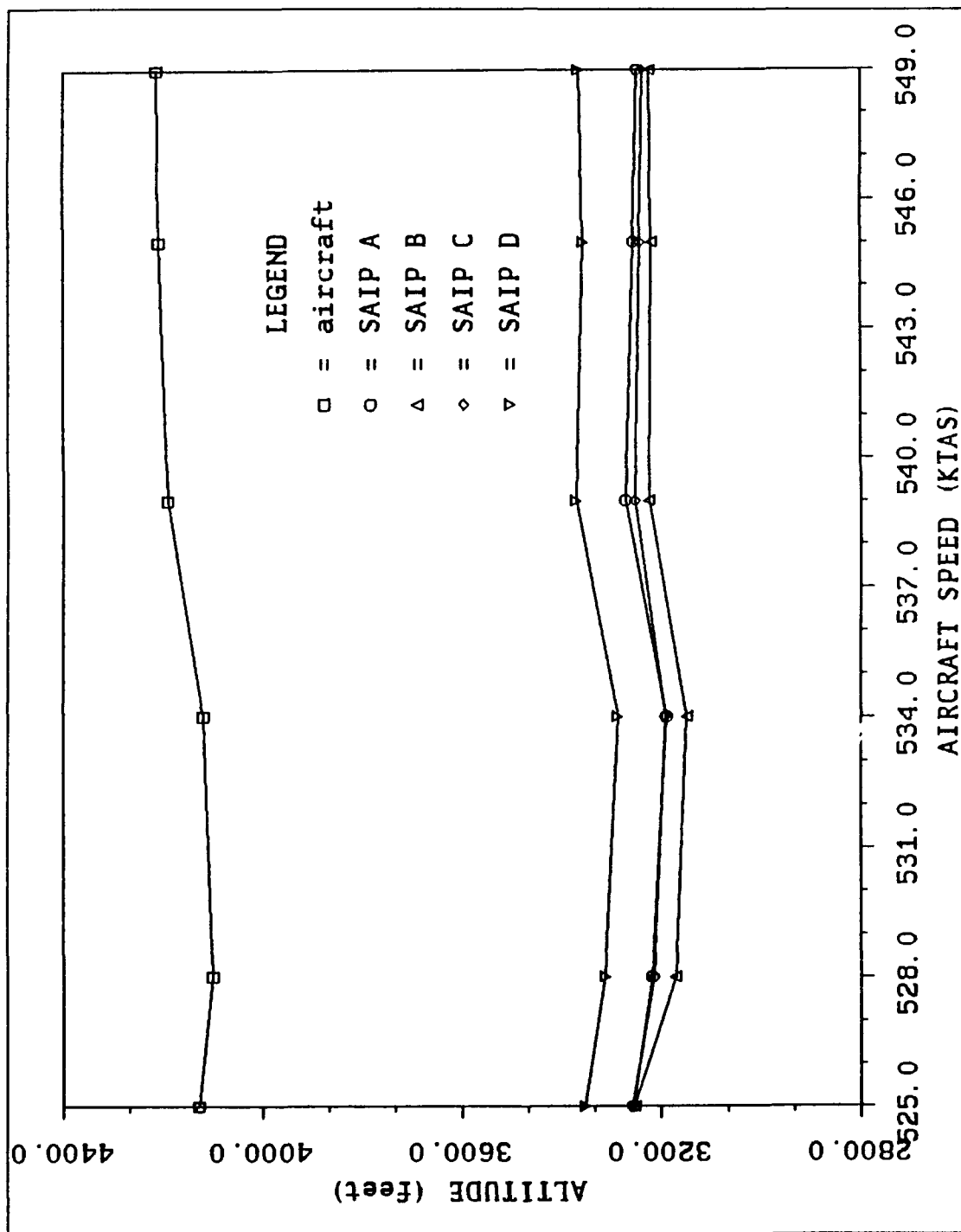
Figure 19. Reported Altitude vs. Aircraft Speed (Run #4: Acceleration)
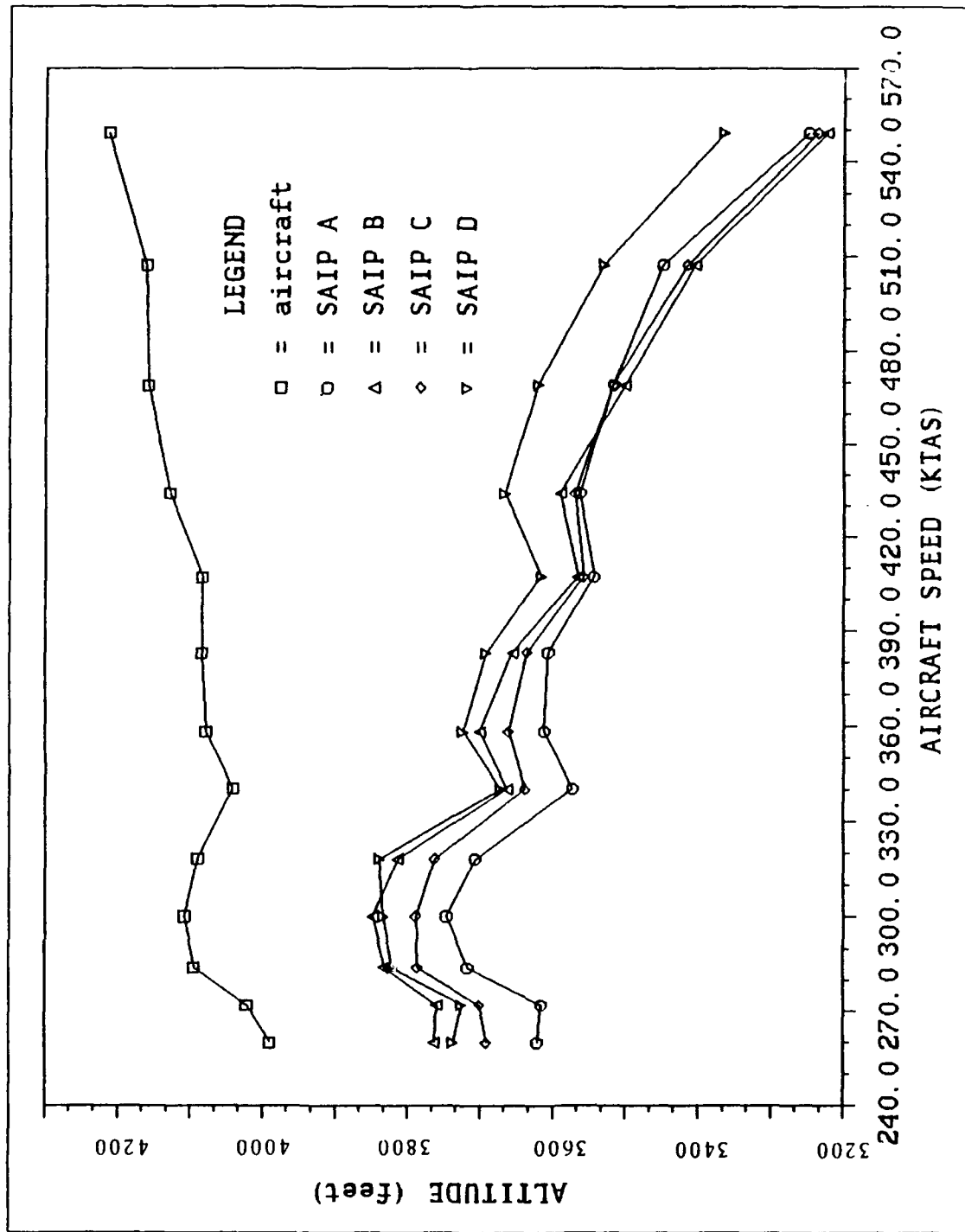
Figure 20. Reported Altitude vs. Aircraft Speed (Run #4: Deceleration)
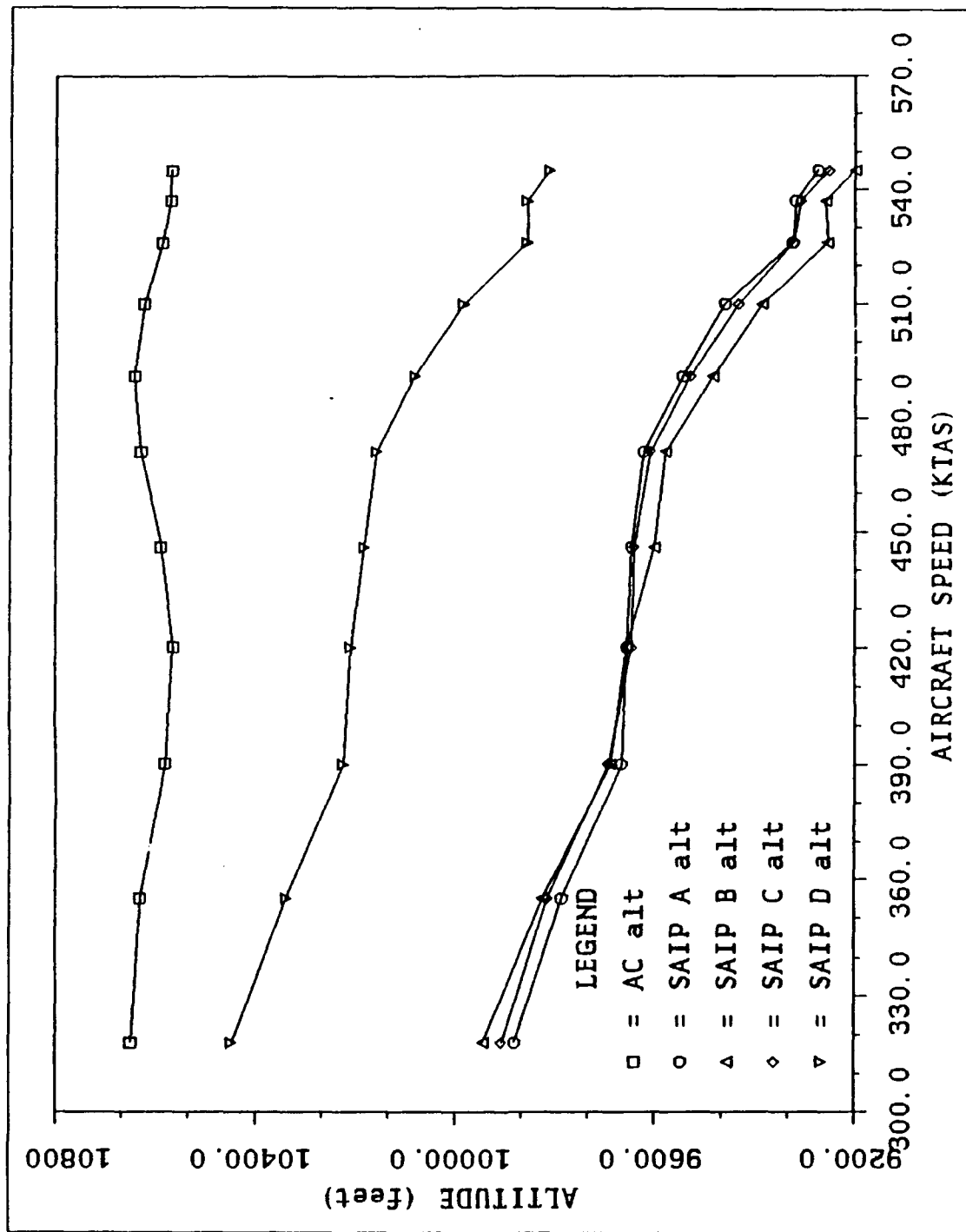
Figure 21. Reported Altitude vs. Aircraft Speed (Run #5: Acceleration)
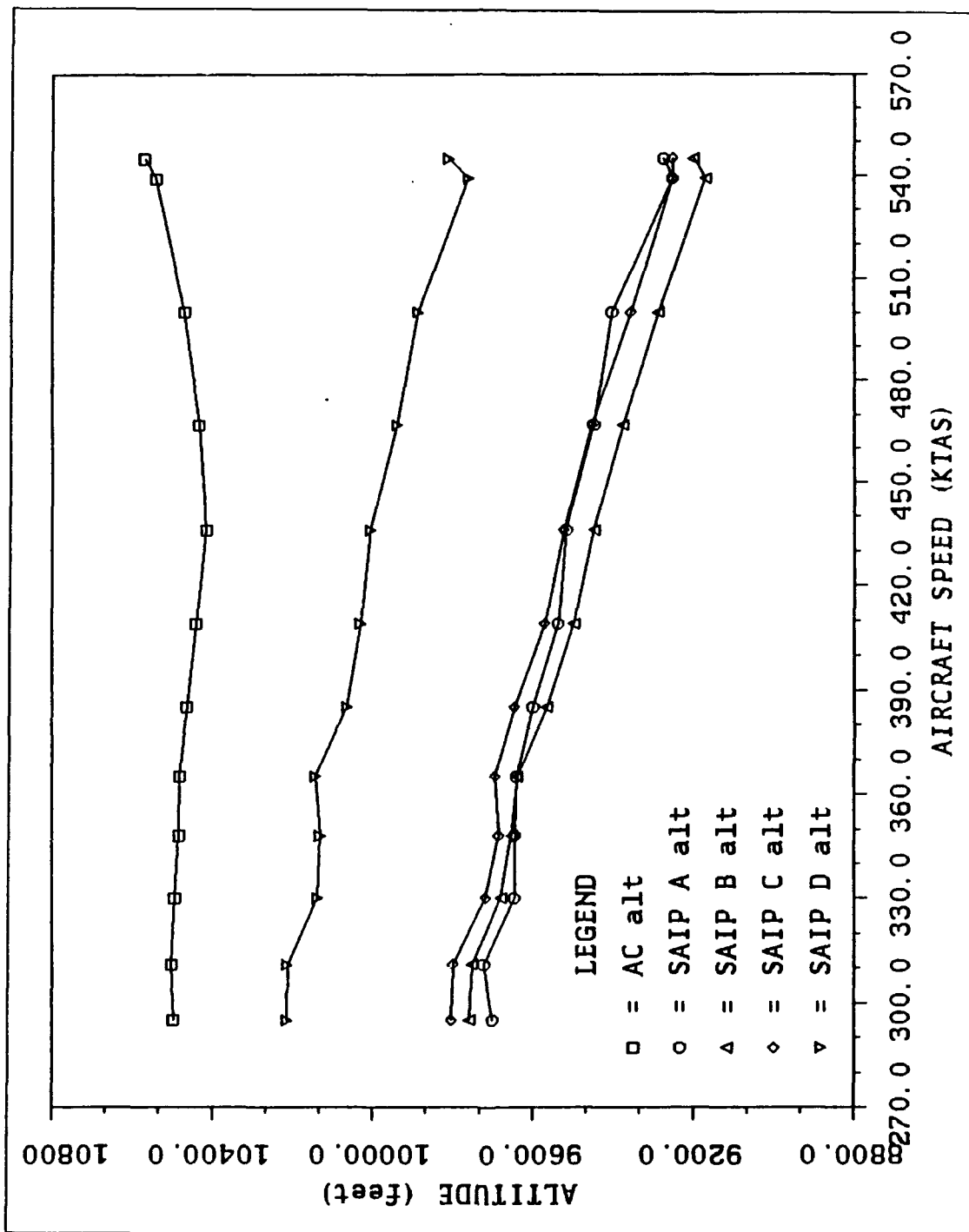
Figure 22. Reported Altitude vs. Aircraft Speed (Run #5: Deceleration)

40
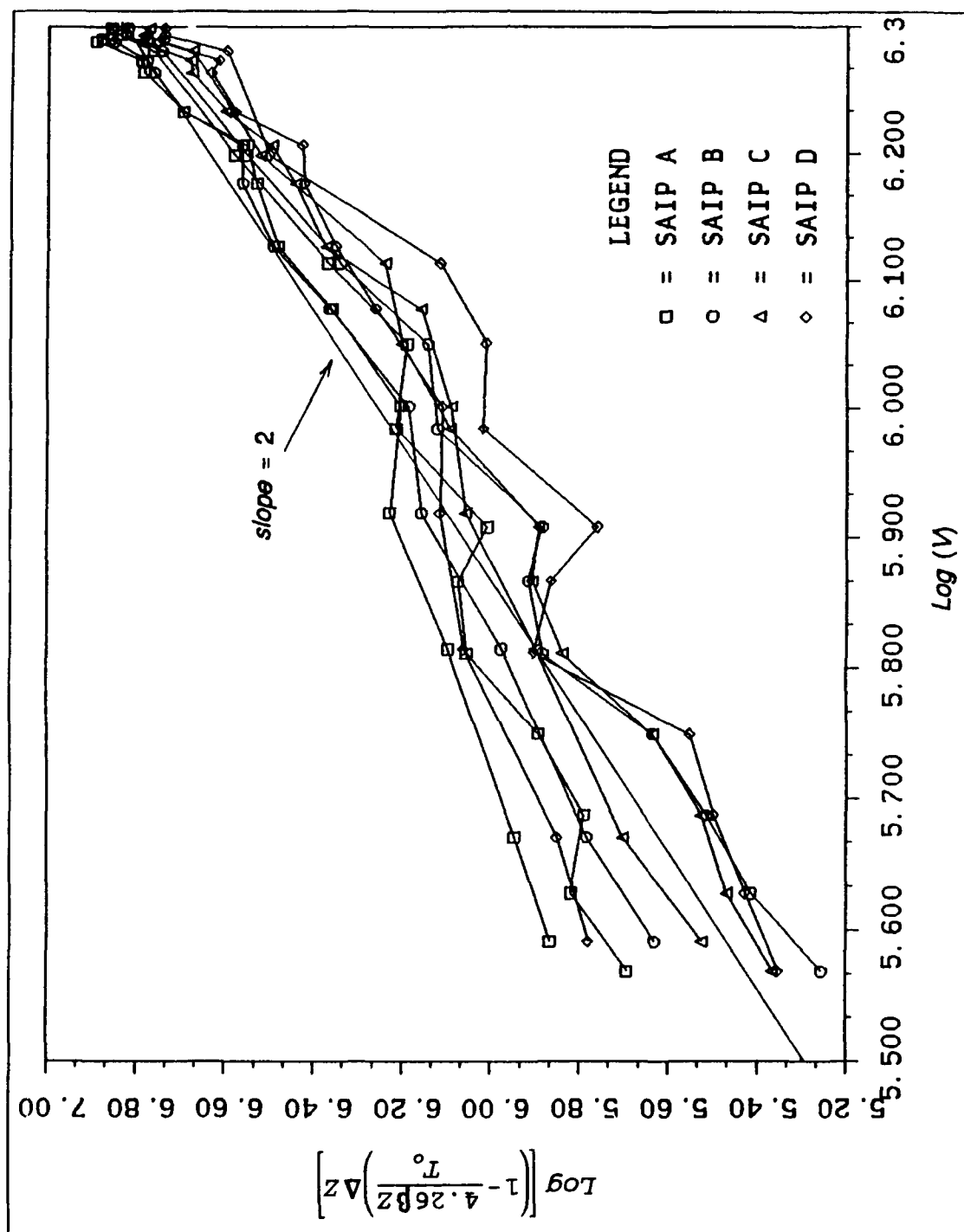
Figure 23. DATAFIT Output Plot (Run #2)

41
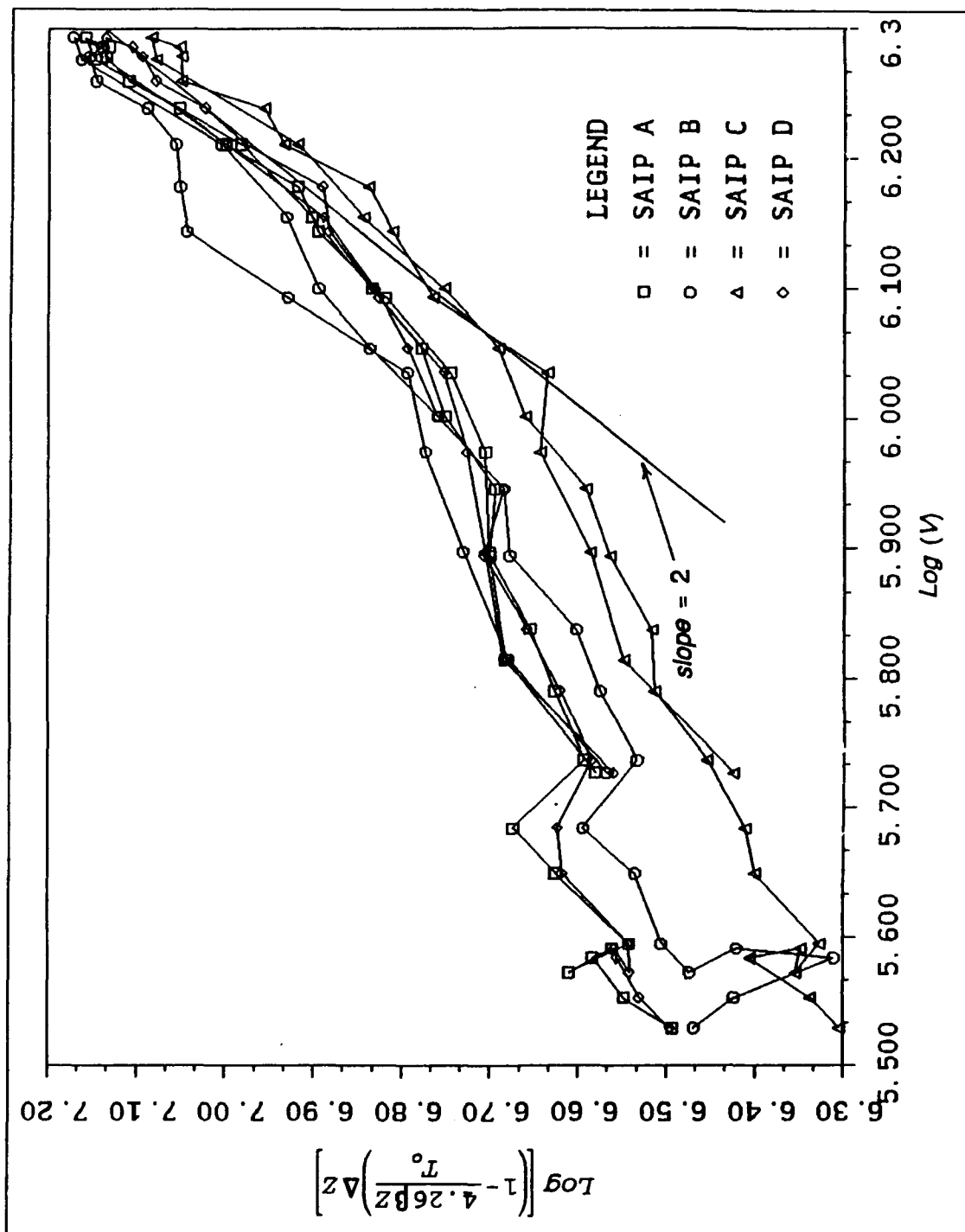
Figure 24. DATAFIT Output Plot (Run #3)

42
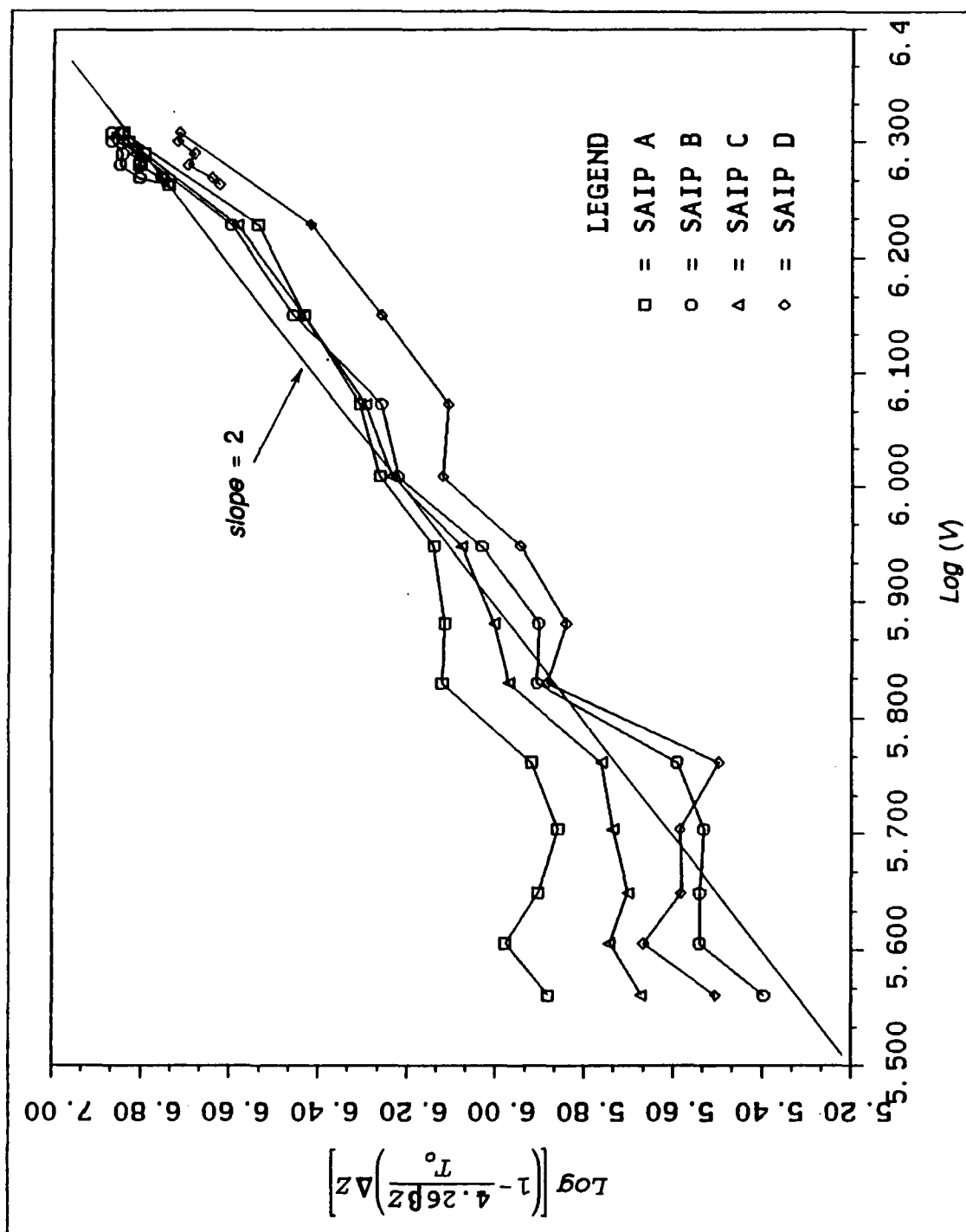
Figure 25. DATAFIT Output Plot (Run #4)

43
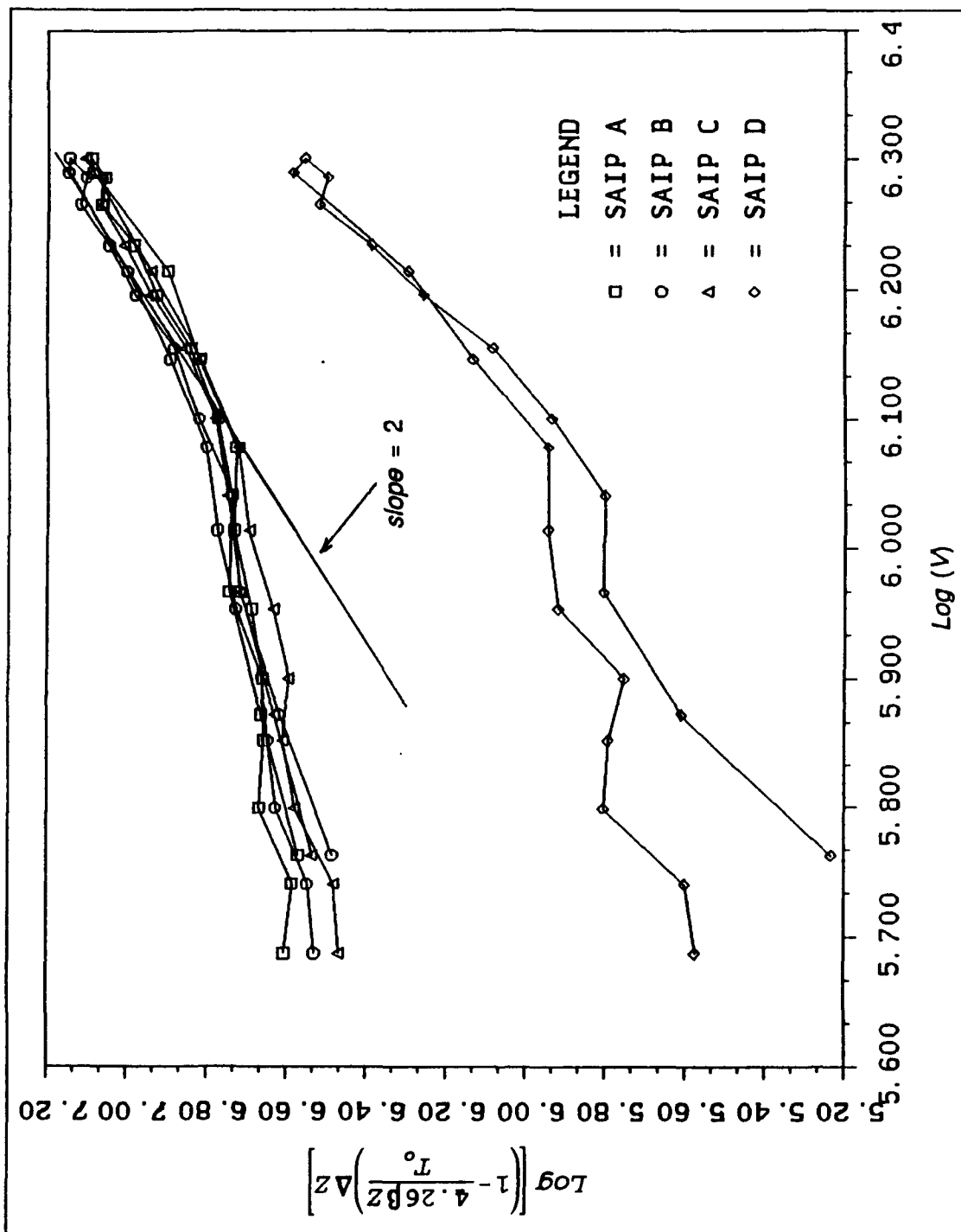
Figure 26. DATAFIT Output Plot (Run #5)

44

4. Altitude Error Density Dependence

By correlating the flight test data in such a way that the aircraft velocity was held constant while the altitude was varied, an analysis could be performed to establish whether a dependence of the SAIP altitude error upon surrounding air density existed. This analysis was conducted by comparing the altitude deficit between the aircraft and each of the individual SAIPs at identical aircraft speeds at both 4,000 and 10,000 feet. Based upon the processed data it was determined that a total of three data points existed where the aircraft speeds were identical at both altitudes and where data was sampled simultaneously. These altitude deficits were then averaged and the ratio between these average values, 0.688, was then calculated.

The investigation of altitude error dependence upon density was performed by recognizing that for any such functional relationship to exist, since the velocities at the two altitudes are equal, the following relation must be satisfied

$$\frac{\rho_{4000}}{\rho_{10000}} = \frac{\left[1 - 4.26 \frac{\beta(4000)}{T_o}\right] \Delta Z_{4000}}{\left[1 - 4.26 \frac{\beta(10000)}{T_o}\right] \Delta Z_{10000}} \tag{17}$$

Thus, the right-hand side ratio, 0.688, was compared with the density ratios for both a cold and hot atmosphere at the corresponding altitudes, 1.329 and

45

1.185, respectively. Since Equation (17) was not satisfied by the empirical data, there is a very low probability that any dependence of SAIP altitude error upon ambient air density existed in the flight tests which were performed.

The fact that the density ratio does not represent the error which was previously shown to depend somewhat on the square of the velocity casts some doubt on the inference that the dynamic pressure of the flow is a fundamental source of the observed SAIP altitude error. The basis of the error is more likely to be found in another parameter which might also manifest a velocity-squared dependence.

IV. WIND TUNNEL APPARATUS AND PROCEDURES

A. WIND TUNNEL APPARATUS

1. Wind Tunnel

The SAIP Nose Cone Assembly (NCA) which was to serve as the test article for the various engineering analyses performed to identify the source of SAIP altitude error was provided by the PMTC Range Development Department (Code 3143). Evaluations of NCA S/N 0040, P/N 2111940-001 were performed in the Naval Postgraduate School low-speed, horizontal-flow, wind tunnel illustrated in Figure 27. This single return tunnel is powered by a 100-horsepower electric motor coupled to a three-blade variable-pitch fan via a four-speed transmission. The tunnel is 64 feet long and ranges from 21.5 to 25.5 feet wide. To straighten the flow through the tunnel, a set of stator blades have been located aft of the fan blades. Additionally, turning vanes have been installed at all four corners of the tunnel, and two fine wire mesh screens have been positioned upstream of the settling chamber to reduce turbulence.[Ref. 10]

The dimensions of the wind tunnel's test section are 45 inches by 32 inches. A reflection plane installed above the base of the test section reduces the available height in this section to 28 inches. The tunnel contraction ratio, as measured by the area of the settling chamber area divided by the test

47
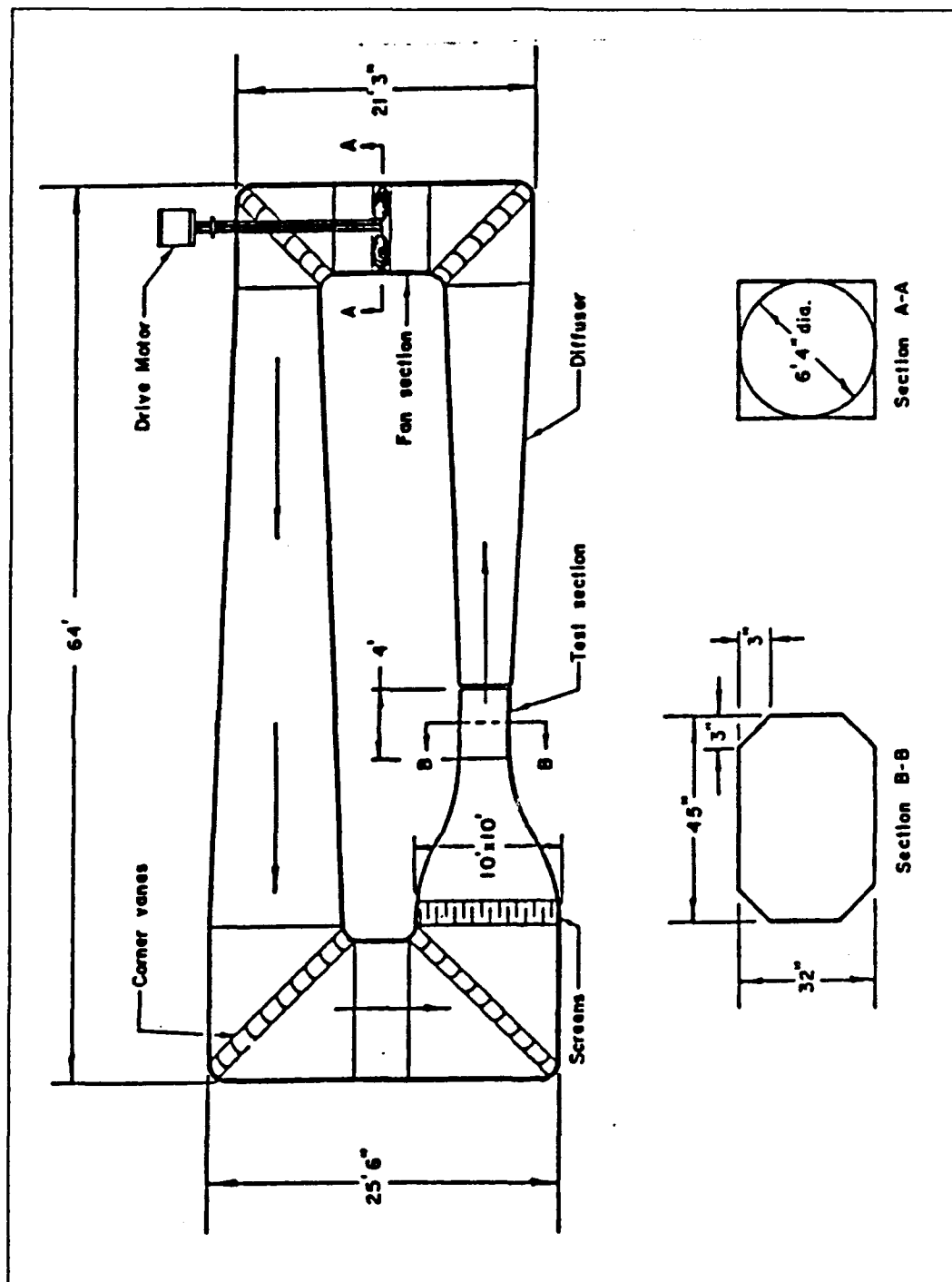
Figure 27. Naval Postgraduate School Wind Tunnel [Ref. 10]

48

section area, is approximately 10:1. Corner fillets which are located within the test section to provide covers over four florescent lights reduce the actual section cross-sectional area from 10 ft^2 to 8.75 ft^2. Similar fillets are installed at wall intersections throughout the tunnel to assist in the reduction of boundary layer effects. Prevention of reduction in freestream pressure due to boundary layer growth within the test section is facilitated by a slight divergence of the walls in this area of the tunnel.[Ref. 10]

A turntable mounted flush with the reflection plane permits operator-controlled changes in the test article pitch angle or angle of attack via a remotely controlled electric motor installed beneath the tunnel. The test section has been designed to operate at atmospheric pressure, and to sustain this constant pressure, breather slots are installed around the circumference of the tunnel to replenish air lost through leakage. The tunnel was designed to generate and maintain flow velocities of up to 290 ft/sec.[Ref. 11]

A dial thermometer extending into the settling chamber of the tunnel is used to measure internal tunnel temperature. Four pressure taps located upstream of the test section in the four adjoining walls are used to measure tunnel static pressure. Additional pressure taps are located in the settling chamber section. The difference between the test section and the settling chamber static pressures is used to measure dynamic pressure. This is accomplished by manifolding the separate tap pressures at the two tunnel locations into two separate lines and then connecting these outputs to a water

49

filled manometer. The tunnel dynamic pressure measured by this manometer is displayed in centimeters of water. Equation (18) is used to calculate the actual wind tunnel velocity, also known as the tunnel Q.[Ref. 10]

$$U_m = \left[\frac{(2)\ (2.0475)\ (P)}{(.93)\ (\rho)} \right]^{\frac{1}{2}} \tag{18}$$

where:

U_m = measured velocity (ft/sec)

2.0475 = conversion factor from cm H_2O to lb/ft^2

P = manometer reading (cm H_2O)

.93 = Empirical Discharge Coefficient (correction for viscosity)

ρ = air density (slugs/ft^3)

2. Service Aircraft Instrumentation Package (SAIP)

a. General

The SAIP pod used in the wind tunnel tests was a second-generation unit which incorporates hardware improvements designed to alleviate the altitude measurement inaccuracies resulting from the first-generation pods' erroneous pressure measurements, as discussed in Section

50

I.A.2. Specifically, the second-generation unit tested was equipped with 12 static ports, each displaced by 30°, oriented circumferentially about the pod's Airflow Sensor Assembly (ASA), as opposed to the single port which existed in the first-generation unit.

b. Nose Cone Assembly

The component of the SAIP pod used in the tests, the Nose Cone Assembly (NCA) depicted in Figure 28, performs two functions required by the SAIP. The first purpose it serves is to support the antenna subsystem which includes the matching and hybrid boards and the antenna elements. The second function of the NCA, and the one of principal concern in this study, is to support the ASA. In the particular configuration which was tested, SAIP Configuration 003, the NCA houses, in addition to the antenna subsystem and ASA, the Air-Data Unit (ADU), the radar altimeter ballast and the antenna filter [Ref. 1]. For the purposes of the NPS wind tunnel tests, the antenna subsystem was not installed.

c. Airflow Sensor Assembly

The ASA consists of an airflow sensor, air lines and connectors, as illustrated in Figure 29. The function of the assembly is to provide to the ADU through six pressure lines the static pressure (one line), dynamic pressure (one line), differential angle-of-attack pressure (two lines), and differential angle-of-sideslip pressure (two lines). The airflow sensor, which
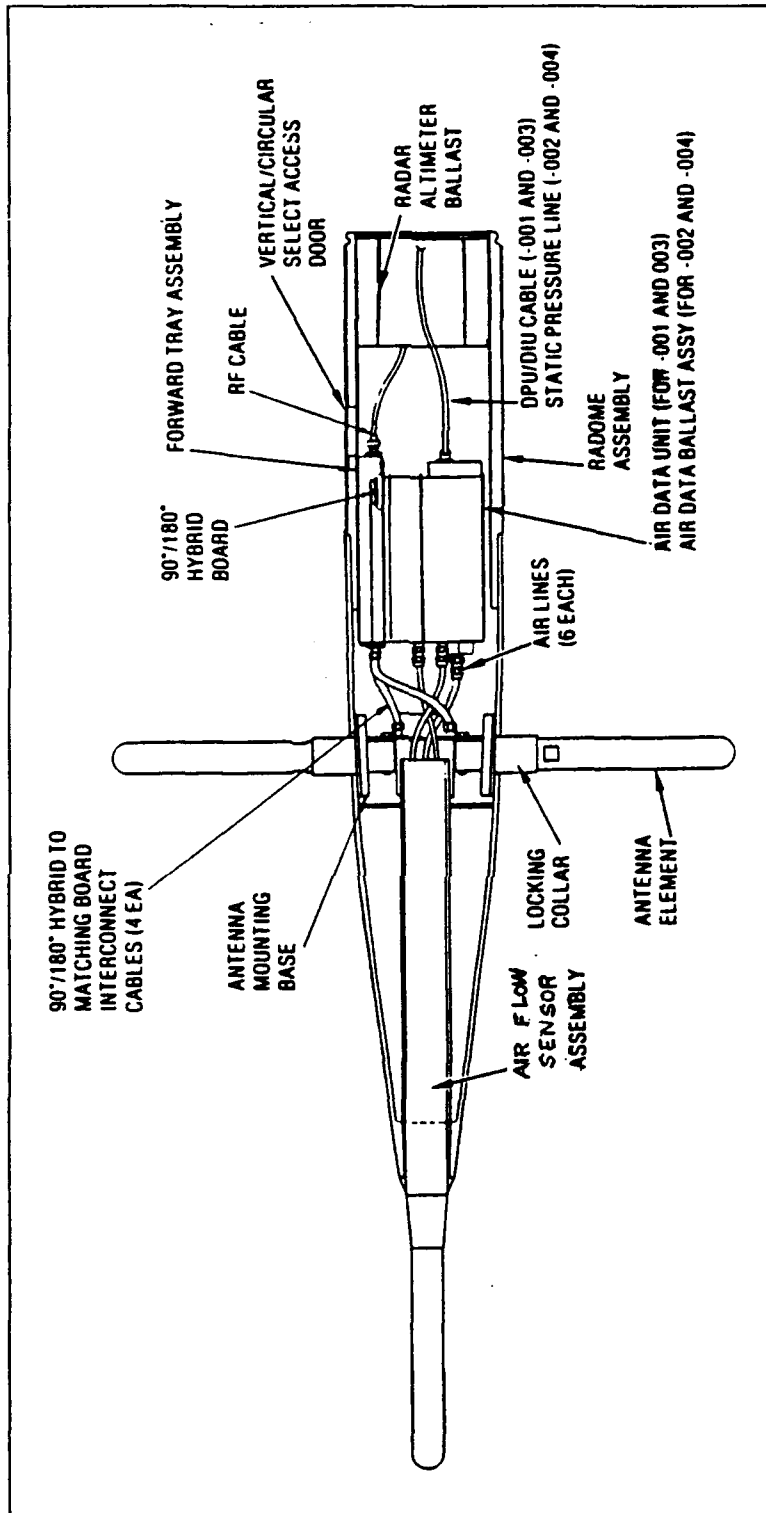
Figure 28. Nose Cone Assembly (NCA) [Ref. 1]

90°/180° HYBRID TO MATCHING BOARD INTERCONNECT CABLES (4 EA)

ANTENNA MOUNTING BASE

AIR FLOW SENSOR ASSEMBLY

LOCKING COLLAR

ANTENNA ELEMENT

AIR LINES (6 EACH)

90°/180° HYBRID BOARD

FORWARD TRAY ASSEMBLY

RF CABLE

VERTICAL/CIRCULAR SELECT ACCESS DOOR

RADAR ALTIMETER BALLAST

DPU/DIU CABLE (-001 AND -003)
STATIC PRESSURE LINE (-002 AND -004)

RADOME ASSEMBLY

AIR DATA UNIT (FOR -001 AND 003)
AIR DATA BALLAST ASSY (FOR -002 AND -004)

52

Figure 29. Airflow Sensor Assembly (ASA) [Ref. 1]

is depicted in Figure 30, incorporates in a hemispherical arrangement a stagnation pressure port at its forward tip and four ports to measure differential angle-of-attack and differential angle-of-sideslip pressures, each located at 90°-offset angles (view C-C). Additionally, 12 static ports which are used in the measurement of barometric altitude are situated around the pod's circumference 3.5 inches aft of the forward tip.

d. Air-Data Unit (ADU)

The function of the ADU is to assimilate the six pressure parameters output from the ASA and provide the analog outputs required to compute altitude, indicated airspeed, true speed, Mach number, angle-of-attack and angle-of-sideslip. On fully operational SAIPs, these analog outputs are subsequently supplied to the Data Processing Unit/Data Interface Unit (DPU/DIU) for digitizing and formatting for downlink communications [Ref. 1]. For the purposes of this study, the ADU was not integrated with the DPU/DIU; instead, the outputs of the ADU were coupled directly to instrumentation designed to record the various output voltages from the unit, as described in Section IV.A.4 below.

The ADU consists of four capacitive pressure transducers which are housed in a single assembly, as well as the associated electronic circuitry used for conditioning of the output signals from the transducers prior to their digitizing and formatting by the DPU/DIU [Ref. 1]. Static pressure is measured by an absolute-type transducer which measures this pressure relative to a
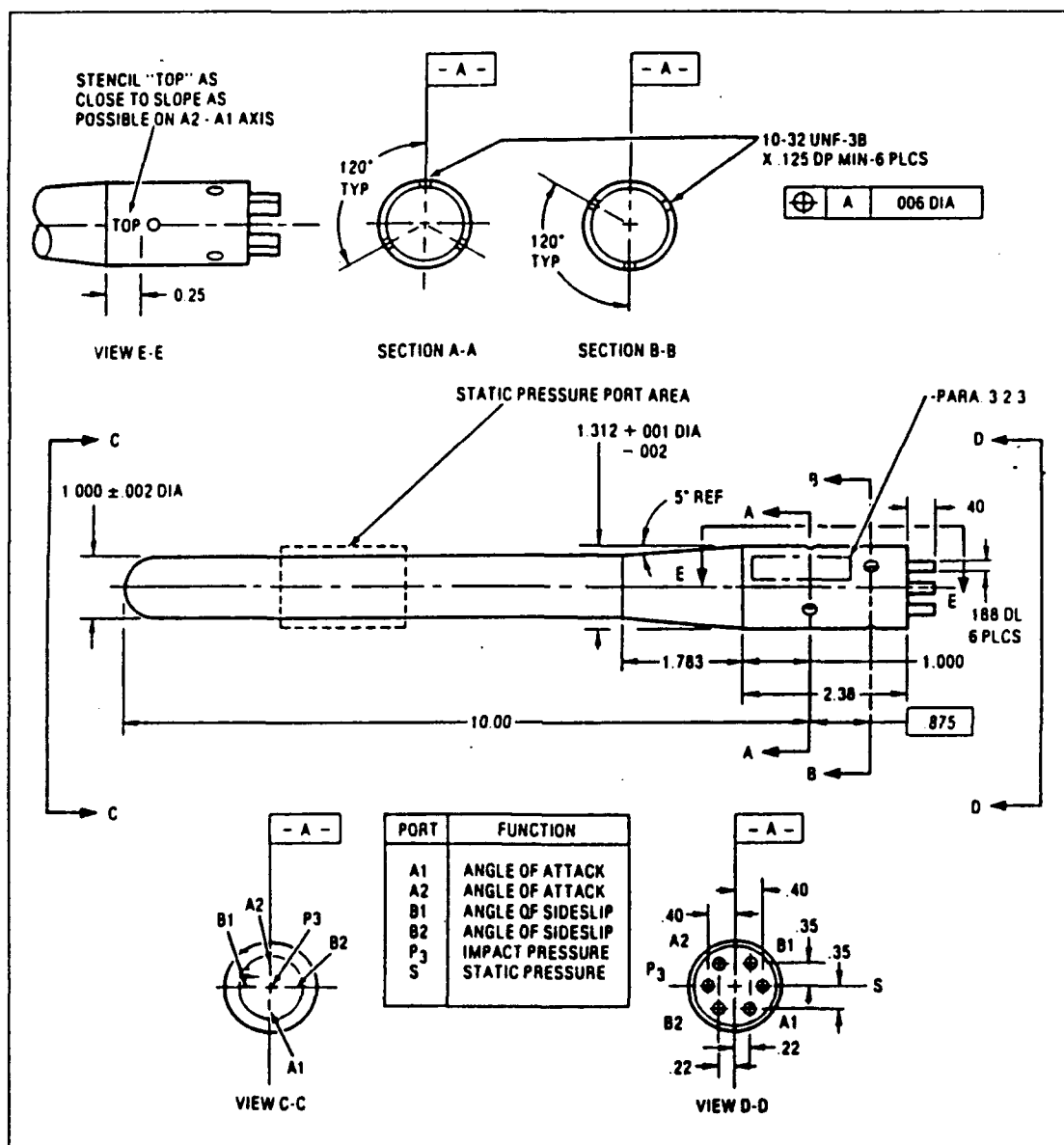
Figure 30. Airflow Sensor [Ref. 1]

vacuum. A single static pressure line extends from the ASA into the static pressure coupler on the input side of the ADU. The remaining three transducers residing in the ADU, used to determine total, angle-of-attack and angle-of-sideslip pressures, are differential capacitive transducers. Pressure lines extend from each of the P3 (total pressure), A1, A2, B1 and B2 pressure ports on the nose of the airflow sensor and are coupled directly into the ADU in a manner similar to the static pressure line.

Once inside the ADU, the sets of angle-of-attack and angle-of-sideslip pressure lines proceed into ports situated on opposite sides of their respective differential pressure transducers. The single P3 line is directed into one side of the total pressure transducer and the other end of this transducer is coupled to the input side of the static pressure transducer (together with the static pressure input) via a one-inch long section of plastic tubing. The outputs of the four transducers are integrated with various electronic circuitry which is housed in the aft end of the ADU and which serves to condition the signals prior to digitizing and formatting for subsequent downlinking by the DPU/DIU.

e. SAIP Calibration

It was determined from preliminary testing that the SAIP NCA which was delivered to NPS for wind tunnel testing was not calibrated in accordance with the SAIP functional specification provided with the test article [Ref. 1]. It was thus deemed necessary to calibrate the unit by applying known positive and negative pressures and subsequently measuring on a digital

voltmeter (DVM) the resultant voltage output from the ADU. A U-tube calibration manometer (Figure 31) with an attached adjustable diaphragm unit which enables the application of a variety of pressures was utilized for this purpose.
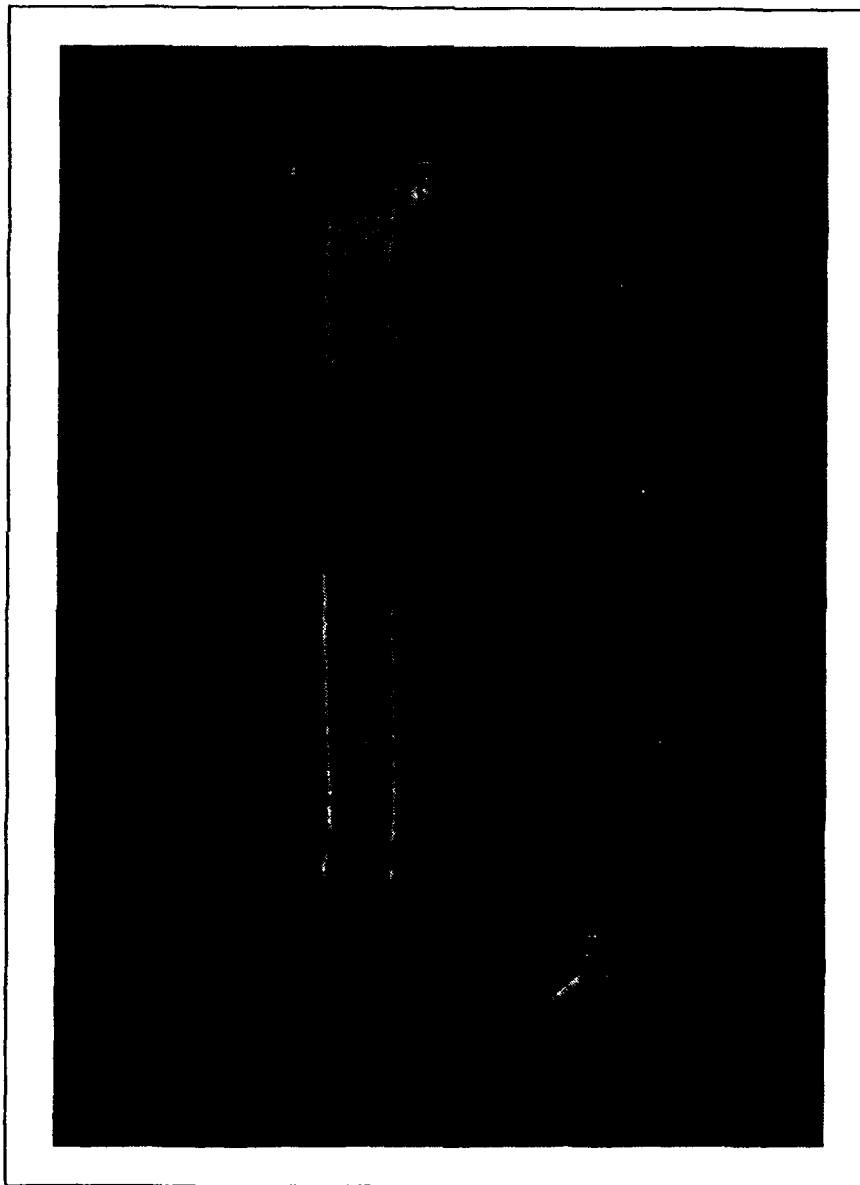
Figure 31. U-Tube Calibration Manometer

The results of this calibration indicate that the incident pressure and resultant voltages vary in a highly linear manner. Consequently, it was a straightforward task to establish calibration curves for the test article (Figure 32).

3. Nose Cone Assembly (NCA) Mounting Assembly

To facilitate secure mounting of the NCA in the wind tunnel's test section and to permit orientation of the probe in a variety of flow directions, the rigid mounting assembly illustrated in Figures 33 and 34 was designed and fabricated. The mechanism was secured to the rotatable disk situated at the base of the tunnel's test section, and was extended vertically into the flow field such that the probe was held in position in the center of the flow. Rotation of the NCA about the vertical axis, representing a variation in the angle ϕ, was controlled by an electric motor which permitted operator-controlled positioning of the angle-of-attack. Constraints imposed by the width of the wind tunnel test section restricted the rotation of the NCA about the vertical axis to $\pm 37.5°$. Additionally, the two clamps built into the top of the V-shaped mounting saddle held the NCA securely at the top of the vertical aluminum strut and permitted the unit to be rotated $\pm 180°$ about its longitudinal axis to simulate variation in the flow angle θ. The capability to both vertically and longitudinally rotate the NCA facilitated the simulation of an adequate range of possible flow impingement directions on an aircraft-mounted SAIP.
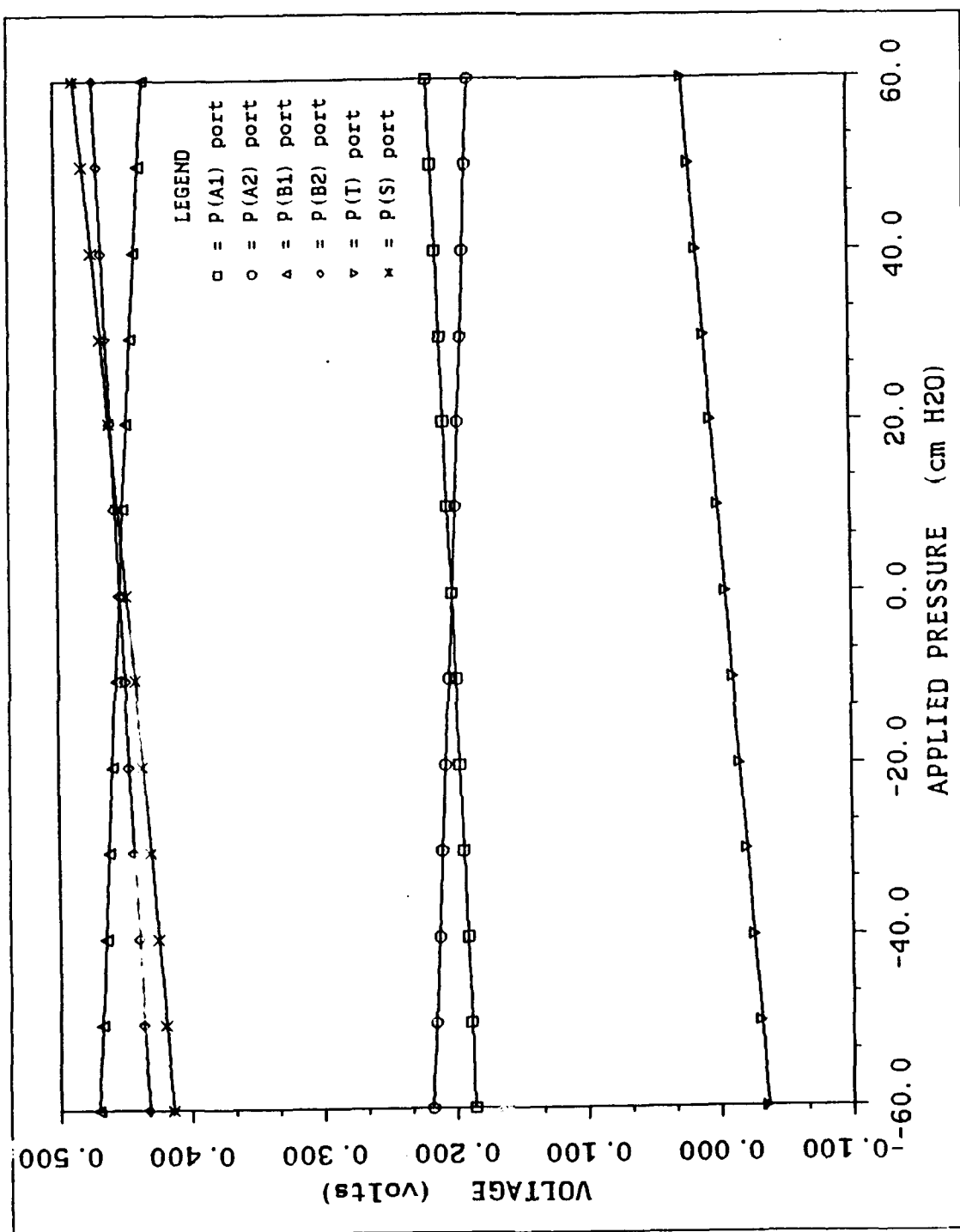
Figure 32. SAIP Calibration Curves

59
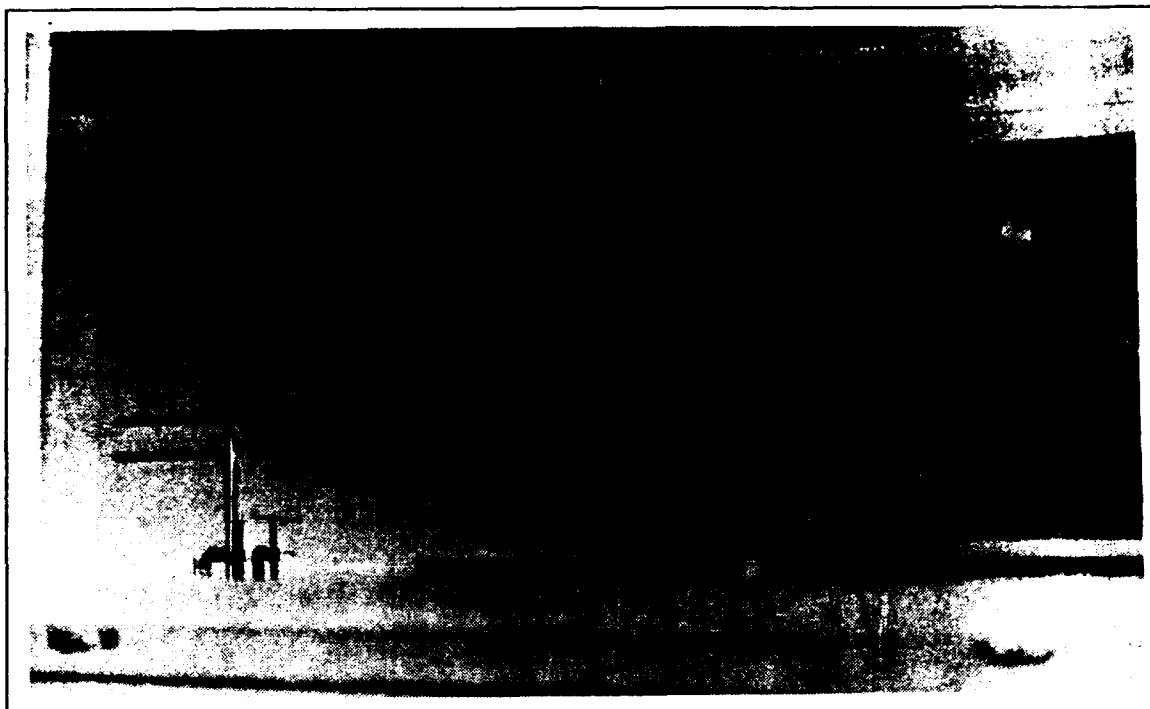
Figure 33. NCA Mounting Assembly (side view)
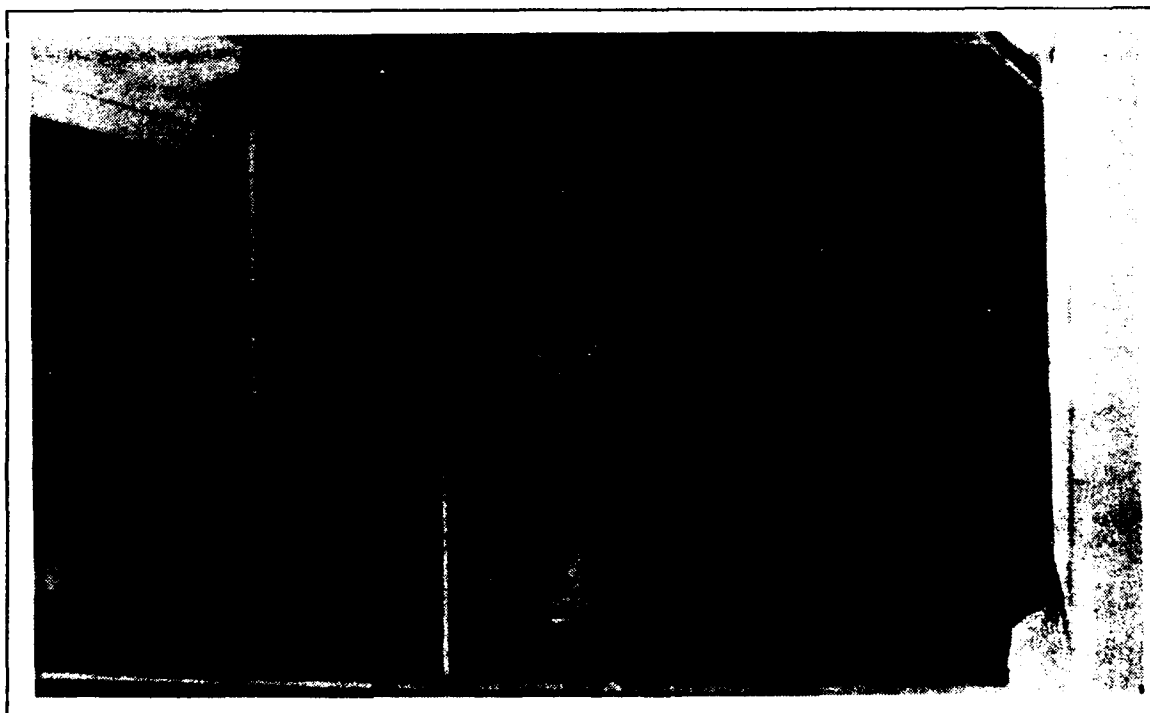
Figure 34. NCA Mounting Assembly (front quarter view)

4. Instrumentation

The NCA was integrated with its instrumentation equipment by coupling the connector plug extending from the output side of the ADU on the test article with an external Fluke Model 8810A Digital Voltmeter (DVM) (Figure 35) via a ±15 volt power supply. The module containing the power
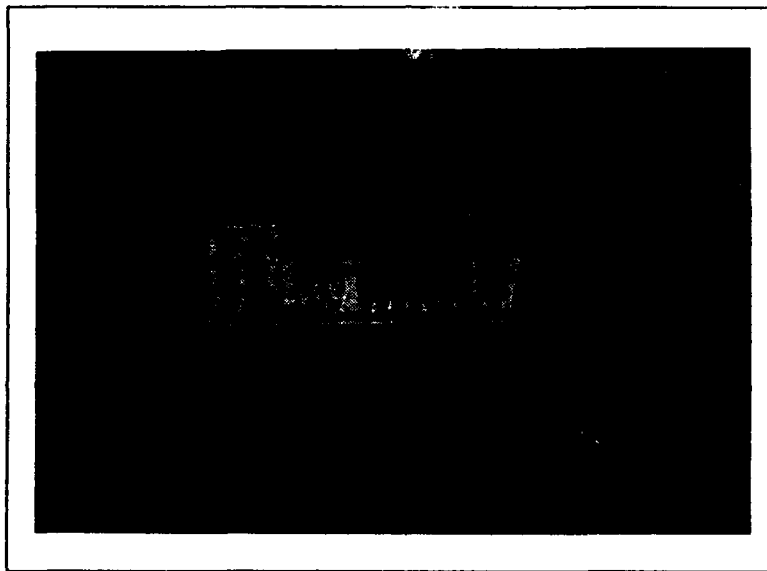
Figure 35. Fluke Model 8810A Digital Voltmeter

supply (Figure 36) was designed to permit manual scanning of the four voltages output from the ADU corresponding to either static pressure, total pressure, angle-of-attack pressure or angle-of-sideslip pressure. The power supply housing also accommodated sampling of the voltage corresponding to

61

the differential pressure existing between the tunnel test section and ambient air outside of the tunnel.
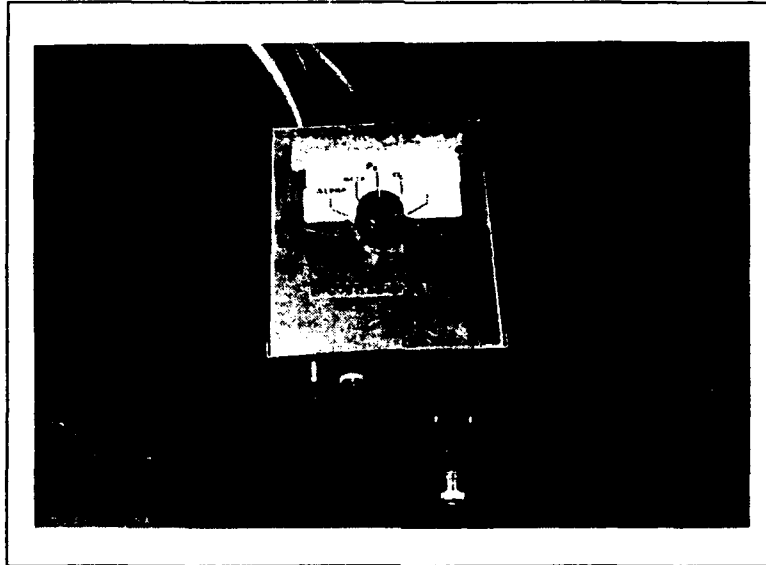
Figure 36. Power Supply Module

While the design of the tunnel is such that the test section is maintained at a nominal pressure of one atmosphere, this pressure actually varied slightly over the duration of the individual tests. To obtain an exact reading of the test section static pressure, a static probe was fabricated and installed in the tunnel directly below the ASA, such that both of the probes' static ports were directly in line with one another (Figures 33 and 34). This stationary static probe facilitated recording of the differential static pressure existing between the tunnel and surrounding ambient conditions, and provided a standard against which the static pressure reported by the SAIP could be

compared. The tunnel static pressure sampled by the stationary static probe was fed into a MKS Baratron Type 223B differential pressure transducer (Figure 37). The output end of the transducer was ported to the atmosphere.
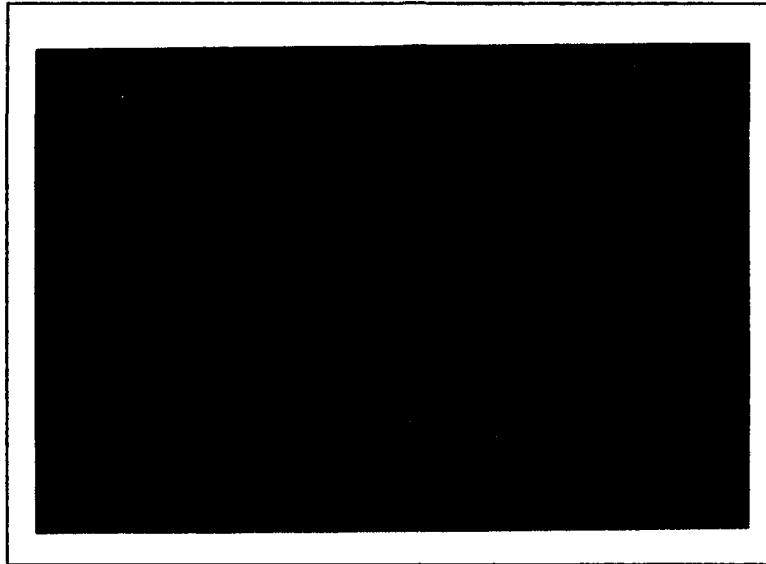
Figure 37. MKS Baratron Type 223B Differential Pressure Transducer

This transducer was driven by the same ±15 volt power source used to power the ADU contained in the NCA. The output signal from this power supply was in the form of a voltage corresponding to the difference in static pressure between the tunnel test section and ambient air. This signal was read from the DVM simultaneously with the four NCA pressure signals.

63

B. WIND TUNNEL PROCEDURES

1. Initial Positioning and Operation

Tests were performed during a total of 15.8 hours of wind tunnel operation, during which time the performance characteristics of the probe were measured in flow speeds ranging from 0 ft/sec to just under 240 ft/sec. Experiments were conducted with a series of sequentially modified flow impingement angles, which represent those to which the SAIP might be exposed in flight. This is done in order to obtain data relevant to the full range of possible flow directions. The probe was initially placed in the tunnel test section oriented at an angle of rotation about its longitudinal axis of $\theta=0°$. A level was placed along the upper edge of the ASA to calibrate the probe's positioning with respect to the horizontal tunnel flow direction, and minor adjustments were made to the tightness of the clamps securing the NCA to level the unit as necessary.

The angle of rotation about the vertical axis was then set at $\phi=0°$ and a steady state flow velocity of 13 cm H_2O (157.8 ft/sec) was established by an adjustment of the tunnel's propeller blade pitch. The four resulting output voltages from the ADU were then recorded along with the voltage corresponding to the differential pressure between the tunnel test section and the ambient air. The turntable supporting the probe mounting mechanism was next rotated clockwise by the remote electrical control panel to orient the probe 5° to the oncoming flow. The propeller blade pitch was then finely adjusted to

64

reestablish a steady flow velocity of 13 cm H_2O. The same five pressure voltages were again registered. This same procedure was followed for probe alignments of +10°, +15°, +20° and +25°, and then identically for -5°, -10°, -15°, -20° and -25°.

2. Reconfiguration

After sweeping ϕ through its full range, the tunnel flow was then reduced to a nominal velocity of 0 ft/sec and the clamps securing the NCA in its saddle were loosened, permitting the probe to be incremented about the angle θ by +15°. The probe was again leveled as necessary, and steady-state flow was again established at 13 cm H_2O. The transducer and static probe voltages at the same set of ϕ angles were similarly recorded. This procedure was repeated until the NCA had been swept from 0° to 180° in 15° increments about θ, and from -25° to +25° in 5° increments about ϕ. At periodic intervals throughout the test sessions, the internal tunnel temperature as measured by the dial thermometer which extends into the settling chamber was recorded.

C. WIND TUNNEL RESULTS

1. Aerodynamic Performance

Data obtained from following the foregoing procedures are illustrated graphically in Figure 38 and tabulated in Appendix E. In the figure, the difference in the static pressure measured by the NCA and the static pressure which actually exists in the surrounding atmosphere is plotted versus the

65
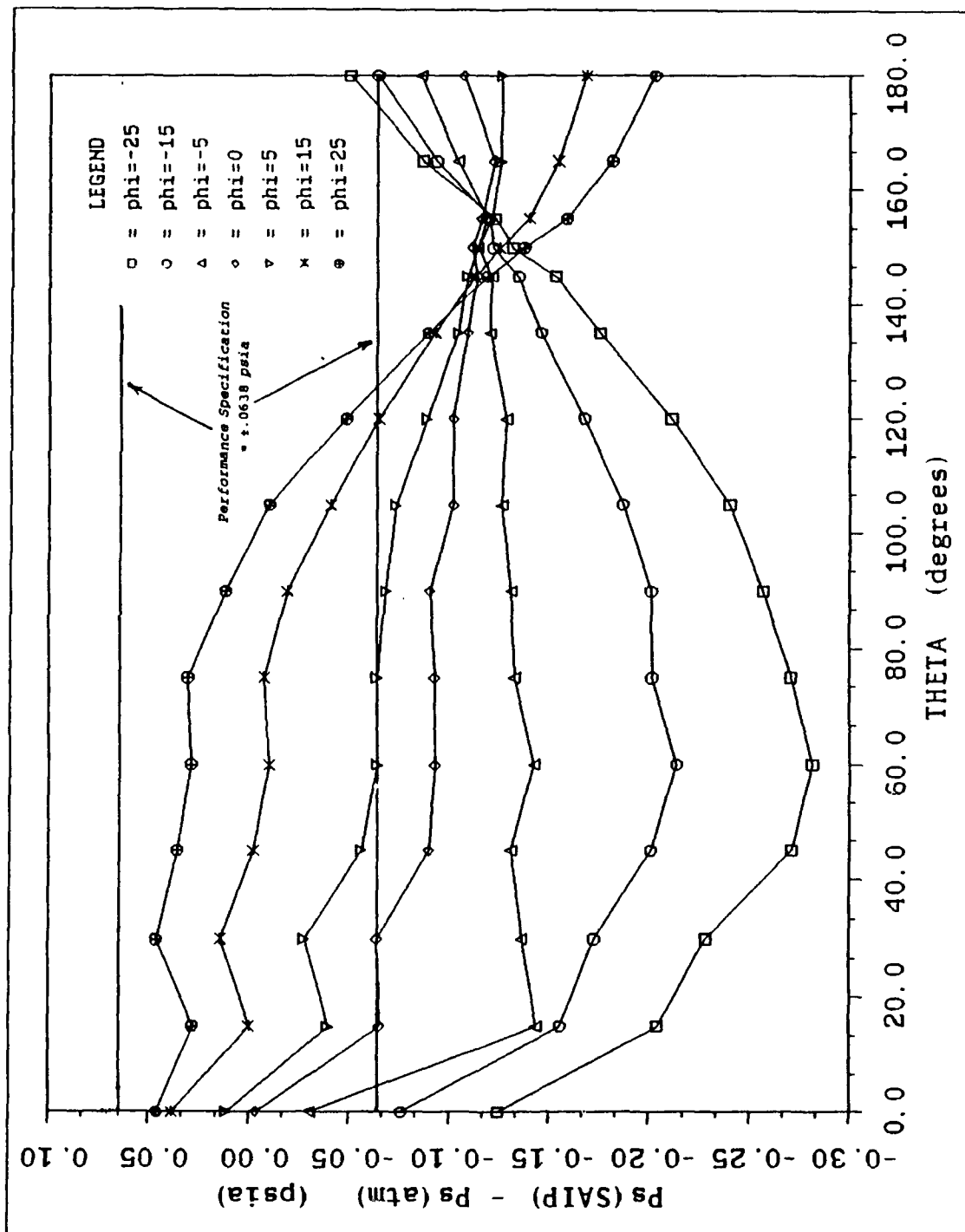
Figure 38. NCA Wind Tunnel Test Results (U_m=157.8 ft/sec)

66

orientation of the NCA with respect to its longitudinal axis. Slight deviations from the nominal 1.0 atmosphere of pressure which exists in the tunnel test section are accounted for in the calculations. It can be seen from the resultant curves in Figure 38 that the variation in pressure differential for the various values of ϕ does not represent the expected value, which should be zero for all orientations of θ. In fact, for larger values of ϕ the data deviate significantly from the expected results.

Figure 38 also reveals that the probe did not meet the $\pm.0638$ psia performance criteria specified in Reference 1 (for sea level operation) over the full range of θ positions for any of the ϕ orientations. Further illustrated by this figure is the convergence of data points at $\theta=150°$. During the course of the wind tunnel tests, it was observed that the pressure differentials converged not only at this orientation, but also at $\theta=-30°$. Because of the paucity of technical documentation on the individual NCA components, the precise cause of these convergences could not be firmly established, although it is speculated that the source of the anomaly may originate in the static pressure line manifolding arrangement existing within the ASA.

2. Temperature Variation

An additional observation made during the course of the tests was that the steady-state static pressure voltage read from the output side of the ADU varied slightly with fluctuations in temperature. These fluctuations were

67

of very small magnitude (generally less than .01 psia) were well within the stipulated performance range (±.0638 psia).

3. Wind Tunnel Configuration

At this point in analysis it became necessary to ascertain if some aspects of the wind tunnel configuration could perhaps be responsible for the deficient NCA performance. The hardware set-up, operating procedures and wind tunnel equipment were all reviewed in an effort to identify possible flaws. After a thorough examination it was determined that the observed NCA performance could not be attributed to any aspect of the experimental procedure. It was then concluded that the probe design itself must exclusively contribute to the erroneous static pressure determinations.

V. ADU PRESSURE SENSITIVITY ANALYSIS

A. ANALYSIS OBJECTIVE

The determination that the inherent aerodynamic characteristics of the NCA were not the sole source of the altitude discrepancies observed in both the flight tests (Section III) and wind tunnel tests (Section IV) resulted in a redirection of investigative effort to examine various other aspects of the test article's design. To supplement the initial ADU calibration described in Section IV.A.2.e, a more comprehensive study was performed to examine the relative interaction between the various pressure lines which interface between the ASA and the individual capacitive pressure transducers housed within the ADU. Of particular concern was any influence which the pressures applied to the total, angle-of-attack and angle-of-sideslip ports on the nose of the ASA might have upon the static pressure measured by the ADU. The possibility of static pressure voltage changes derived from incremental pressure adjustments caused by flow dynamics at the front of the probe would reveal a possible in-flight static pressure dependence upon air flow dynamic pressure.

B. ANALYSIS PROCEDURE

1. System Test

A system-level test was performed upon the NCA in an effort to assess the overall performance of the both the ASA and the ADU as they function collectively in response to frontal port pressure fluctuations. This investigation was performed by utilizing the aforementioned U-tube calibration manometer (Figure 31), which was used to generate the original SAIP calibration curves (Figure 32). Using a methodology similar to that described in Section IV.A.2.e, known positive and negative pressures were individually applied to the total, angle-of-attack and angle-of-sideslip pressure ports located on the airflow sensor, and the voltage corresponding to static pressure was subsequently read from the DVM. A second system-level test was performed by applying identical pressures to the five frontal ports simultaneously. Since dynamic pressure acts simultaneously upon all five frontal ports in flight, by applying pressure to the ports concurrently and monitoring ADU performance, the effect of dynamic pressure upon the airborne SAIP could be realistically simulated and assessed.

2. Component Test

A separate component-level pressure sensitivity test was performed in an effort to independently evaluate the performance of the two individual components, and thus to isolate the source of any potential dynamic pressure

error. In this test, the ADU was physically dec(: led from the airflow sensor and removed from the NCA, and known pressures were then applied to the input side of the ADU. The purpose of this analysis was to isolate the influence of the airflow sensor and its attached pressure lines from the ADU. By applying pressure "downstream" of the airflow sensor, it would be possible to conclude that any static pressure voltage fluctuations which might occur upon application of pressure to the input side of the ADU would originate as errors from within the ADU itself and not from the attached airflow sensor or coupling airlines.

C. ANALYSIS RESULTS

1. System Test

The initial system-level tests revealed that the application of pressure individually to each port on the airflow sensor resulted in a fairly significant deviation in measured ADU static pressure voltage. These results, illustrated in Figure 39, indicate that the sensitivity of the static pressure voltage to frontal port pressure varies in a relatively linear fashion, in a manner similar to the SAIP calibration curves. The fact that a definite fluctuation in the static pressure output voltage occurred upon application of these pressures to the frontal pressure ports is a startling discovery, as static pressure should remain independent of, and isolated from, any dynamic pressure influence. This revelation serves to possibly identify a fundamental
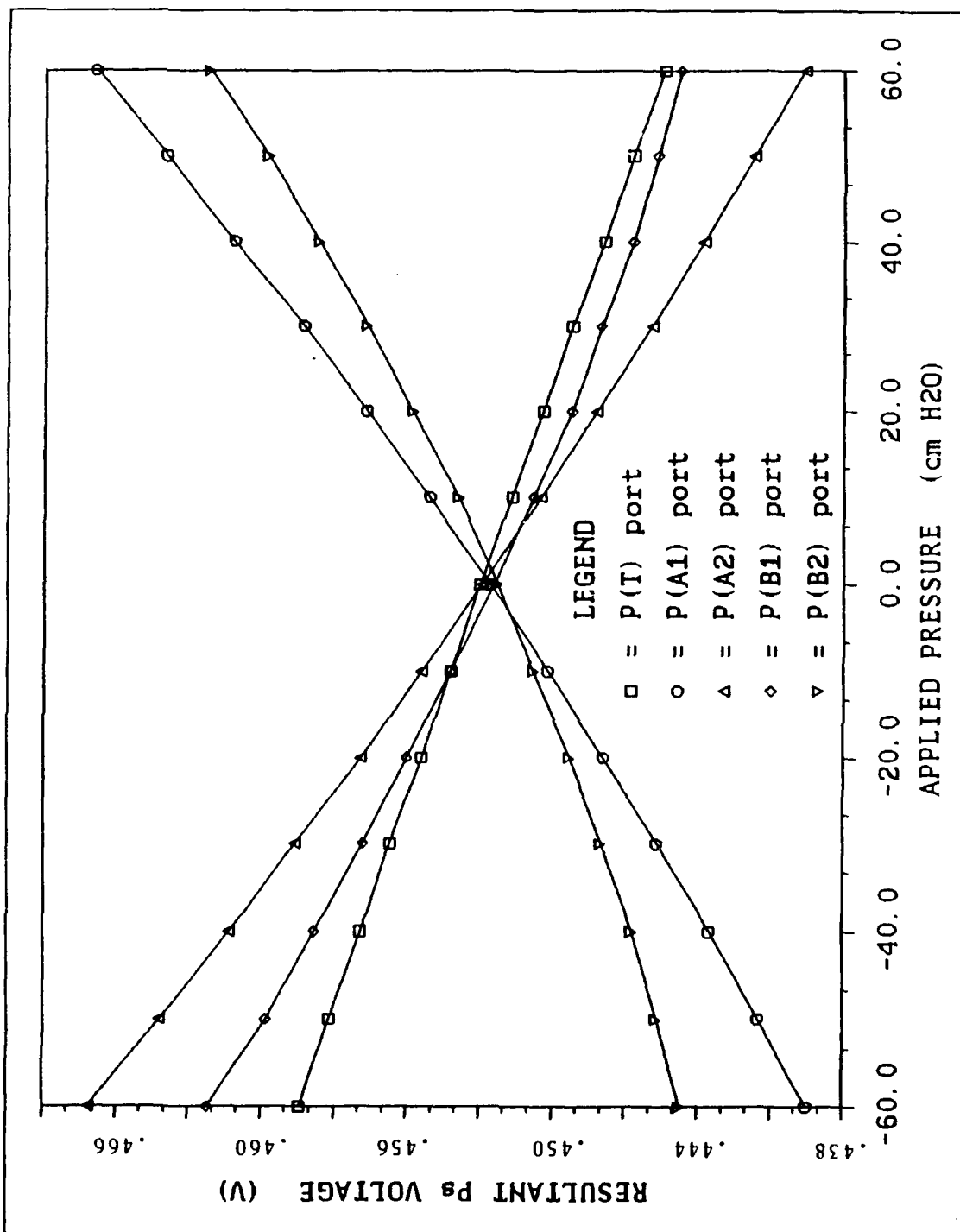
Figure 39. System-Level Pressure Sensitivity Analysis Performance (individual port pressure)

problem with the existing SAIP design, which could potentially be introducing significant errors into the system's altitude determination capability.

The second system-level evaluation resulted in the curve depicted in Figure 40. The difference in the static pressure measured by the NCA and that existing in the ambient environment, $P_s(SAIP) - P_s(atm)$, has been plotted versus the applied pressure (in centimeters of H_2O) in order for the units to correspond to those measured in the wind tunnel tests. The figure illustrates distinctly the linearly decreasing trend of the pressure differential with increases in applied pressure. This trend would suggest that in level flight, as the dynamic pressure increases (as a result of increasing aircraft velocity), the static pressure measured by the SAIP would decrease linearly. This experimental result seemingly contradicts the results obtained in the flight test which was analyzed in Section III. There it was revealed that the SAIP pods consistently reported lower altitudes (as a result of higher static pressures) than that of the aircraft, and that this negative position error was aggravated by increased aircraft velocities (Figures 15-22). Accordingly, the flight tests revealed that the static pressure sensed by the probes actually *increased*, not decreased as seen in the wind tunnel results, with increasing dynamic pressure.

2. Component Test

The process of disconnecting the ADU from the ASA, removing this transducer unit from the NCA and then applying incremental pressures to the
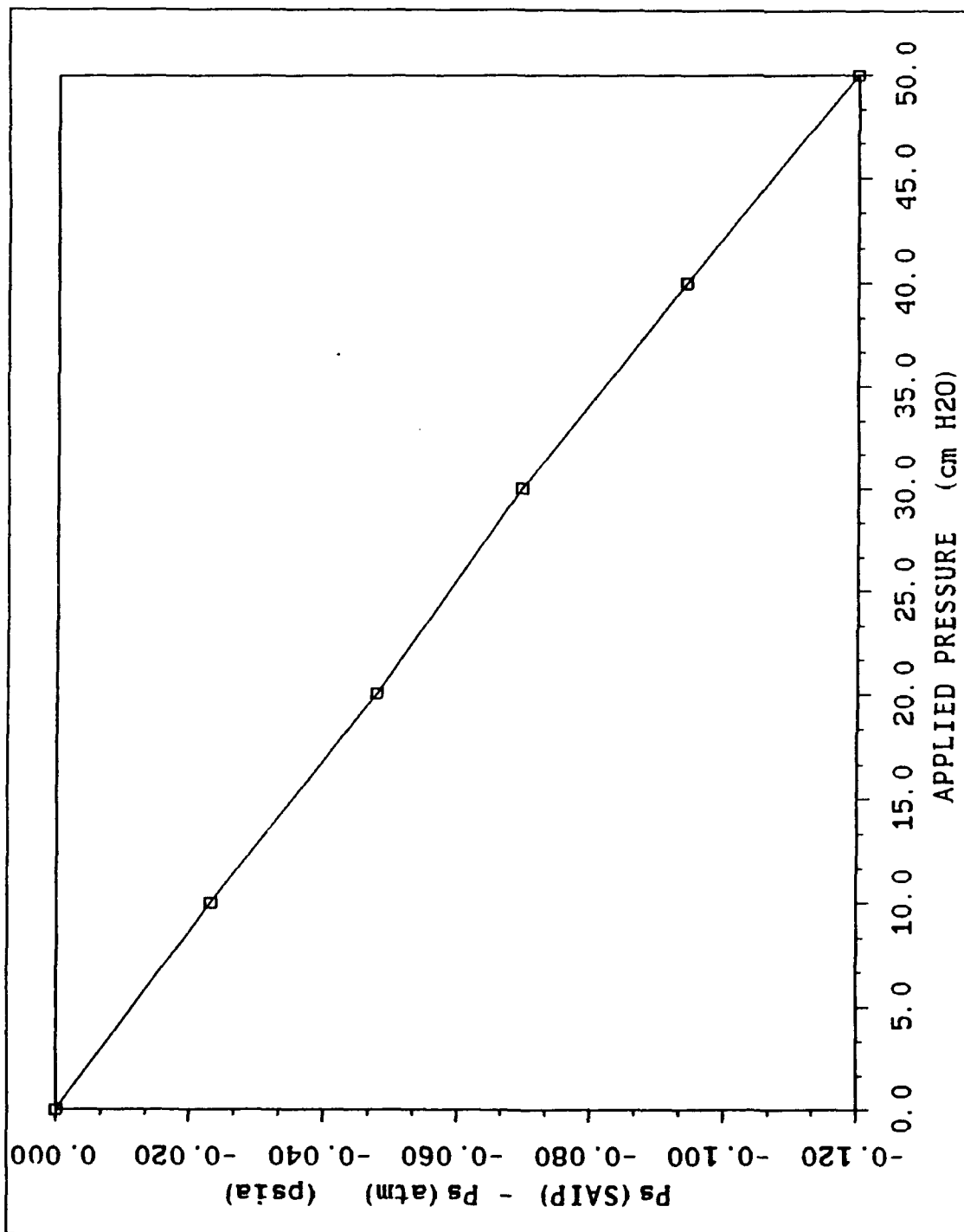
Figure 40. System-Level Pressure Sensitivity Analysis Performance (multiple port pressure)

input side of the unit resulted in the curves illustrated in Figure 41. Examination of these curves reveals that they are identical to those obtained by applying the same set of pressures to the dynamic pressure ports on the nose of the ASA. The straightforward conclusion which can thus be drawn is that the ASA is correctly transferring the pressures impinging upon the frontal ports to the ADU, and that any static pressure anomalies which are experienced are not caused by deficiencies in the ASA design, but originate as errors from within the ADU.
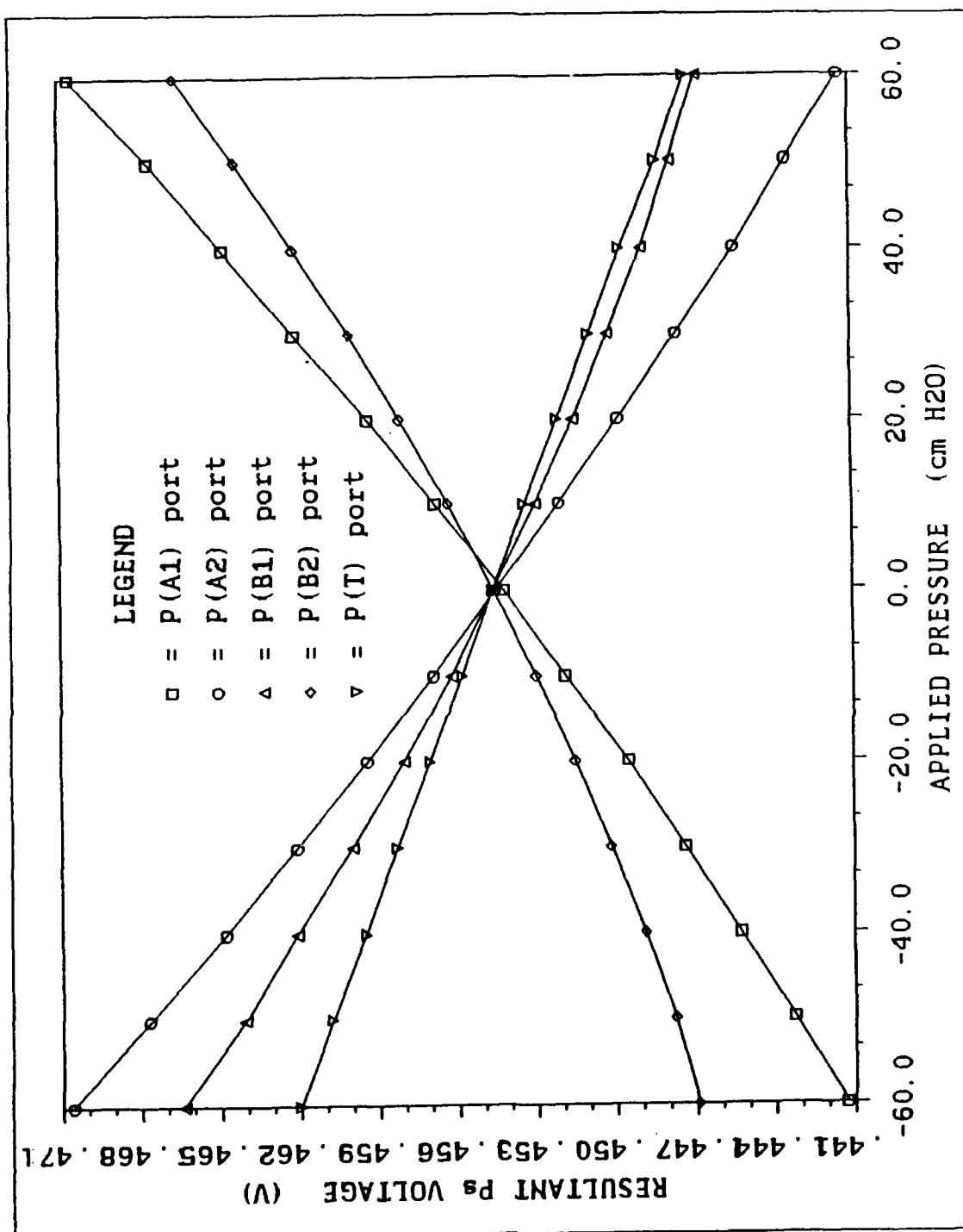
Figure 41. ADU Calibration Curves

76

VI. SUPPLEMENTAL TESTING

A. GENERAL

A two-phased approach was undertaken to confirm the suspected source of SAIP altitude error and to isolate the specific hardware component(s) contributing to the error. The initial effort was directed towards wind tunnel testing of a NCA modified to isolate frontal port dynamic pressures which appear to influence ADU static pressure measurements. The second area of investigation included a study of the internal electronics of the ADU in an attempt to identify possible interference problems with the unit.

B. WIND TUNNEL ANALYSIS

1. Wind Tunnel Procedures

a. *Dynamic Pressure Isolation Tests*

Tests in which air flow dynamic pressure was isolated from the NCA airflow sensor were performed to verify the possible interference of dynamic pressure with measured static pressure. Procedures similar to those employed during the initial wind tunnel tests of the NCA were utilized in the tests to verify the dynamic pressure influence upon pod accuracy. The test article was initially fitted with a very thin-membrane sleeve which was secured over the frontal port area of the airflow sensor and which precluded dynamic

pressure impingement upon the total, angle-of-attack and angle-of-sideslip ports while permitting undisturbed flow over the length of the sensor. The NCA was then mounted in the tunnel test section and instrumented in a manner identical to the initial wind tunnel tests.

The same flow velocity established during the initial tests, 13.0 cm H_2O, corresponding to approximately 158 ft/sec, was maintained during this wind tunnel test. By exposing the test article to common flow conditions, the performance of the SAIP which was modified with the protective sleeve could be readily compared with that of the baseline unit used in the first tests. Trials were conducted by varying the θ orientation in 22.5° increments from 0° to 180°. Similarly, the probe was rotated about ϕ at orientations of 25°, 10°, 5°, 0°, -5°, -10° and -25° during the tests.

b.   *Flow Velocity Effects--Baseline NCA*

During the testing period an additional trial was run to evaluate the baseline (unmodified) pod's performance under a range of flow velocities. In this test the sleeve was removed from the ASA and the tunnel flow velocity was incremented from 0 to 30.0 cm H_2O (0 to 239.7 ft/sec) in steps of 1.0 cm H_2O. Both the θ and ϕ orientations of the NCA were maintained at 0° during the test.

c. *Flow Velocity Effects--Modified NCA*

A final test was performed in the wind tunnel to measure the modified pod's performance under conditions of changing flow velocity. A procedure identical to that employed in the previous trial was implemented, with the exception that the sleeve used to isolate the frontal ports was installed to preclude dynamic pressure impingement upon the ports.

2. Wind Tunnel Results

a. *Dynamic Pressure Isolation Tests*

Isolation of the five frontal ports of the airflow sensor from the impinging flow by a shielding sleeve produced markedly different results from those obtained in the previous wind tunnel test of the unshielded NCA. The resultant curve from the dynamic pressure isolation test appears in Figure 42, and the corresponding data is tabulated in Appendix F. The most significant result from tests of the modified NCA was that the overall magnitude of the pressure differential was appreciably reduced from that obtained with the baseline unit. While this differential varied from approximately -.28 psia to .05 psia with the baseline test article (Figure 38), the range of variation in tests of the modified unit was only on the order of -.02 psia to .04 psia. Taking into account the accuracy and precision of the measurement instruments used, the performance of the modified NCA in the wind tunnel tests was well within
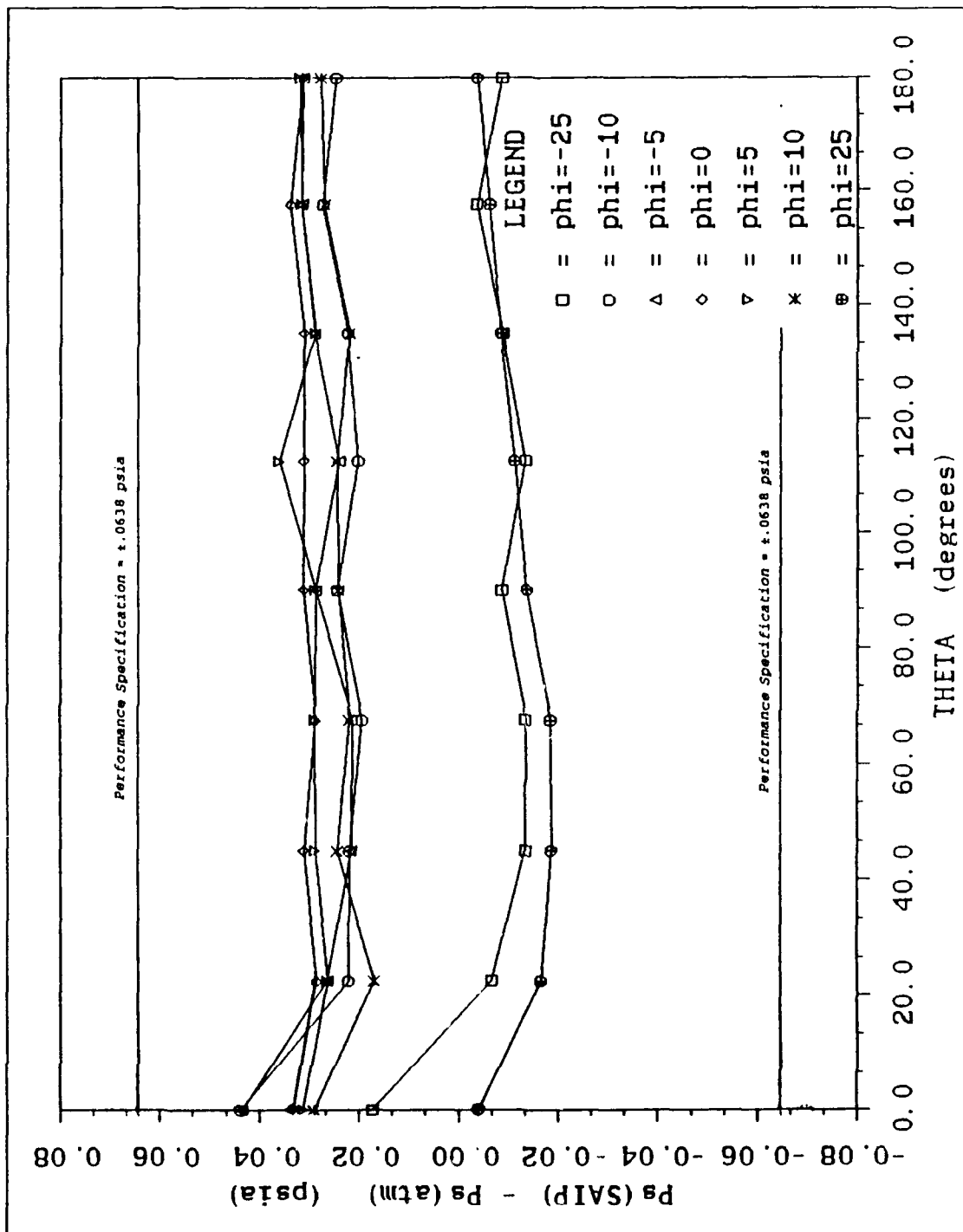
Figure 42. NCA Dynamic Pressure Isolation Test Wind Tunnel Results (U_m=157.8 ft/sec)

80

the prescribed limits on accuracy for sea level operation of ±.0638 psia at all orientations.[Ref. 1]

Figure 42 also reveals that the sleeve effectively eliminated the "sinusoidal" variation of the pressure differential with changes in θ which was observed in the previous wind tunnel trials. The figure correctly indicates that variations in φ of at least 25° should not affect the static pressure which is calculated by the system, and additionally that no effect of θ is discernable. Also notable is the fact that when the modified NCA was rotated about φ in either the positive or negative direction (at a fixed θ orientation), the pressure differential generally decreased. This is a departure from the results observed with the baseline NCA, where rotations about φ in the positive direction caused an increase in the differential while negative rotations about φ resulted in a decrease in this parameter (Figure 38).

b. Flow Velocity Effects--Baseline NCA

The investigation of baseline (uncovered) NCA static pressure determination accuracy as a function of flow velocity resulted in the plot illustrated in Figure 43. Under the existing test conditions, a correctly performing NCA would be described by a straight horizontal line. This curve depicts the decrease in NCA-reported static pressure with increase in dynamic pressure. This general trend corresponds with what was observed in the system-level ADU pressure sensitivity analysis (where incremental pressures were applied simultaneously to all five frontal ports and static pressure voltage

81
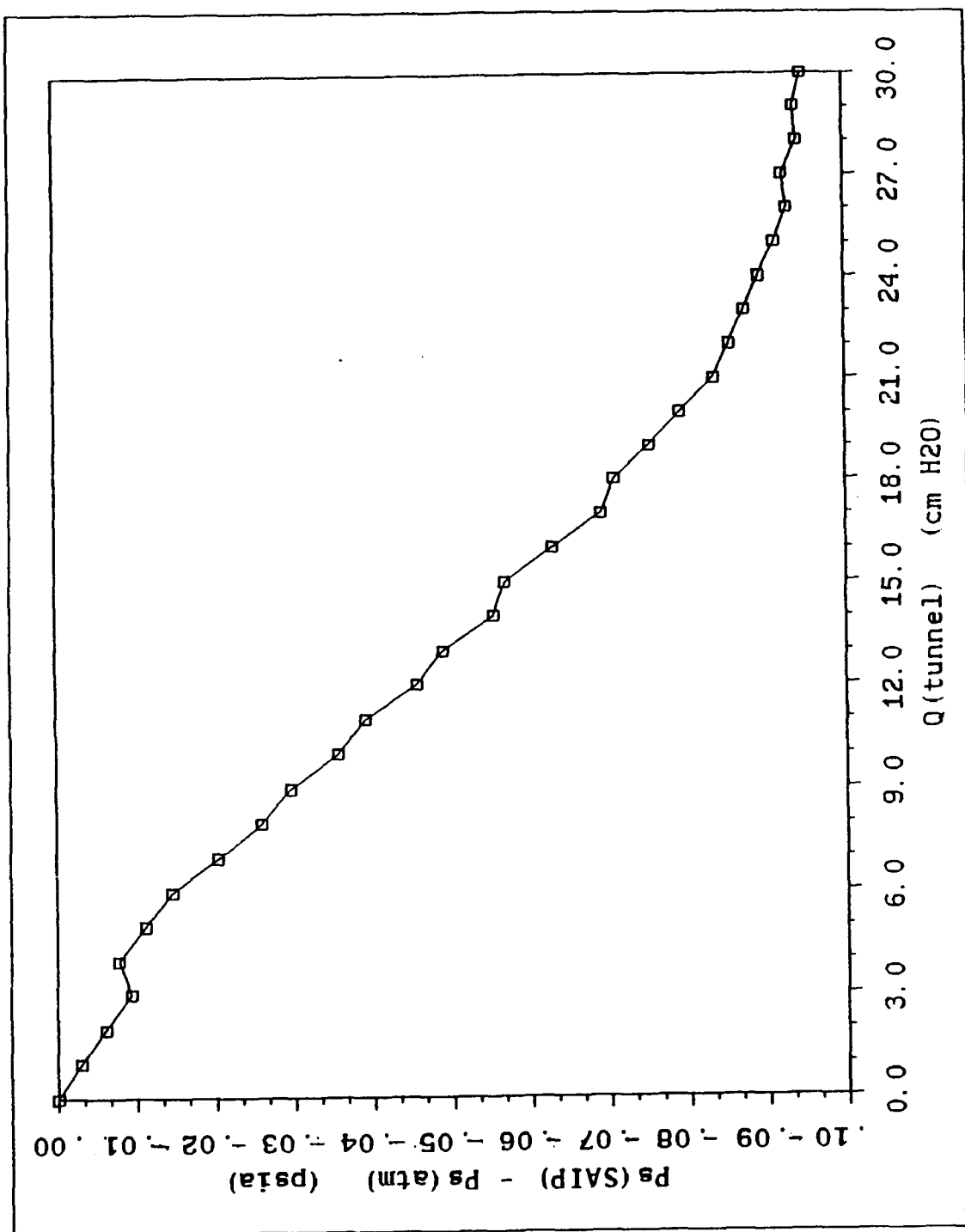
Figure 43. Velocity Dependent Pressure Differential--Baseline NCA

was subsequently recorded) described in Section V.C.1 (Figure 40), though the static pressures reported by the NCA during the sensitivity analysis were somewhat greater in magnitude than those observed in the wind tunnel tests. These results, however, do not correlate well with what was observed from the analysis of SAIP flight tests in Section III. In the flight test analysis it was revealed that increasing aircraft velocities led to a decrease in the reported SAIP altitude, which would correspond to an *increase* in static pressure sensed by the units. The slope observed in the wind tunnel test is exactly opposite to what was experienced in flight.

c. *Flow Velocity Effects--Modified NCA*

It can be seen from the results of the investigation of modified NCA performance over a range of flow velocities, Figure 44, that the shielded probe reports higher static pressures as the dynamic pressure impinging upon the frontal ports is increased. It was anticipated that the shielding would possibly result in a constant static pressure output from the ADU because of the elimination of dynamic pressure interference which, it was conjectured, was introducing errors into the probe's determination of static pressure.

The revelation that the utilization of a protective sleeve resulted in a curve of approximately equal slope as that obtained from tests of the unprotected probe, but of opposite sign, portends the possibility that some sort of correction circuitry has been included among the components residing within the ADU, the design of which could possibly incorporate a variable capacitance

83
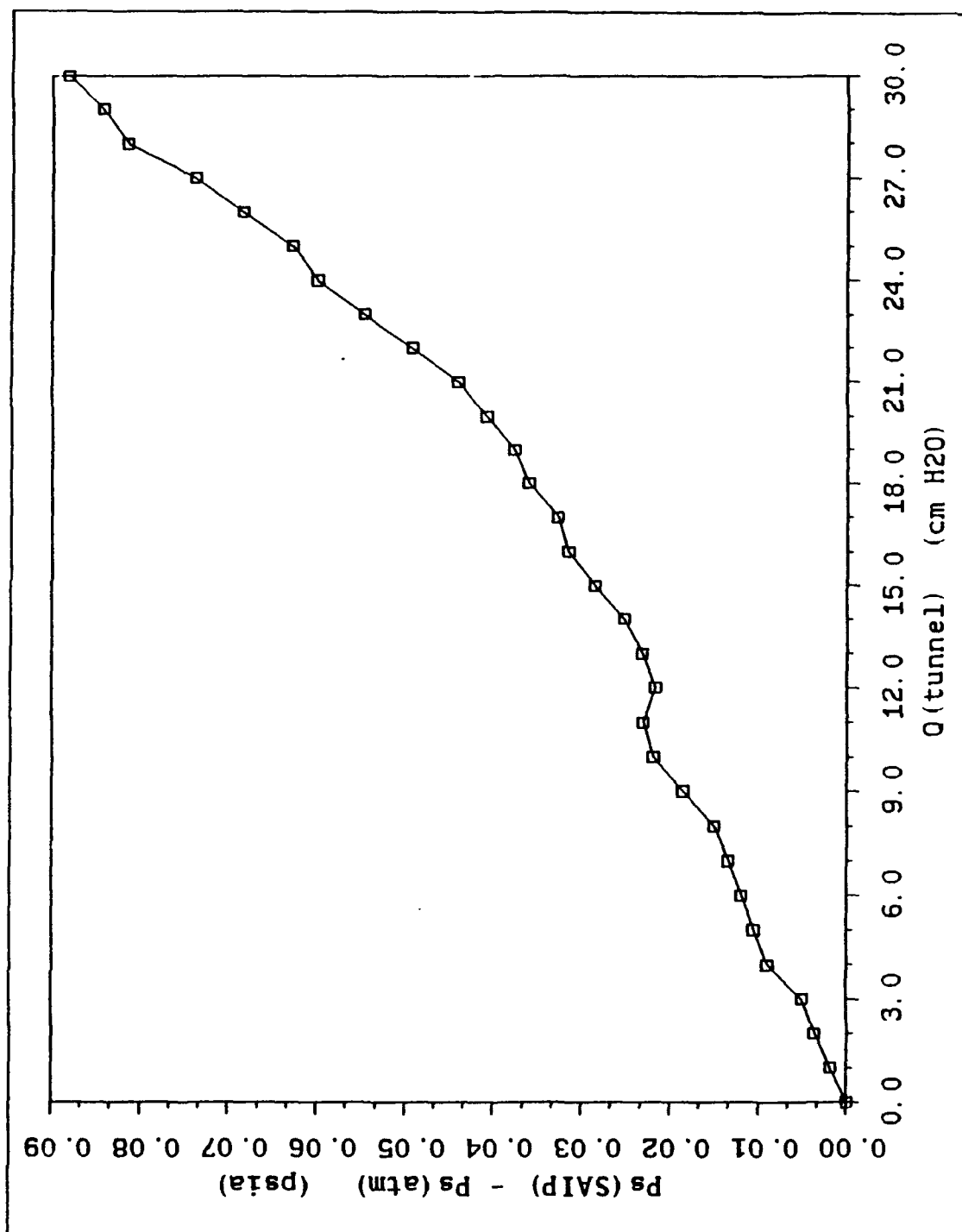
Figure 44. Velocity Dependent Pressure Differential--Modified NCA

84

transducer system [Ref. 12]. This circuitry could possibly be utilized to attempt to correct ADU static pressure output readings which appear to vary at sea-level (assuming no such corrective capabilities were designed into the system) according to the trend depicted in Figure 43.

In order to reconcile the NCA's behavior as measured in the wind tunnel experiments with the observed performance at 4,000 and 10,000 feet during flight tests, one would have to conjecture the existence of "correction circuitry". Because this matter is not of aerodynamic origin and because ADU circuit documentation is not available to NPS at this time, this matter is considered outside of the scope of this thesis.

C. ADU TRANSDUCER ISOLATION ANALYSIS

1. Analysis Procedure

The pressure transducer isolation test was designed to identify components in the ADU which may be contributing electronic or pneumatic interference to the system. The existence of such components could precipitate errors in ADU static pressure determination. This test was performed by isolating each of the three differential-type pressure transducers (total, angle-of-sideslip and angle-of-attack) from the ADU circuitry, applying incremental pressures to the input junctions of the static pressure transducer and then reading the resultant static pressure voltage. Procedurally, the first transducer to be isolated was the total pressure transducer. This particular

85

transducer possesses both a pneumatic interface with the static pressure transducer and an electronic interface with the signal conditioning circuitry, and thus both of these effects were independently isolated. The angle-of-sideslip pressure transducer was then electronically isolated from the system (together with the previously disconnected total pressure transducer), the same incremental pressures were the applied to the static port, and the resultant static pressure voltage was again recorded. Finally, the angle-of-attack transducer was electronically disconnected and the same procedures were followed with all three differential transducers isolated from the circuitry, thus precluding interference of any of the three devices with the remainder of the system.

2. Analysis Results

The results of disconnecting various combinations of the total, angle-of-attack and angle-of-sideslip pressure transducers, applying a series of graduated pressures to the static pressure input port to the ADU and subsequently measuring the ADU static pressure voltage are illustrated in Figure 45 and tabulated in Appendix G. Figure 45 illustrates that when all three transducers are connected (together with the static pressure transducer), the normal in-flight operating configuration, the resultant output is on the order of .45-.46 volts, just as observed in the SAIP calibration curves (Figure 32) discussed in Section IV.A.2.e. The curve representing this configuration,

86

seen along the bottom of Figure 45, exhibits a linear variation with pressure and has a reciprocal slope of 113.70 psia/volt.

Other combinations of pressure transducer connections led to the remaining curves seen in Figure 45. A particularly interesting and significant result can be seen in the grouping of curves plotted in the top region of the figure. When the ADU was configured with any of combinations of transducers represented by these curves, the resultant output voltage varied from approximately 5.0 to 6.0 volts.

The importance of this result is that the general range of voltages spanned by these curves corresponds precisely with the range which the SAIP functional specification [Ref. 1] stipulates the probe's output should lie in for the given pressures. It will be recalled that during the preliminary study of SAIP calibration (Section IV.A.2.e), the output of the ADU did not appear to correlate with the static pressure/output voltage relationship outlined in the functional specification. In fact, as discussed in the first paragraph of this subsection, the output took the form of the bottom curve in Figure 45.

Another critical system characteristic revealed by the figure is highlighted by the fact that the five curves which converge at the top of Figure 45 all possess reciprocal slopes of approximately 2.58 psia/volt. This result again corresponds almost exactly with the specified performance criterion of an ADU static pressure/output voltage relationship of 2.5 psia/volt [Ref. 1]. The close correspondence of these slopes, coupled with the high degree of

LEGEND

□ = P(T)+P(A)+P(B) connected

○ = P(T)+P(A) connected

△ = P(A)+P(B) connected

◇ = P(A) connected

▽ = P(B) connected

✕ = P(T) connected

⊕ = no transducers connected

APPLIED PRESSURE (cm H2O)

RESULTANT P(s) VOLTAGE (V)
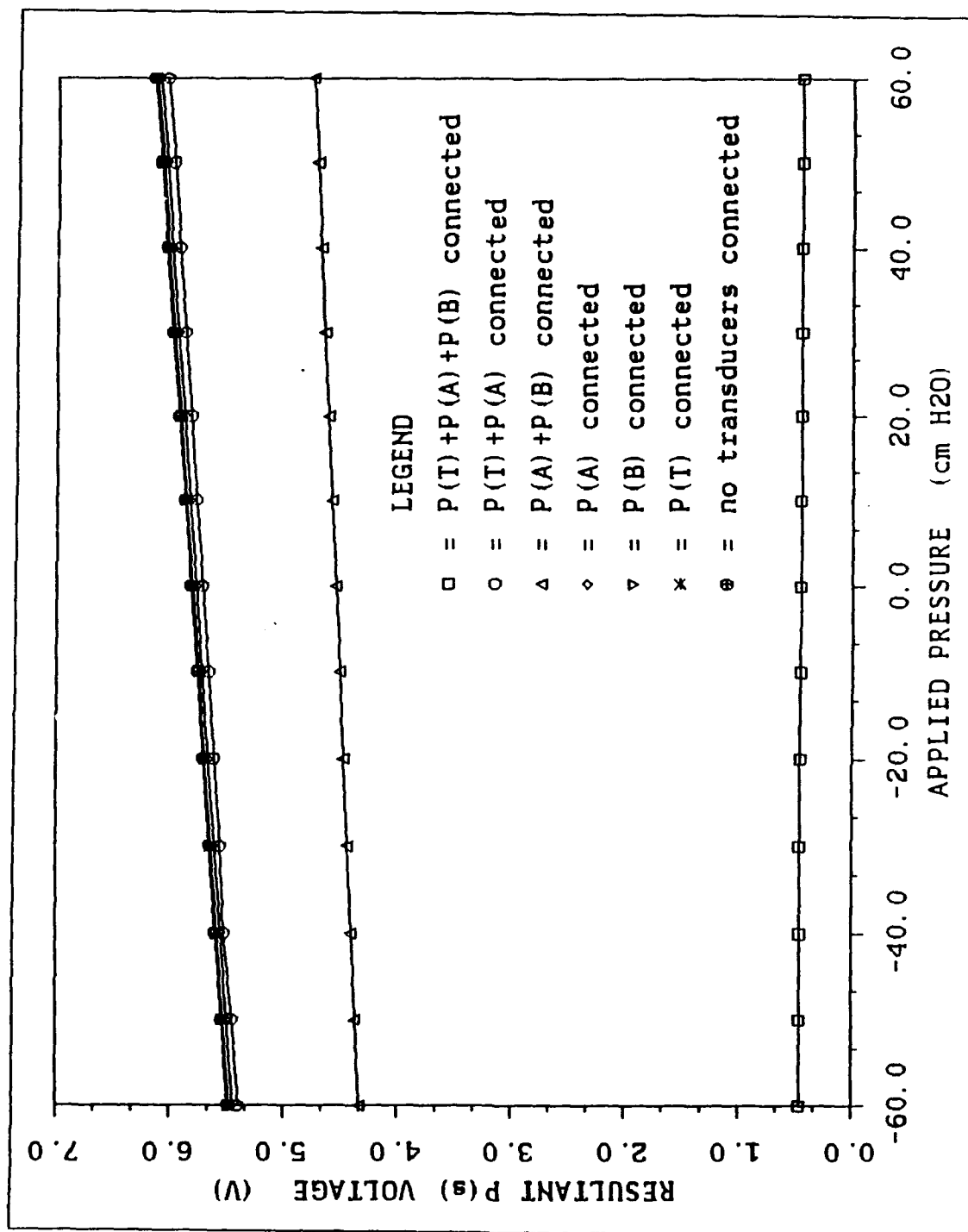
Figure 45. ADU Transducer Isolation Analysis Results

correlation between the overall magnitudes of the specified and empirical voltages, strongly suggests that by electrically isolating the three differential transducers from the remainder of the ADU circuitry, the originally specified performance of the ADU can be recovered and SAIP altitude determination errors can be eliminated.

VII. CONCLUSIONS AND RECOMMENDATIONS

A. CONCLUSIONS

Based upon the results of the multifaceted investigation of SAIP altitude determination error involving in-flight evaluations, wind tunnel testing and pressure sensitivity studies, a number of conclusions have been established:

Flight Tests

- The second-generation SAIP design incorporating 12 static ports provided essentially identical performance during flight tests as did the first-generation single static port unit. Both designs failed to meet the required altitude accuracy established in the SAIP functional specification [Ref. 1].

- SAIP altitude error manifests a functional relationship which is somewhat dependent upon the square of the velocity of the impinging air flow.

- SAIP altitude error cannot be conclusively attributed to dynamic pressure impingement upon the probe's frontal ports because of the lack of dependence of this error upon ambient air density.

- Neither the relative wing station position of the SAIP on the test aircraft nor either the presence or absence of a centerline fuel tank had a measurable influence upon SAIP altitude determination accuracy.

Wind Tunnel Tests

- While the static ports located on the airflow sensor are not positioned sufficiently aft of the probe's leading edge to meet recommended criterion, the aerodynamic characteristics of the second-generation SAIP design are sufficient to accurately assimilate and transfer static pressure data from the probe's Airflow Sensor Assembly (ASA) to the input ports of the Air Data Unit (ADU) [Ref. 5].

90

- The interim redesign concept involving the elimination of SAIP dynamic pressure processing through the use of a shielding sleeve, while ineffective in eliminating altitude determination errors introduced by changing flow velocities, is effective in excluding errors associated with varying flow impingement angles.

Pressure Sensitivity Testing

- SAIP altitude errors originate as the result of electrical interference introduced by the existence of total, angle-of-attack and angle-of-sideslip differential pressure transducers in the same ADU circuitry as that supporting the processing of static pressure signals. No evidence was found to support the postulate that pneumatic interference, either within the ASA or the ADU, is contributing to inaccuracies in SAIP-reported altitudes.

- Required SAIP altitude determination performance, as outlined in the system's functional specification (Reference 1), can be recovered by electrical isolation of the total, angle-of-attack and angle-of-sideslip pressure transducers from the static pressure transducer and remaining ADU circuitry. Equivalent performance can alternatively be achieved by electrically isolating either the angle-of-attack or angle-of-sideslip transducers (or both) from existing electronics.

B. RECOMMENDATIONS

Recommendations for achieving an accurate SAIP altitude determination capability are suggested as follows:

- Further wind tunnel testing should be performed to evaluate the static pressure measurement accuracy of a SAIP Configuration -003 Nose Cone Assembly (NCA) containing an ADU which has been modified in such a manner that the three differential-type pressure transducers used to process total, angle-of-attack and angle-of-sideslip pressures are electrically isolated from all ADU circuitry.

- The successful completion of the foregoing series of wind tunnel tests should sanction a similar modification of operational ADUs to facilitate the elimination of current SAIP altitude deficiencies and the recovery of requisite system performance. A near-term improvement could include

91

simply severing the electrical leads carrying power to the individual differential pressure transducers.

- A circuit redesign of the ADU should be undertaken to permit simultaneous processing of static, total, angle-of-attack and angle-of-sideslip pressure information without the attendant degradation of static pressure measurement accuracy.

- Additional investigation should include a study of the relative value and extractability of data processed by the total, angle ʿ-attack and angle-of-sideslip pressure sensors with regard to the capability of the data to furnish supplemental information on aircraft position, attitude, velocity, acceleration, etc.

- Evaluate the sensitivity of the existing absolute- and differential-type pressure transducers and associated ADU electronics to effects introduced by three-dimensional aircraft acceleration, and compare the resultant performance with the system's functional requirements.

- Novel techniques should be studied for measuring the above aircraft parameters. One such investigation might include using a multiplicity of ports on the body of the SAIP, thereby eliminating the need for the total, angle-of-attack and angle-of-sideslip pressure ports on the nose of the airflow sensor. The capabilities of computer-based systems to interpret probe pressure readings is expanding, and could permit replacement of the existing pressure line manifolding arrangement with a system capable of yielding flow direction and Mach number in addition to static pressure.

APPENDIX A. PRESSURE CALCULATION PROGRAM

```
00010 REM   CALCULATION OF P/Pinf AND Cp AS A
00015 REM   FUNCTION OF Minf, PHI AND THETA
00020 OPEN "CP.OUT" FOR OUTPUT AS #3
00030 DIM P(7)
00035 DIM Cp(7,65)
00040 G=1.4
00080 PRINT "INPUT FREE-STREAM MACH NUMBER"
00090 INPUT Minf
00110 PRINT "Minf          PHI          THETA    P/Pinf          Cp"

00116 REM SWEEP PHI FROM 0 TO 90 DEGREES
00117 REM IN 15 DEGREE INCREMENTS
00118 FOR J=0 TO 6
00119 P(J)=J*.261799388

00120 REM SWEEP THETA FROM -180 DEGREES TO 180 DEGREES
00122 T=-3.239767424
00125 FOR I=1 TO 65
00132 T=T+.098174770

00135 REM CALCULATIONS
00140 F(J)=4*(SIN(P(J)))^2*(SIN(T))^2 + (COS(P(J)))^2
00150 A(J)=(Minf^2)*F(J)
00160 B=1+((G-1)/2)*Minf^2
00170 C(J)=((G-1)/2)*(Minf^2)*F(J)
00180 M(J)=SQR(A(J)/(B-C(J)))
00190 P1(J)=(B/(1+((G-1)/2)*M(J)^2))^(G/(G-1))
00195 Cp(J,I)=(P1(J)-1)*(2/(G*Minf^2))
00209 NEXT I
00210 NEXT J

00211 REM PRINT LOOPS
00212 FOR J=0 TO 6
00213 T=-3.239767424
00214 FOR I=1 TO 65
00215 T=T+.098174770
00216 PRINT Minf,P(J),T,P1(J)
00217 PRINT #3; T;Cp(0,I);Cp(1,I);Cp(2,I);                    &
      Cp(3,I);Cp(4,I);Cp(5,I);Cp(6,I)
00218 NEXT I
00219 NEXT J

00220 PRINT "ANOTHER RUN? (1=Y,2=N)"
00230 INPUT Q
00250 IF Q=1 GO TO 30
00255 CLOSE #3
00260 END
```

APPENDIX B. DATASTAT PROGRAM

```
C  THIS PROGRAM CALCULATES THE MEAN VALUE AND
C  STANDARD DEVIATION OF A SET OF INPUT ALTITUDES

      PROGRAM DATASTAT
      IMPLICIT REAL (A-Z)
      INTEGER*2 K
      CHARACTER*20 NAME

      DIMENSION AC(100), A(100), DA(100), VA(100),
     ;B(100), DB(100),VB(100),
     ;C(100), DC(100),VC(100),
     ;D(100), DD(100),VD(100)

      WRITE(6,*) 'ENTER THE NAME OF THE INPUT FILE'
      READ(5,'(20A)') NAME
      WRITE(*,*) 'INPUT COLUMN LENGTH'
      READ(5,'(A)') K
      OPEN(UNIT=15,FILE=NAME,STATUS='OLD')

      DO I=1,K
        READ(15,*) AC(I),A(I),B(I),C(I),D(I)
        WRITE(6,*) AC(I),A(I),B(I),C(I),D(I)
      END DO

C  CALUCULATE DIFFERENCE
      DO 70 I=1,K
          DA(I)=AC(I)-A(I)
          DB(I)=AC(I)-B(I)
          DC(I)=AC(I)-C(I)
          DD(I)=AC(I)-D(I)
          WRITE(22,*) DA(I),DB(I),DC(I),DD(I)
70 CONTINUE

C  CALCULATE SUM OF DIFFERENCES
      SA=0
      SB=0
      SC=0
      SD=0
      DO 80 I=1,K
         SA=SA+DA(I)
         SB=SB+DB(I)
         SC=SC+DC(I)
         SD=SD+DD(I)
80 CONTINUE
```

```
C   CALCULATE MEAN VALUE
      MA=SA/K
      MB=SB/K
      MC=SC/K
      MD=SD/K

C   CALCULATE VARIANCE
      DO 90 I=1,K
        VA(I)=(AC(I)-A(I))**2
        VB(I)=(AC(I)-B(I))**2
        VC(I)=(AC(I)-C(I))**2
        VD(I)=(AC(I)-D(I))**2
   90 CONTINUE

C   CALCULATE SUM OF DIFFERENCES
      VARA=0
      VARB=0
      VARC=0
      VARD=0
      DO 100 I=1,K
        VARA=VARA+VA(I)
        VARB=VARB+VB(I)
        VARC=VARC+VC(I)
        VARD=VARD+VD(I)
  100 CONTINUE

C   CALCULATE STANDARD DEVIATION
      SIGMAA=SQRT(VARA/K-(MA**2))
      SIGMAB=SQRT(VARB/K-(MB**2))
      SIGMAC=SQRT(VARC/K-(MC**2))
      SIGMAD=SQRT(VARD/K-(MD**2))

      WRITE(*,*) 'MEAN VALUE OF SAIP A DIFFERENCE=', MA
      WRITE(*,*) 'MEAN VALUE OF SAIP B DIFFERENCE=', MB
      WRITE(*,*) 'MEAN VALUE OF SAIP C DIFFERENCE=', MC
      WRITE(*,*) 'MEAN VALUE OF SAIP D DIFFERENCE=', MD
      WRITE(*,*) 'STD DEV OF SAIP A DIFFERENCE=', SIGMAA
      WRITE(*,*) 'STD DEV OF SAIP B DIFFERENCE=', SIGMAB
      WRITE(*,*) 'STD DEV OF SAIP C DIFFERENCE=', SIGMAC
      WRITE(*,*) 'STD DEV OF SAIP D DIFFERENCE=', SIGMAD

      STOP
      END
```

APPENDIX C. DATAFIT PROGRAM

```
C   THIS PROGRAM CALCULATES DATA FOR PLOTTING
C   AND SUBSEQUENT POLYNOMIAL FIT

      PROGRAM DATAFIT
      IMPLICIT REAL (A-Z)
      INTEGER*2 K
      CHARACTER*20 NAME

      DIMENSION AC(100),A(100),DA(100),FA(100),LOGFA(100),
     ;B(100),DB(100),FB(100),LOGFB(100),
     ;C(100),DC(100),FC(100),LOGFC(100),
     ;D(100),DD(100),FD(100),LOGFD(100),
     ;V(100),LOGV(100)

      WRITE(6,*) 'ENTER THE NAME OF THE INPUT FILE'
      READ(5,'(20A)') NAME
      WRITE(*,*) 'INPUT COLUMN LENGTH'
      READ(5,'(A)') K
      OPEN(UNIT=15,FILE=NAME,STATUS='OLD')

      DO I=1,K
        READ(15,*) V(I),AC(I),A(I),B(I),C(I),D(I)
        WRITE(6,*) V(I),AC(I),A(I),B(I),C(I),D(I)
      END DO

C   CALCULATE DIFFERENCE
      DO 70 I=1,K
      DA(I)=AC(I)-A(I)
      DB(I)=AC(I)-B(I)
      DC(I)=AC(I)-C(I)
      DD(I)=AC(I)-D(I)
      WRITE(22,*) DA(I),DB(I),DC(I),DD(I)
 70   CONTINUE

      DO 80 I=1,K
        FA(I)=(1-.000006880928*AC(I))*DA(I)
        FB(I)=(1-.000006880928*AC(I))*DB(I)
        FC(I)=(1-.000006880928*AC(I))*DC(I)
        FD(I)=(1-.000006880928*AC(I))*DD(I)
 80   CONTINUE

      DO 90 I=1,K
        LOGV(I)=LOG(V(I))
 90   CONTINUE
```

```
      DO 100 I=1,K
         LOGFA(I)=LOG(FA(I))
         LOGFB(I)=LOG(FB(I))
         LOGFC(I)=LOG(FC(I))
         LOGFD(I)=LOG(FD(I))
100 CONTINUE

      DO 110 I=1,K
      WRITE(6,*) LOGV(I),LOGFA(I),LOGFB(I),LOGFC(I),
     ;LOGFD(I)
      WRITE(23,*) LOGV(I),LOGFA(I),LOGFB(I),LOGFC(I),
     ;LOGFD(I)
110 CONTINUE

      STOP
      END
```

APPENDIX D. DATASTAT AND DATAFIT INPUT DATA

RUN #2

IRIG time	Relative run time	Speed (KTAS)	AC alt (feet)	SAIP A alt (feet)	SAIP B alt (feet)	SAIP C alt (feet)	SAIP D alt (feet)
2:46:00	0.0000	268	4034	3671	3747	3776	3701
2:46:10	0.1667	290	4048	3655	3714	3740	3691
2:46:20	0.3333	335	4050	3593	3645	3675	3609
2:46:30	0.5000	372	4038	3517	3553	3599	3573
2:46:40	0.6667	404	4056	3547	3556	3602	3593
2:46:50	0.8333	436	4062	3468	3465	3576	3524
2:47:00	1.0000	458	4048	3376	3369	3445	3458
2:47:10	1.1667	481	4061	3356	3333	3415	3428
2:47:20	1.3333	496	4130	3409	3402	3448	3494
2:47:30	1.5000	509	4142	3310	3310	3386	3402
2:47:40	1.6667	525	4174	3264	3284	3356	3392
2:47:50	1.8333	530	4206	3291	3301	3386	3438
2:48:00	2.0000	538	4192	3179	3219	3274	3310
2:48:10	2.1667	539	4140	3140	3159	3235	3271
2:48:20	2.3333	544	4182	3202	3238	3282	3314
2:48:30	2.5000	541	4225	3264	3278	3314	3356
2:48:40	2.6667	534	4238	3346	3363	3422	3484
2:48:50	2.8333	492	4051	3310	3330	3353	3366
2:49:00	3.0000	452	3992	3392	3409	3465	3527
2:49:10	3.1667	424	4018	3517	3540	3511	3599
2:49:20	3.3333	397	4008	3494	3540	3553	3586
2:49:30	3.5000	368	4050	3632	3681	3678	3724
2:49:40	3.6667	353	4046	3599	3665	3668	3684
2:49:50	3.8333	334	3978	3540	3609	3625	3602
2:50:00	4.0000	314	3972	3599	3684	3684	3707
2:50:10	4.1667	295	3988	3652	3733	3730	3737
2:50:20	4.3333	278	4004	3658	3773	3760	3770
2:50:30	4.5000	262	4006	3701	3809	3786	3789

IRIG time	Relative run time	Speed (KTAS)	AC alt (feet)	SAIP A alt (feet)	SAIP B alt (feet)	SAIP C alt (feet)	SAIP D alt (feet)
2:53:40	0.0000	307	10544	9767	9777	9879	9783
2:53:50	0.1667	335	10533	9672	9675	9780	9670
2:54:00	0.3333	364	10513	9636	9610	9731	9632
2:54:10	^.5000	393	10520	9639	9577	9692	9621
2:54:20	U.6667	418	10526	9610	9564	9705	9603
2:54:30	0.8333	443	10538	9551	9436	9603	9544
2:54:40	1.0000	466	10543	9478	9308	9564	9491
2:54:50	1.1667	482	10553	9463	9308	9547	9493
2:55:00	1.3333	498	10559	9377	9308	9452	9404
2:55:10	1.5000	512	10564	9318	9272	9432	9354
2:55:20	1.6667	523	10561	9242	9193	9318	9282
2:55:30	1.8333	533	10556	9203	9178	9314	9258
2:55:40	2.0000	537	10559	9210	9200	9314	9246
2:55:50	2.1667	541	10584	9199	9180	9298	9231
2:56:00	2.3333	532	10597	9226	9206	9318	9243
2:56:10	2.5000	498	10542	9380	9354	9452	9361
2:56:20	2.6667	471	10530	9457	9426	9518	9472
2:56:30	2.8333	446	10526	9524	9462	9603	9528
2:56:40	3.0000	426	10540	9593	9536	9672	9578
2:56:50	3.1667	404	10540	9618	9610	9698	9610
2:57:00	3.3333	382	10527	9656	9665	9741	9665
2:57:10	3.5000	363	10532	9656	9675	9767	9650
2:57:20	3.6667	343	10532	9695	9738	9803	9692
2:57:30	3.8333	327	10520	9706	9747	9793	9711
2:57:40	4.0000	310	10518	9731	9777	9833	9738
2:57:50	4.1667	294	10499	9646	9711	9843	9688
2:58:00	4.3333	284	10492	9679	9749	9843	9685
2:58:10	4.5000	269	10706	9957	9984	10ı02	9957
2:58:20	4.6667	263	10775	9973	10075	10154	10026
2:58:30	4.8333	268	10504	9742	9842	9888	9744
2:58:40	5.0000	266	10435	9656	9842	9783	9677
2:58:50	5.1667	258	10506	9754	9842	9897	9767
2:59:00	5.3333	252	10564	9852	9869	9974	9850

RUN #4

IRIG time	Relative run time	Speed (KTAS)	AC alt (feet)	SAIP A alt (feet)	SAIP B alt (feet)	SAIP C alt (feet)	SAIP D alt (feet)
3:53:40	0.0000	525	4127	3256	3254	3258	3352
3:53:50	0.1667	528	4100	3218	3171	3214	3312
3:54:00	0.3333	534	4119	3189	3149	3192	3287
3:54:10	0.5000	539	4190	3271	3224	3252	3370
3:54:20	0.6667	545	4208	3255	3219	3242	3356
3:54:30	0.8333	549	4212	3248	3223	3236	3364
3:54:40	1.0000	507	4161	3449	3405	3415	3530
3:54:50	1.1667	469	4158	3517	3501	3517	3620
3:55:00	1.3333	434	4128	3563	3590	3570	3666
3:55:10	1.5000	407	4084	3544	3566	3558	3616
3:55:20	1.6667	383	4084	3606	3655	3635	3691
3:55:30	1.8333	358	4078	3612	3701	3661	3724
3:55:40	2.0000	340	4041	3573	3663	3638	3672
3:55:50	2.1667	318	4090	3707	3814	3763	3839
3:56:00	2.3333	300	4108	3747	3848	3789	3834
3:56:10	2.5000	284	4094	3717	3832	3786	3821
3:56:20	2.6667	272	4022	3616	3760	3701	3725
3:56:30	2.8333	260	3990	3621	3763	3691	3737

RUN #5

IRIG time	Relative run time	Speed (KTAS)	AC alt (feet)	SAIP A alt (feet)	SAIP B alt (feet)	SAIP C alt (feet)	SAIP D alt (feet)
3:58:20	0.0000	318	10648	9879	9942	9905	10446
3:58:30	0.1667	355	10630	9785	9823	9813	10336
3:58:40	0.3333	390	10580	9666	9689	9692	10223
3:58:50	0.5000	420	10564	9655	9656	9646	10208
3:59:00	0.6667	446	10588	9646	9600	9640	10181
3:59:10	0.8333	471	10629	9622	9579	9609	10157
3:59:20	1.0000	491	10642	9544	9484	9528	10080
3:59:30	1.1667	510	10622	9460	9385	9432	9982
3:59:40	1.3333	526	10586	9324	9254	9322	9855
3:59:50	1.5000	537	10570	9318	9259	9308	9855
4:00:00	1.6667	545	10568	9274	9200	9252	9810
4:00:10	1.8333	539	10541	9252	9170	9252	9760
4:00:20	2.0000	500	10469	9403	9288	9356	9886
4:00:30	2.1667	467	10433	9448	9375	9452	9938
4:00:40	2.3333	436	10415	9517	9447	9522	10005
4:00:50	2.5000	409	10440	9537	9498	9570	10029
4:01:00	2.6667	385	10464	9600	9565	9646	10064
4:01:10	2.8333	365	10481	9641	9639	9694	10142
4:01:20	3.0000	348	10484	9646	9654	9685	10131
4:01:30	3.1667	330	10494	9646	9680	9718	10137
4:01:40	3.3333	311	10503	9723	9752	9800	10212
4:01:50	3.5000	295	10497	9701	9759	9803	10213

APPENDIX E. NCA WIND TUNNEL TEST DATA

PHI (degrees)

THETA (degrees)	-25	-20	-15	-10	-5	0
-35	-.0892	-.0878	-.0888	-.0850	-.0874	-.0860
-30	-.1079	-.1017	-.0979	-.0927	-.0903	-.0903
-25	-.1225	-.1114	-.0980	-.0966	-.0928	-.0856
0	-.1247	-.1041	-.0762	-.0508	-.0301	-.0037
15	-.2043	-.1812	-.1558	-.1207	-.1438	-.0654
30	-.2284	-.2006	-.1727	-.1328	-.1365	-.0641
45	-.2713	-.2362	-.2011	-.1661	-.1310	-.0901
60	-.2814	-.2464	-.2137	-.1786	-.1426	-.0931
75	-.2708	-.2430	-.2017	-.1704	-.1329	-.0931
90	-.2569	-.2339	-.2012	-.1661	-.1311	-.0905
105	-.2401	-.2171	-.1868	-.1541	-.1263	-.1022
120	-.2112	-.1892	-.1676	-.1469	-.1287	-.1022
135	-.1752	-.1617	-.1459	-.1373	-.1205	-.1094
145	-.1531	-.1431	-.1344	-.1258	-.1210	-.1138
150	-.1319	-.1243	-.1219	-.1181	-.1142	-.1118
155	-.1228	-.1214	-.1200	-.1186	-.1186	-.1162
165	-.0867	-.0901	-.0936	-.0970	-.1042	-.1224
180	-.0502	-.0536	-.0642	-.0773	-.0855	-.1071

PHI (degrees)

THETA (degrees)	5	10	15	20	25
-35	-.0874	-.0971	-.1043	-.1129	-.1287
-30	-.0879	-.0927	-.1013	-.1051	-.1137
-25	-.0832	-.0856	-.0894	-.0932	-.0970
0	.0108	.0300	.0382	.0464	.0450
15	-.0399	-.0149	-.0005	-.0150	.0280
30	-.0280	-.0030	.0139	.0317	.0461
45	-.0564	-.0276	-.0025	.0201	.0356
60	-.0642	-.0343	-.0103	.0148	.0288
75	-.0642	-.0295	-.0079	.0148	.0302
90	-.0686	-.0387	-.0195	-.0032	.0114
105	-.0734	-.0579	-.0411	-.0233	-.0102
120	-.0892	-.0782	-.0651	-.0569	-.0487
135	-.1046	-.0964	-.0930	-.0973	-.0896
145	-.1090	-.1090	-.1128	-.1152	-.1190
150	-.1142	-.1239	-.1253	-.1291	-.1377
155	-.1210	-.1306	-.1402	-.1503	-.1589
165	-.1258	-.1378	-.1547	-.1681	-.1815
180	-.1264	-.1456	-.1687	-.1869	-.2027

APPENDIX F. DYNAMIC PRESSURE ISOLATION TEST DATA

THETA	PHI (degrees)						
(degrees)	-25	-10	-5	0	5	10	25
0.0	.0173	.0438	.0434	.0333	.0312	.0290	-.0042
22.5	-.0066	.0222	.0264	.0285	.0263	.0170	-.0165
45.0	-.0134	.0220	.0216	.0311	.0288	.0244	-.0186
67.5	-.0135	.0194	.0214	.0287	.0289	.0220	-.0185
90.0	-.0086	.0244	.0287	.0312	.0288	.0242	-.0136
112.5	-.0134	.0202	.0240	.0311	.0360	.0244	-.0112
135.0	-.0088	.0224	.0290	.0311	.0288	.0220	-.0084
157.5	-.0036	.0274	.0316	.0338	.0316	.0270	-.0062
180.0	-.0088	.0246	.0312	.0312	.0318	.0276	-.0038

APPENDIX G. ADU TRANSDUCER ISOLATION ANALYSIS DATA

Transducers Connected

Pressure (cm H2O)	P(T) +P(A) +P(B)	P(T) +P(A)	P(A) +P(B)	P(A)	P(B)	P(T)	none
-60	.4618	5.3920	4.3339	5.4401	5.4711	5.4744	5.4865
-50	.4606	5.4460	4.3696	5.4958	5.5267	5.5301	5.5418
-40	.4593	5.5185	4.4053	5.5505	5.5818	5.5847	5.5967
-30	.4581	5.5530	4.4409	5.6067	5.6370	5.6407	5.6531
-20	.4569	5.6070	4.4758	5.6628	5.6929	5.6946	5.7084
-10	.4556	5.6599	4.5114	5.7169	5.7474	5.7496	5.7639
0	.4544	5.7151	4.5465	5.7710	5.8030	5.8065	5.8198
10	.4532	5.7675	4.5805	5.8280	5.8595	5.8623	5.8745
20	.4519	5.8208	4.6149	5.8820	5.9153	5.9164	5.9296
30	.4507	5.8735	4.6494	5.9370	5.9698	5.9717	5.9865
40	.4494	5.9267	4.6837	5.9930	6.0257	6.0299	6.0414
50	.4486	5.9798	4.7178	6.0486	6.0816	6.0857	6.0957
60	.4468	6.0327	4.7530	6.1043	6.1374	6.1411	6.1523

LIST OF REFERENCES

1. *Function Specification for the Service Aircraft Instrumentation Package (SAIP)*, Pacific Missile Test Center Specification PMTC-CD-EL-697-76A, 31 March 1989.

2. NATOPS Flight Manual, UH-1H Aircraft, NAVAIR 01-110HCE-1, p. III-11-18, 1 March 1988.

3. Memorandum of David Muskat (PMTC, Code 1062), Serial 8800/1062 to Wayne Biesecker (PMTC, Code 3144), Subject: SAIP Static Barometric Pressure Measurement Quality, 12 July 1989.

4. *Mission Data Summary Tapes*, Numbers 12, 17, 27 and 30, Pacific Missile Test Center, Range Data Processing Center, 27 September 1989.

5. Benedict, Robert P., *Fundamentals of Temperature, Pressure and Flow Measurements*, Third Edition, pp. 350-354, John Wiley and Sons, Inc., 1984.

6. Anderson, John D., *Fundamentals of Aerodynamics*, pp. 150-152, McGraw Hill, Inc., 1984.

7. Schlichting, Herman, *Boundary Layer Theory*, Seventh Edition, pp. 20-21, McGraw Hill, Inc., 1979.

8. Zucker, Robert D., *Fundamentals of Gas Dynamics*, pp. 112-116, Matrix Publishers, Inc., 1977.

9. Murphy, R. C., Test Plan for Extended Area Test System Altitude Improvement, Pacific Missile Test Center, 11 September 1989.

10. Department of Aeronautics, *Laboratory Manual for Low Speed Wind Tunnel Testing*, Naval Postgraduate School, Monterey, CA, 1989.

11. Viniotis, John J., *Flowfield Effects of Launch on a Vertically-Launched Missile*, Master's Thesis, Naval Postgraduate School, Monterey, CA, June 1989.

12. Considine, Douglas M., <u>Process Instruments and Controls</u>, Third Edition, pp. 3.68-3.70, McGraw Hill, Inc, 1985.

INITIAL DISTRIBUTION LIST

		No. Copies
1.	Defense Technical Information Center Cameron Station Alexanderia, VA 22304-6145	2
2.	Library, Code 52 Naval Postgraduate School Monterey, California 93943-5002	2
3.	Chairman Department of Aeronautics, Code AA Naval Postgraduate School Monterey, CA 93943-5000	1
4.	Commander Pacific Missile Test Center, Code 3333 Point Mugu, CA 93042-5000	3
5.	Commander Naval Air Test Center Attn: Range Directorate (Mr. Mike Payne) Patuxent River, MD 20670-5304	1
6.	Commander Naval Air Systems Command (PMA248) Washington, DC 20361	2
7.	Professor Oscar Biblarz Department of Aeronautics, Code AA/Bi Naval Postgraduate School Monterey, CA 93943-5000	1
8.	LT Eric L. Pagenkopf Department of Aeronautics, Code AA/Pa Naval Postgraduate School Monterey, CA 93943-5000	1

9. LT Steven R. Eastburg
    211 Southview Drive
    Cherry Hill, NJ 08034

    2